Master's thesis

NTNU
Norwegian University of Science and Technology
Faculty of Engineering
Department of Marine Technology

Karoline Eriksen

Numerical investigation of a bottom-fixed wind turbine in severe environmental conditions

Numerisk undersøkelse av en bunnfestet vindturbin under tøffe miljøforhold

Master's thesis in Marine technology
Supervisor: Marilena Greco
June 2019

NTNU
Kunnskap for en bedre verden

Karoline Eriksen

Numerical investigation of a bottom-fixed wind turbine in severe environmental conditions

Numerisk undersøkelse av en bunnfestet vindturbin under tøffe miljøforhold

Master's thesis in Marine technology
Supervisor: Marilena Greco
June 2019

Norwegian University of Science and Technology
Faculty of Engineering
Department of Marine Technology

NTNU
Kunnskap for en bedre verden

NTNU Trondheim
Norwegian University of Science and Technology
Faculty of Engineering Science and Technology
Department of MarineTechnology

MASTER THESIS IN MARINE TECHNOLOGY

Spring 2019

FOR

Karoline Eriksen

Numerical investigation of a bottom –fixed wind turbine in severe environmental conditions

(Numerisk undersøkelse av en bunnfestet vindturbin under tøffe miljøforhold)

Steep shallow-water waves can lead to important hydrodynamic loads when interacting with bottom fixed wind turbines. Nonlinear and viscous effects, as well as influence of the sea bottom, represent important features in the wave-body interaction. Presence of collinear current in general matters.
A preliminary project work was performed to document the state of the art. A mono-pile, combined with the DTU 10 MW Reference Wind Turbine, was selected as fixed platform concept. A North Sea site with a water depth of 20 m was identified for the investigations. Relevant environmental conditions were documented and relevant incident-wave theories were discussed. The open-source CFD platform OpenFOAM was selected as research tool. As preliminary step, 2D flow conditions in the cross-section plane were carried out. The solver was used for verification/validation studies to simulate a fixed circular cylinder in steady and in oscillatory ambient flow, both in laminar and in turbulent conditions.

Objective
The present master thesis aims to investigate numerically a bottom-fixed mono-pile wind turbine interacting with shallow-water waves during severe environmental conditions and to assess the relevance of three-dimensional flow, turbulence and viscosity.

The work should be carried out in steps as follows:

1. Summarize major findings/outcomes from the project thesis and complement, if necessary, the literature survey in order to identify state-of-the-art of the problem. Discuss range of relevant non-dimensional parameters for the selected case study of a fixed wind turbine in a specific site and in relevant environmental conditions. Select a deterministic wave-modelling representative of severe/extreme wave conditions in the selected site, including multi-directional wave conditions.
2. Describe the numerical method selected as research tool and its basic assumptions. Perform a systematic study to clarify the differences between the numerical results obtained in the project thesis and the reference solutions and to complete the verification study.
3. Apply the numerical method to investigate the 3D mono-pile in severe/extreme wave conditions, reproduced as learned in step 1. The studies should be performed assuming practically zero viscosity, using a laminar-flow formulation and, possibly, using a simplified turbulent-flow formulation.
4. Use the numerical method to study the wave-body interactions as 2D in the cross-sectional plane using a laminar-flow formulation. Use the 2D simulations to estimate

the hydrodynamic loads on the structure and integrate them for a comparison against the corresponding 3D simulations. Examine comparatively the flow features along the body.

5. Draw the conclusions from the studies and discuss possible further research steps.

The work may show to be more extensive than anticipated. Some topics may therefore be left out after discussion with the supervisor without any negative influence on the grading.

The candidate should in her report give a personal contribution to the solution of the problem formulated in this text. All assumptions and conclusions must be supported by mathematical models and/or references to physical effects in a logical manner.

The candidate should apply all available sources to find relevant literature and information on the actual problem.

The thesis should be organised in a rational manner to give a clear presentation of the work in terms of exposition of results, assessments, and conclusions. It is important that the text is well written and that tables and figures are used to support the verbal presentation. The thesis should be complete, but still as short as possible. In particular, the text should be brief and to the point, with a clear language. Telegraphic language should be avoided.

The thesis must contain the following elements: the text defining the scope (i.e. this text), preface (outlining project-work steps and acknowledgements), abstract (providing the summary), table of contents, main body of thesis, conclusions with recommendations for further work, list of symbols and acronyms, references and (optional) appendices. All figures, tables and equations shall be numerated.

The supervisor may require that the candidate, in an early stage of the work, present a written plan for the completion of the work. The plan should include budget for the use of computer and laboratory resources that will be charged to the department. Overruns shall be reported to the supervisor.

From the thesis it should be possible to identify the work carried out by the candidate and what has been found in the available literature. It is important to give references to the original source for theories and experimental results.

Supervisor : Marilena Greco
Co-supervisor : Andrea Califano
Co-supervisor : Claudio Lugni

Submitted : January 15th 2019
Deadline : June 11th 2019

Marilena Greco
Supervisor

Abstract

The market for renewable energy is increasing along with developing technology and the interest for extending the wind energy market to offshore areas. By this motivation an objective is made to investigate a bottom-fixed monopile wind turbine interacting with shallow-water waves and to assess relevance of three-dimensionality, flow features, turbulence and viscosity. In order to investigate higher order phenomena of this bottom fixed wind turbine, some investigations and literature study of the state of the art are done. Based on the findings of these studies, a relevant site for further investigation is chosen to be at a location in the North Sea. The geometry to be investigated is chosen to be a monopile for the bottom-fixed wind turbine foundation. The environmental parameters from the site are then included in a CFD study that is conducted by the use of the open-source program OpenFOAM. A Cnoidal wave theory is chosen and implemented into the CFD set-up by use of the plug-in waves2FOAM. An initial mesh-convergence study in 2D is verified by comparing the results to previously done studies. An investigation of the accuracy of the simulated Cnoidal waves is done by simulating waves in an empty pool, measure the instant wave heights by probes and comparing this result to analytically obtained waves by use of Cnoidal wave theory. This comparison give very promising results, with almost identical waves. It is shown that use of the plug-in waves2FOAM is efficient and easy to implement into the study and is therefore chosen for further use as wavemaker.

With the aim of studying 3D flow and 3D effects, fully 3D simulations of the monopile cylinder in extreme waves are carried out for three different wave conditions. Several 2D studies of the cylinder at different heights of the waves are also conducted. Using these results for integration by use of "strip theory", an estimated 3D result for the drag- and lift forces is obtained. The integrated results are then used for comparison to the 3D results. The comparison show that the drag-forces from the 3D simulation are approximately four times higher than the results from the integrated 2D simulations. The integrated lift force show bigger variation in the time series and thereby higher peaks. It is seen that the 2D simulations with an unsteady boundary condition inlet show irregular pressure behaviour that may be the reason for some deviations in the results. The flow pattern confirm this irregularity in the pressure behaviour. The 3D flow behaves as expected and demonstrates wave run-up at the rear of the cylinder as can be caused by steep and long waves in shallow waters.

Viscosity is investigated by conducting a 3D simulation with the same wave condition but with practically zero viscosity. The results show a decrease in the viscous force components by less than 3%. The turbulence simulations give in 2D a clearer steady state condition and diminished forces ($\sim$ 50%). This can also be affected by the pressure boundaries. The turbulent simulation in 3D give different wave profiles than for the other 3D cases which was unexpected. This results in lower forces acting on the cylinder and no separation behaviour.

Sammendrag

Markedet for fornybar energi øker i takt med teknologiutvikling og interesse for å utvikle vindenergimarkedet til havområder. Utfra denne motivasjonen er det av interesse å undersøke en bunnfestet vindturbin i grunt vann og utforske relevansen av tre-dimensjonalitet og kort-kammede bølger. Undersøkelser og litteratur-studie av nåværende forsking blir gjennomført for å undersøke hva som er gjort i forbindelse med høyere ordens krefter på slike strukturer. Basert på funnene av disse studiene gjøres en utgreiing om et relevant geografisk sted som er et aktuelt sted å plassere vindturbinen. Valget faller på en lokasjon i Nordsjøen og miljøfaktorene på stedet blir dermed utforsket og inkludert i en CFD studie. Disse studiene er gjort ved bruk av programvaren OpenFOAM. En høyere ordens bølgeteori blir brukt for å simulere bølgene på stedet. Cnoidal bølger er valgt for å representere disse på en god måte. Disse blir implementert inn i CFD oppsettet ved hjelp av ekstrapakken waves2FOAM. En mesh blir først opprettet i 2D for å gjennomføre en konvergens-studie. Resultatene blir deretter sammenlignet med tidligere studier, og det kommer her frem at oppsettet gir samsvarende resultater med hva som er funnet tidligere. Modellen er dermed validert. Også bølgene valideres; dette ved å simulere 2D bølger i et tomt basseng og deretter sammenligne bølgeprofil med analytiske bølger regnet ut ved hjelp av bølgeteorien. Også her samsvarte resultatene godt og det konkluderes med at waves2FOAM er et bra verktøy som kan brukes videre.

Med mål om å studere 3D strømning og effekter blir det gjennomført komplette 3D simuleringer av vindturbin-fundamentet under harde værforhold. Flere 2D studier av sylinderen ved forskjellige bølgehevinger blir også gjennomført. Ved å integrere 2D resultatene ved hjelp av «stripe-teori», finner man et estimert 3D resultat for kreftene som virker på sylinderen. Disse integrerte resultatene kan dermed brukes for sammenligning med 3D resultatene. Sammenligningen viser at de viskøse (drag) kreftene fra 3D simuleringen omtrent er fire ganger høyere enn de integrerte kreftene. Løft kreftene fra de integrerte resultatene viser større variasjoner i tidsseriene og har dermed høyere topper. 2D simuleringene viser uregelmessigheter i forhold til trykket som kan være grunnen til avvikene i resultatene. Strømningsbildet rundt sylinderen viser at trykk-oppførselen i disse simuleringene trenger å bli undersøkt grundigere. Strømningsbildet i 3D simuleringene er som forventet og viser bølge oppløp rett bak sylinderen. Dette er et fenomen som sees ved bratte og lange bølger i grunt vann.

Effekten av viskositet er undersøkt ved gjennomføring av en 3D-simulering med de samme bølgeparameterne som tidligere, men med omtrent null viskositet i væsken. Resultatene viser en minking i de viskøse kraft komponentene som er mindre enn 3%. Turbulent simuleringene gir en klarere stabil tilstand i 2D og en minking i krefter på rundt 50%. Dette kan også ha blitt påvirket av trykk-grensebetingelsene og løsnings-koden som er brukt. Turbulent simuleringen i 3D gir avvikende bølgeprofiler i forhold til de andre 3D-simuleringene. Dette var ikke forventet og resulterer i lavere krefter som virker på sylinderen og ingen separasjon.

Preface

This project is carried out in order to complete the course TMR4930, master's thesis in marine technology. This completes the requirements for obtaining the master in marine technology at the Norwegian University of Science and Technology (NTNU). The work has been conducted during the spring semester of 2019 and is a continuation of the specialization project done during the fall semester of 2018 that is mandatory for the class TMR4520, specialization project in marine hydrodynamics.

I am very grateful to my supervisor, professor Marilena Greco (NTNU) for all guidance and help with the work. Thank you for all your ideas and encouragements and for always staying positive. I would also like to express my gratitude towards my co-supervisors Andrea Califano and Claudio Lugni. Thank you Claudio for answering my e-mails and questions. Thank you Andrea for all the time you have put into practical help and guidance that I have received during our meetings. I would also like to direct a big thank you to Tufan Arslan for all the help with the supercomputer and other technical issues. Thank you for meeting with me for practical help, instruction and installation of software. Thank you to Hoaran Li for help with solving issues related to the simulation set-up and issue solving. Also, I would like to direct my appreciation to my friends at the office, my boyfriend and my family for all the encouragements and support. Finally, thank you to my father, Frode Eriksen, for proof-reading and support.

Trondheim, June 10, 2019

Karoline Eriksen

Karoline Eriksen, candidate number 10029

Contents

List of Tables

List of Figures

Abbreviations

OWT	Offshore Wind Turbine
WT	Wind Turbine
CFD	Computational Fluid Dynamics
RWT	Reference Wind Turbine
Re	Reynolds Number
CN	Courant Number
CFL	Courant Friedrichs Lewy number
BC	Boundary Conditions
OF	OpenFOAM
LES	Large-Eddy Simulation
RANS	Reynolds-Averaged Navier-Stokes equation
RST	Reynolds-Stress Transport
ARS	Algebraic Reynolds-Stress
VOF	Volume of Fluid Method for Multiphase Flow
WC	Wave case
CPU	Central processing unit

Nomenclature

D	Diameter [m]
H	Wave height [m]
T	Wave/flow period [s]
t	Time [s]
T_p	Peak wave period [s]
$H_s/H_{1/3}$	Significant wave height [m]
d	Water depth [m] (in general) / time step ratio (courant number)
λ	Wave length [m]
ζ_a	Wave amplitude [m]
U_w	Wind velocity [m/s]
C_D	Drag coefficient
C_L	Lift coefficient
g	Gravitational acceleration $[m/s^2]$
S	Wave steepness parameter
μ	Shallow water parameter
U_r	Ursell parameter
k	Wave number
ρ	Density $[kg/m^3]$
σ_y	Yield Strength [MPa]
μ	Poisson's ratio
Re	Reynold's number
U/V	Incoming stream velocity [m/s]
u	Velocity vector
a	Incoming stream acceleration $[m/s^2]$
L	Characteristic length [m]
ν	Kinematic viscosity $[m^2/s]$
S	Strouhal number
f_v	Vortex shedding frequency [1/s]
C_{Fx}	Force coefficient
C_M	Mass coefficient
KC	Keulegan Carpenter number
cn, sn, dn	Jacobian elliptic functions
η	Water surface elevation [m]
θ	Phase angle [deg]
h	Mean water depth [m]
K, E	Complete elliptic integrals
c	Wave celerity / ratio of the time step (Introduction to CFD)
m	Cnoidal wave key parameter
q_ϕ	Source or sink of ϕ
α	VOF variable

Chapter 1

Introduction

The climate changes that are happening in the world have been visible for several decades. In order to limit the damages, the UN have decided on a 2-degree Celsius climate goal by 2030, UN (2018). In order to achieve this goal it is necessary to reduce the emissions of climate gasses such as Co2.This can be done by using alternative resources or decreasing the energy consumption. However, DNV-GL (2018) predicts that the global energy demand is increasing and will continue to do so until the year 2030. The electricity consumption will possible more than double until the mid-century. On this background it will be vital to increase the renewable energy production. According to DNV-GL (2018), wind energy along with solar PV can supply more than two-thirds of that electricity. The energy transition outlook states; "more renewables and more carbon capture and storage is needed to meet the ambitions of the Paris Agreement".

Wind energy is an important contributor to renewable energy sources. Wind energy can be produced both onshore and offshore. Offshore installations are still quite new on the market and new solutions are in the developing phase. There is also a trend indicating an increase in windmill size. Increasing size demands bigger areas, and this has been one of the motivations for developing offshore wind solutions. These solutions can either be constructed to float or installed on the sea bottom. Floating installations are still in the testing phase, one example being the Hywind park consisting of six floating wind turbines which each has a capacity of five [MW]. This is the world's first floating wind park and was according to Equinor (2018) installed during the fall of 2017. However, most of the existing structures at sea today are bottom-fixed ones. The monopile is one of these bottom-fixed structures that are most commonly utilized for carrying offshore wind turbines. The dimensions may vary, but the geometry is a single pile connected to the sea bottom. These piles are exposed to loads from wind and waves as well as the loads from the turbine. It is predicted that the monopile will continue to dominate the offshore wind turbine market because they are cost effective and relatively easy to install, Bouzid (2018).

With increased and more complex structures, the interest in studying higher order phenomena, such as ringing for these offshore bottom-fixed structures has grown, Kristiansen and Faltinsen (2017). Ringing, along with other higher order phenomena, is yet to be fully investigated and understood. Ringing is in this thesis defined as transient resonant oscillations in a structure that are induced by waves. This includes oscillations induced from both waves and higher order wave forces, Rosenlund (2013). It has been discovered that this phenomena can cause great damage under certain conditions. For developing and cost-minimizing it is extremely important to investigate higher order phenomena for offshore wind turbines (OWT). This thesis aims to investigate a bottom-fixed monopile wind turbine (WT) interacting with shallow water waves. Because of lack of knowledge in this area, it is also of interest to assess the relevance of viscosity, three dimensional flow and turbulence.

This Master thesis is a continuation of a project thesis that was written by the undersigned during the fall of 2018. In the project thesis the state of the art was documented and a monopile combined with a 10 [MW] reference WT was selected as the fixed platform concept. Some preliminary studies were conducted in the open-source Computational Fluid Dynamics (CFD) tool OpenFOAM. This work will be continued in this Master thesis. It is necessary to repeat some of the topics previously covered and include them in this Master thesis for further elaboration. This is done in order to fully describe the phenomena and discoveries. Some results from the project thesis are also included in order to compare and discuss its relevance and possible impact.

1.1 Outline of Master Thesis

The thesis is structured in a manner that should be easy to follow. First, the state of the art is addressed and some of the previous project thesis work is summarized and extended. A site description and WT specifications are given along with environmental conditions. Necessary background theory is then described in the following chapter. Next, the method for solving some of the research questions below will be to use the numerical tool OpenFOAM along with an additional plug-in for wave modelling. The procedure and a description of the numerical tool along with its limitations and assumptions are described. Further, an overview of the relevant set-up and boundary conditions are given along with results for each simulation type. A discussion follows after each result section. The discussion sections includes reference work. Lastly, a conclusion with recommendations for further work and research topics is given.

1.1.1 Research Questions and Objective

The objective of the Master thesis is to investigate a bottom-fixed monopile WT interacting with shallow water waves during severe environmental conditions and to assess the relevance of three-dimensional flow, turbulence and viscosity. This is done by answering the following research questions:

- What are the relevant parameters for the selected case study at a specific site and with the given environmental conditions?
- Can representative results be obtained by use of CFD simulations in a reasonable amount of time?

- Will turbulence, three-dimensional flow and viscous effects be of importance?
- Will the code be able to simulate steep waves in shallow waters in an efficient and good way?
- Do the results from a three-dimensional CFD investigation cohere with strip theory used on results from the two dimensional CFD simulations?

1.2 Summary of Literature Study

This section provides a summary of the literature study that was performed for the project thesis. The state of the art of bottom-fixed WT in shallow waters and steep waves was investigated to make a foundation for the project- and master thesis work. It was discovered that several research projects have aimed at solving issues related to bottom fixed monopile wind turbines. Different aspects have been investigated, and structures of increasing size have been installed at sea. An important trend is that the turbine size along with monopile dimensions are rapidly increasing.

1.2.1 Experimental Research

The magnitude of the nonlinear wave loads will be higher for finite water depth than for deep waters according to Bachynski et al. (2017). This was their motivation for doing experimental tests of a monopile in shallow waters with the aim of investigating ringing phenomena in irregular waves. Other similar studies have been performed as well for different water depths and different waves. Table 1.1 show selected experimental studies that aim at studying wave effects on monopiles. The table is taken from Bachynski et al. (2017).

Table 1.1: Selected experimental studies concerning wave effects on monopiles. Taken from Bachynski et al. (2017)

	Facility	Scale	Water depth [m]	Model	Waves
Wienke and Oumeraci (2005)	FZK	1:9.8	39.2-44.1	Rigid	DBr
de Vos et al. (2007)	Aalborg Uni.	1:57.5	20.1-28.7	Rigid	R, ULS I, LC
Zang et al. (2010)	DHI	1:27.6	13.9	Rigid	DBr
de Ridder et al. (2011)	MARIN	1:30	30	Flexible	R, DBr, FLS I, LC
Nielsen et al. (2013)	DHI	1:36.6	16.6-20.1	Rigid	ULS I, SC
Nielsen et al. (2013)	DHI	1:80	20.8-40.8	Rigid/ flexible	ULS I, SC
Bachynski et al. (2017)	NTNU/ Sintef Ocean	1:48	19-27	Rigid/ flexible	ULS I, LC

The experimental work presented in Table 1.1 focus on different aspects, and make different assumptions. In the work conducted by Wienke and Oumeraci (2005), breaking waves acting on a slender cylinder pile is examined. Plunging breaking waves are considered, and their study can therefore be in use for examining short-duration slamming loads. In the work of de Vos et al. (2007), the run-up around the pile is investigated. Both regular and irregular waves are included. Comparisons of their results and previous studies and theories show that the shape of foundation affect the results to a big degree. Zang et al. (2010) found that the second order parasitic waves had importance for the ringing phenomena. However, their study is not conclusive. Testing by de Ridder et al. (2011) was very extensive, and examines breaking waves effects. Nielsen et al. (2013) use a sloped bottom for their experiments (1:25), and they include both regular- and irregular waves. Short-crested waves are also included. They found that steep and breaking waves give significant vibration responses. This can imply ringing phenomena, and they conclude that steep waves can have significant responses in short-crested seas.

Bachynski et al. (2017) carried out experiments for 20 three-hour duration realizations of four different sea states. They did this for two different models and two water depths. This way, they were able to get a profound result basis. In some tests, the physical wave in the experiments showed to have more non-linearity than a 2nd order model could capture. This means that the non-linear wave model underestimates the maximum hydrodynamic forces and moments acting on the rigid monopile. However, the tests showed that the model could estimate the response fairly well. The non-linear model captured the ringing phenomena to a much higher degree than the linear model. More about the numerical model they used can be found in Section 1.2.2. Their research concluded that second-order phenomena such as ringing was seen in the flexible single degree-of-freedom model for steep waves.

1.2.2 Numerical Research

As discussed in Section 1.2.1, Bachynski et al. (2017) did a numerical investigation of a bottom fixed monopile in steep waves and shallow waters, and compared the results to the experimental results they did for the same conditions. Their model was created in RIFLEX, and consisted of beam elements. The wave load model in use is based on a modified Morison model. Their results showed that the modified Morison approach gave higher springing responses for the flexible model, but gave quite accurate springing results in extreme conditions. The over-prediction was most visible for short waves in shallow waters.

Paulsen et al. (2014) did a numerical study of a circular cross-section in finite water depth with steep waves. It was done by solving the two-phase incompressible Navier-Stokes equations, and their conclusions say that *"the secondary load cycle is an indicator of strongly nonlinear flow rather than a direct contributor to the resonant forcing"*. In their paper, they present research on a nonlinear wave forcing on a bottom-mounted circular cylinder in intermediate water depths. This is done by implementing a fully nonlinear Navier-Stokes solver, where the viscous boundary layer effects at the cylinder and at the seabed are neglected. Using the stream function theory solution of Fenton (1988), the incident waves are generated. Recent work conducted by Kristiansen and Faltinsen (2017) investigate a local run-up phenomena that is observed during experimental testing. A 2D Navier-Stokes simulation was conducted, and the resulting pressure due to flow separation can qualitatively explain the local rear run-up. This is done by investigating the flow around a circular cylinder by a large-eddy simulation (LES) solver.

Extensive numerical work was carried out by Schloer et al. (2013) were the aim was to investigate extreme waves and the significance on non-linearity for irregular waves. Steep waves from nonlinear theory got implemented in the study of an offshore monopile wind turbine. A fully nonlinear potential flow model was used for calculation of the wave kinematics, while the wave forces was calculated by Morison's equation. The potential flow solver was compared with a CFD-solver, where waves got implemented as well. The study showed how important the wave non-linearity is in the design of offshore wind turbines.

Chapter 2

Problem Description

In this chapter, the WT is defined in terms of dimensions and specifications. The surrounding conditions are also addressed in terms of water depth, environmental conditions (wind, waves, current and tide) and soil conditions. The range of relevant non-dimensional parameters for the selected case are discussed and a deterministic wave-modelling that is representative of extreme wave conditions is selected. Multi-directional wave conditions are assessed.

2.1 Wind Turbine Specifications

The specifications of the wind turbine are taken from the DTU 10 [MW] WT. This reference WT was chosen based on the findings summarized in Section 1.2. The 10 [MW] turbines will be of great interest for the future as the trend is showing that the size of the turbines and the turbine supports are getting bigger in order to increase the production and be more economically viable. The key parameters of the turbine are important for the geometry of the monopile. These are listed in Table 2.1 and are taken from Velarde (2016).

Table 2.1: Key parameters for the DTU 10 [MW] wind turbine

Wind Regime	IEC Class 1A
Rotor Orientation	Clockwise rotation - Upwind
Control	Variable Speed, Collective Pitch
Cut in wind speed	4 m/s
Cut out wind speed	25 m/s
Rated wind speed	11.4 m/s
Rated power	10 MW
Number of blades	3
Rotor diameter	178.3 m
Hub diameter	5.6 m
Hub height	119.0 m
Drivetrain	Medium speed, Multiple-Stage Gearbox
Minimum rotor speed	6.0 rpm
Maximum rotor speed	9.6 rpm
Maximum generator speed	480.0 rpm
Gearbox ratio	50
Maximum tip speed	90.0 m/s
Hub overhang	7.1 m
Shaft tilt angle	5.0 deg
Rotor precone angle	-2.5 deg
Blade prebend	3.332 m
Rotor mass	227962 kg
Nacelle mass	446036 kg
Tower mass	628442 kg

The monopile tower for the 10 [MW] DTU reference wind turbine (RWT), has a design and properties as shown in Tables 2.2 and 2.3. The base diameter is 8.3 m, and increase linearly to 5.5 m at the top. The total tower height is 115.63 m. All properties and dimensions can be found in Velarde (2016).

Table 2.2: Tower Material Parameters for the DTU 10 MW RWT

Density, ρ $[kg/m^3]$	8500
Yield strength, $\sigma_y [MPa]$	355
Young's modulus, $E[N/m^2]$	2.10E+11
Shear modulus, $G[N/m^2]$	8.08E+10
Poisson's ratio, μ	0.3

Table 2.3: Monopile Tower Design Parameters

Height [m]	Outer Diameter [m]	t [mm]
0	8.3	38
11.5	8.0215	38
23	7.7431	36
34.5	7.4646	34
46	7.1861	32
57.5	6.9076	30
69	6.6292	28
80.5	6.3507	26
92	6.0722	24
103.5	5.7937	22
115.63	5.5	20

An illustration of the DTU RWT is shown in Figure 2.1.

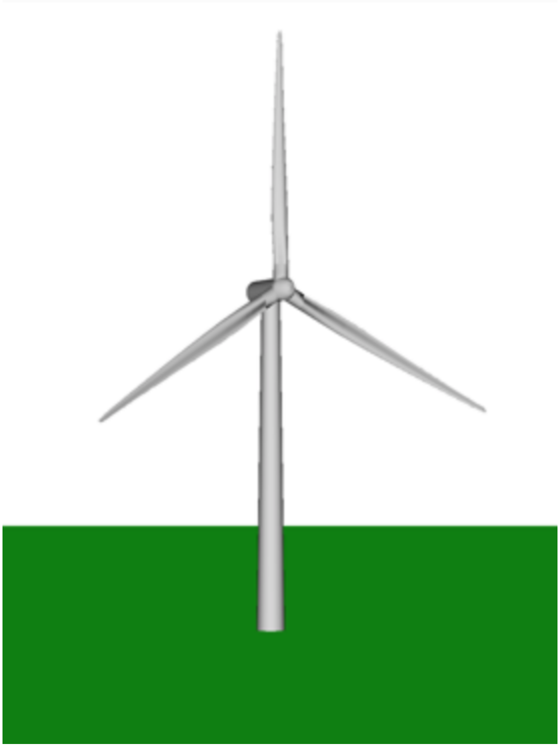

Figure 2.1: DTU 10 MW RWT, picture courtesy of hawc2.dk

2.2 Site specifications

The selected WT design will be implemented into a suitable location. It is important that the water is shallow due to limitation of the monopile height. At the same time, the selected site should provide a lot of wind resources and be suitable for a wind park. In this section, the selected site for this project is presented and the relevant parameters that are important to consider when choosing a site is discussed. After, the environmental- and soil conditions at the site are presented. By determining the relevant wave conditions, the extreme conditions can be numerically represented. A wave modelling method for the selected site will therefore be discussed at the end of the Section. The Marine Renewable Integrated Application Platform, MARINA, is a project that aims at developing technology for the renewable marine energy industry. Parts of the project focus on identifying new concepts and locations, and in this connection they have published an article concerning possible European sites for development and concept comparison, Li et al. (2013). The sites discussed in the work of Li et al. (2013) represents both shallow water- and deep water sites in the North Sea and the Atlantic Ocean. They are chosen based on the consideration of the average wind and wave energy resources available at sites, as well as extreme conditions. The extreme conditions will often give a good indication of the cost of developing offshore platforms at the actual site. The sites are chosen based on a comparison of predicted costs and energy outputs. Figure 2.2 shows the investigated and chosen sites from the work of Li et al. (2013).

Figure 2.2: Investigated sites. Picture courtesy of Li et al. (2013)

For bottom fixed concepts, the sites with shallow waters are of interest. For this thesis, site number 17 (close to 15) is chosen for further investigation. This is located in the center of the North Sea, and more information about the site is shown in Table 2.4. All information about the site is taken from Li et al. (2013).

Table 2.4: General Site Information - North Sea Center

Water Depth $[m]$	~ 20
Distance to shore $[km]$	60
Average wind power density at 80 m height $[W/m^2]$	850.95
Average wave power density $[kW/m]$	12.79
50-year mean wind speed at 10 m height $[m/s]$	26.49
50-year significant wave height $[m]$	8.62
Mean value of $T_p[s]$	6.70

The data used in the article by Li et al. (2013) is taken from the research project FINO3 that is run by the Research and Development Center Fachhochschule Kiel GmbH (GmbHm (2019)). More information is available on their website concerning wind conditions, wave conditions and foundation. This is further described in Section 2.2.1.

2.2.1 Relevant Parameters

There are several relevant parameters that are important to consider when studying possible sites for an offshore wind farm. Logistics, economy and environment are examples of categories that should be looked in to. According to Bailey (2016), offshore environments for wind farms have different environmental factors than the onshore wind farms. The winds are stronger and have more horizontal uniformity, also called wind shear. This is caused by the lack of terrain or surface roughness that hinder the wind. The local metocean environment consists of various atmospheric and oceanographic conditions that vary through time. Storms and extreme values must be assessed as well as standard operating conditions. These parameters can according to Bailey (2016) be summarized in following three categories:

- Meteorological variables such as wind
- water- and sea bed-related variables
- Joint characteristics

When the WT experience extreme conditions, the turbine will be parked. This way, the meteorological variables such as wind will not be implemented in this analysis. They are however important for a fully integrated WT analysis. The input that will be of importance for this analysis, are the parameters that decide the loading and the boundary conditions for the CFD simulation. This will be the water- and sea bed-related variables in particular. More concrete, these will be the wave height, period and direction, along with seabed geometry and bathymetry.

Other parameters that are important to consider are the soil parameters, corrosion, marine growth and scour protection. The soil parameters decide the pile-soil interaction due to lateral loads. Corrosion can severely damage the construction and in worst case lead to failure. It is therefore necessary to consider a protection method against corrosion. Marine growth increase the area that is exposed to loads. If the area increases, the structure is exposed to more loads. It can therefore be important to consider an increase in area when considering loads on the structure. Scour protection is very important for monopiles in order to secure a good connection between the construction and the sea bed. In worst case, the foundation for the WT can be severely altered in operation. This can lead to an unstable construction and failure.

Last, practical parameters such as distance to shore, power cables and other parameters that influence the economy and logistics should be considered. Available natural resources (wind and waves) is the most important when it comes to site selection, but the implementation ability in the sense of practical issues are factors of great importance. However, this is outside the scope of the research topic for this thesis and will not be closely looked into.

Environmental Conditions

Based on 43 years of observations, the hourly average threshold values for wind speeds are given in Table 2.5.

Return Period [years]	**Wind Speed [m/s]**
1	27.8
10	31.4
20	32.5
50	33.8
100	34.8

Table 2.5: Threshold values for wind speeds on an hourly average, taken from GmbHm (2019)

Ignoring the wind strengths, the most frequent wind is given as west direction, and is illustrated in Figure 2.3.

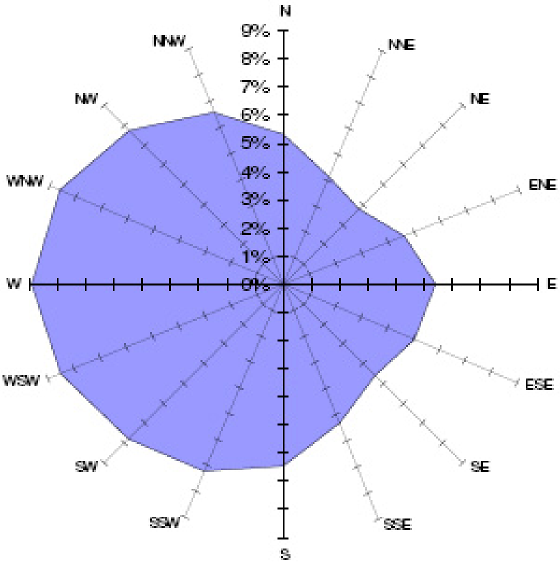

Figure 2.3: Most frequent wind directions, picture courtesy of GmbHm (2019)

Other meteorological parameters are given in Table 2.6.

Mean air temperature	9.5 degrees Celsius
Daily extreme temperatures	(-10) - (-30) degrees Celsius
Salt content of sea water	3.5 %
Stormy days	25 per year

Table 2.6: Meteorological parameters taken from GmbHm (2019)

The design water level according to GmbHm (2019) is 26.3 m due to tide and storm surge. However, the water depth in use will be 20 m. The design waves are given in Table 2.7.

Parameters	**50 years**	**30 years**	**10 years**
H1/3	9.2m	8.9m	8.3m
Hmax	17.9m	17.3m	16.2m
Crest height	18.0m	17.7m	16.4m
Wave length, λ	170-232m	166-224m	158-216m
Wave period, T	10.7-13.9s	10.6-13.6s	10.2-13.1s

Table 2.7: Parameters of the design wave and its return periods, taken from GmbHm (2019)

The wave headings are recorded by a wave buoy in the applicable area. The recordings clearly indicate that the main heading of the waves is west-southwest and that the extreme events for the most part occur with west to north-west directions. The statistical records of the heading of the waves are illustrated in Figure 2.4.

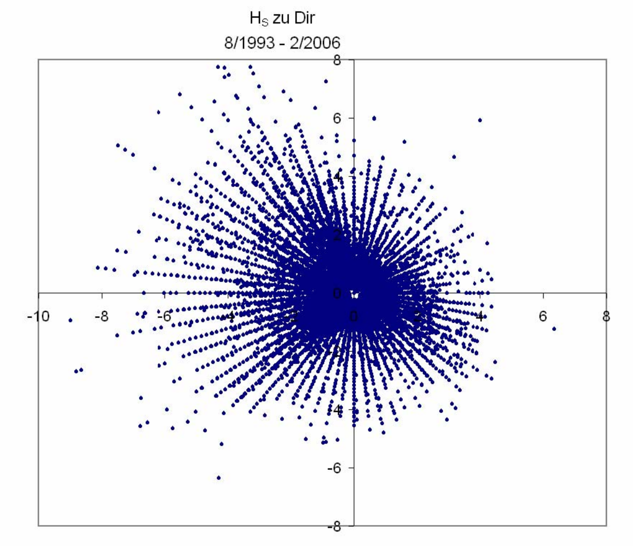

Figure 2.4: Wave measurements from a WaveRider wave buoy in the years 1993-2006, picture courtesy of GmbHm (2019)

Li et al. (2013) made environmental contour surfaces that illustrate the combinations of H_s and T_p that gives a fifty-year return state for the environmental conditions. They use a 2-parameter Weibull distribution for making the contours shown in Figure 2.5. The H_s and T_p values vary with different wind speeds. The two-dimensional H_s and T_p contours are shown in Figure 2.6. The data used for making these contours is taken from site 15 (very close to site 17) and is assumed to be representative for both sites. The weather data was sampled at an hourly frequency in the years 2001-2010. A lognormal distribution is used for tail fitting. More details about the process can be found in Li et al. (2013). It is clear that the significant wave heights and their periods correspond well to the measurements done by GmbHm (2019) that are presented in Table 2.7.

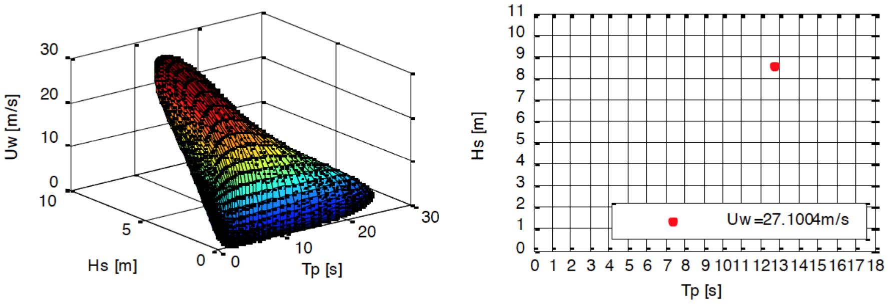

Figure 2.5: Environmental contours for site

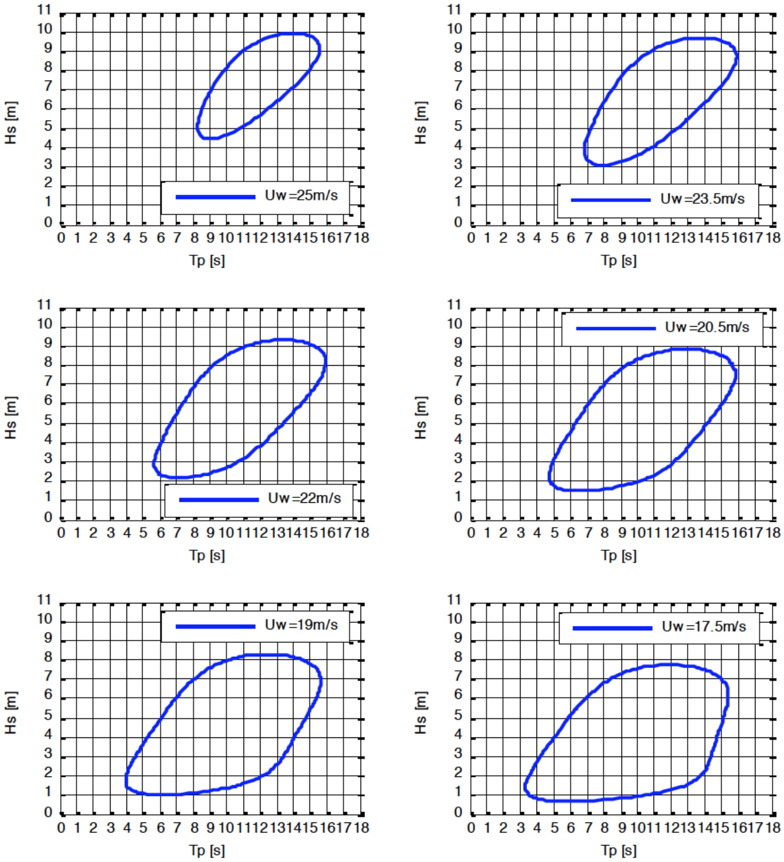

Figure 2.6: Environmental contours for site

The conditions corresponding to the maximum mean wind speed and the maximum significant wave height are shown in Table 2.8.

Table 2.8: Environmental conditions on the 50-year contour surfaces with maximum U_w or maximum H_s, taken from Li et al. (2013)

Parameter	**Maximum U_w**	**Maximum H_s**
U_w [m/s]	27.1	25.3
H_s [m]	8.6	9.9
T_p [s]	12.7	14

Water current will be important for this study, as current induce a higher particle velocity around the cylinder. Hence, it is also important to take into account in the design of offshore structures. For extreme conditions, surface current speed with a 10-year return period should according to the offshore standard by DNV-GL (2010) normally be used. Some typical surface current speeds with a return period of 10 years, are given by DNV-GL (2010), and shown in Table 2.9.

Table 2.9: Surface current speeds with a 10-year return period at different locations

Norwegian Sea (Haltenbanken)	0.90 m/s
North Sea (Troll)	1.50 m/s
North Sea (Greater Ekofisk area)	0.55 m/s

Soil Conditions

Structural damping is caused by the surrounding environment. According to Merz et al. (2009), the structural damping of vibrations can be due to following sources:

- Aerodynamic damping (rotor translation)
- Hydrodynamic damping (structure motion relative to the surrounding water)
- Structural damping (friction between members, material damping)
- Soil damping (comes from soil-foundation interactions)

Nonlinear soil behaviour can be found both in the longitudinal and transverse directions. The soil-foundation interaction will be influenced by the conditions at site. A seismic investigation has been conducted in an area of $2x2\ km^2$ around the site, GmbHm (2019). The seismology show a plateau for the first horizon about 2 m below the seabed. According to GmbHm (2019), a higher position of the horizon can mean that a more homogeneous layer would be encountered. It was also clear that low penetration depths of the seismic sound waves indicated a firm sedimentary compaction. Pressure sounding and core drilling was executed at the site as well. For specifications of this testing, reference is given to GmbHm (2019). According to these tests, the site "consists of medium-dense to very dense sand deposits with partial gravelly and silty constituents". Characteristic values concerning the site is given in Table 2.10 and is taken from GmbHm (2019).

Table 2.10: Soil characteristics concerning the site, taken from GmbHm (2019)

Depth under ground	y [$\frac{kN}{m^3}$]	ϕ [deg]	c_k [$\frac{kN}{m^2}$]	$E_{s,k}$ [$\frac{MN}{m^2}$]	$E_{dyn,k}$ [$\frac{MN}{m^2}$]
0.0-0.5	17/9	27.5	0	40	100
0.5-3.0	19/11	53.0	0	80	160
3.0-6.0	18/10	30.0	0	40	100
6.0-14.6	19/11	37-5	0	120	300
14.6-26.0	19/11	40.0	0	220	400
26.0-35.0	19/11	42.5	0	250	500

Here, ϕ is the angle of internal friction, y is the saturated unit weight of the sand, C_k the effective cohesion, $E_{s,k}$ the secant stiffness and $E_{dyn,k}$ the unloading and reloading stiffness.

Chapter 3

Background

This Chapter is devoted to describing the necessary theoretical background for the thesis. The chapter is based on previous work done in relation to the initial case study. In this previous work it was discovered that the choice of wave theory is very important and will be dependent on the water conditions, i.e. the water depth of the chosen area to be investigated. The breaking of waves will be affected by water depth and waves in the area. This effect will be important for shallow waters according to Camp et al. (2003). Other factors that will be of importance are the bathymetry of the site and surrounding weather conditions, including wind, waves and current. It was decided in the preparation work that for shallow waters, a Cnoidal wave theory is a good choice, while for intermediate waters a Stokes wave theory is the better choice.

In this Chapter, the background theory for flow phenomena, wave theories and computational fluid dynamics (CFD) is given. An investigation concerning different theories and methods is given in order to give sufficient foundation for the selections and methods used for the rest of the thesis. Other aspects will be considered as well. The stochastic parameters will be influenced by distance to shore. The stiffness of the soil at the site decides the necessary length (in addition to water depth) of the monopile.

3.1 Flow Theory

The water flow around a circular cylinder can to a certain degree be described by the Reynolds number, Re. The Reynolds number is given by Equation (3.1), where L is the characteristic length of the body, U is the incoming stream velocity and ν is the kinematic viscosity.

$$Re = \frac{UL}{\nu} \tag{3.1}$$

The fluid particles that are in contact with a body in a real fluid, will have the same velocity as the body. The result is a developing boundary layer around the body with increasing velocity corresponding to the distance between the body and the particles. This phenomena is described in more detail by for example Pettersen (2018). Figure 3.1 illustrates the expected vortex shedding for a circular cylinder at different Reynolds numbers.

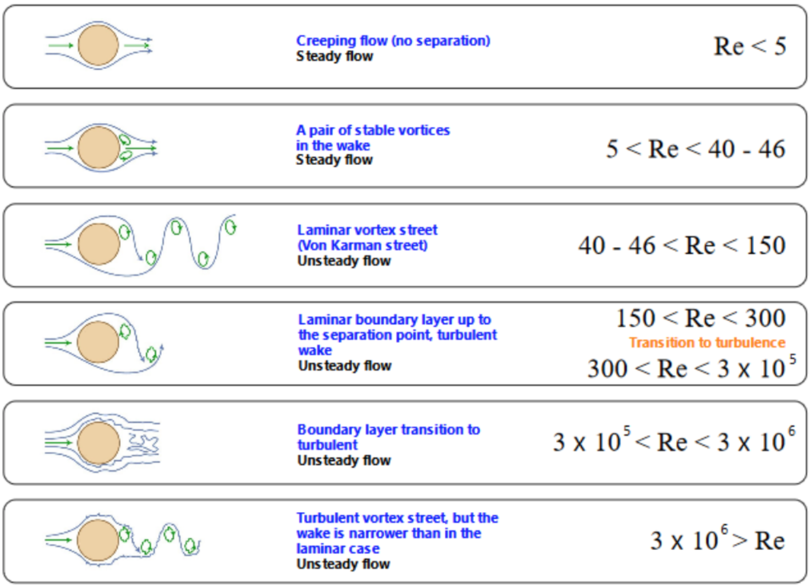

Figure 3.1: Vortex shedding behind a cylinder for different Reynolds numbers

The four last illustrations in Figure 3.1 show vortex shedding that is given by a lift- and a drag force. The lift force will oscillate with the same frequency as the vortex shedding frequency, f_v. its sign will also oscillate between negative and positive. In comparison, the drag force will oscillate with the same sign and double frequency when there is vortex shedding. There exists a relationship between the diameter of the cross section, the stream velocity and the vortex shedding frequency. This relationship is given by Strouhals number, S, and is given in Equation (3.2). this number is without dimensions and will be constant for a large range of Reynolds numbers. Within this range, its value will be approximately 0.2, Pettersen (2018).

$$S = \frac{f_v D}{U} \tag{3.2}$$

3.1.1 Forces on a Cylinder

The in-line forces for a cylinder in oscillatory flow is given by two terms; the mass part and the drag part. The mass part is given by inertia forces that are proportional to the acceleration, while the drag part is proportional to the velocity squared. The two terms are given by Equations (3.3) and (3.4). These are known as Morison's equation, and is described by Morison et al. (1950).

$$F_x = F_M + F_D \tag{3.3}$$

$$F_x = \rho \frac{\pi D^2}{4} C_M \frac{\delta U}{\delta t} + \frac{\rho}{2} C_D |U| U \tag{3.4}$$

Here, F_M and F_D are the mass- and drag- forces respectively. The coefficients, C_M and C_D depends on the Reynolds number, Re, and the Keulegan Karpenter number, KC. The KC number is given by Equation (3.5).

$$KC = \frac{U_0 T}{D} \tag{3.5}$$

Here, U_0 is the flow velocity and T is the flow period. For small numbers of KC, the mass term of the Morison equation will dominate. At larger values of KC, the viscous effects will be more pronounced, and thereby increasing the importance of the drag term. Figure 3.2 illustrates this dependence and is given by Sarpkaya (1976).

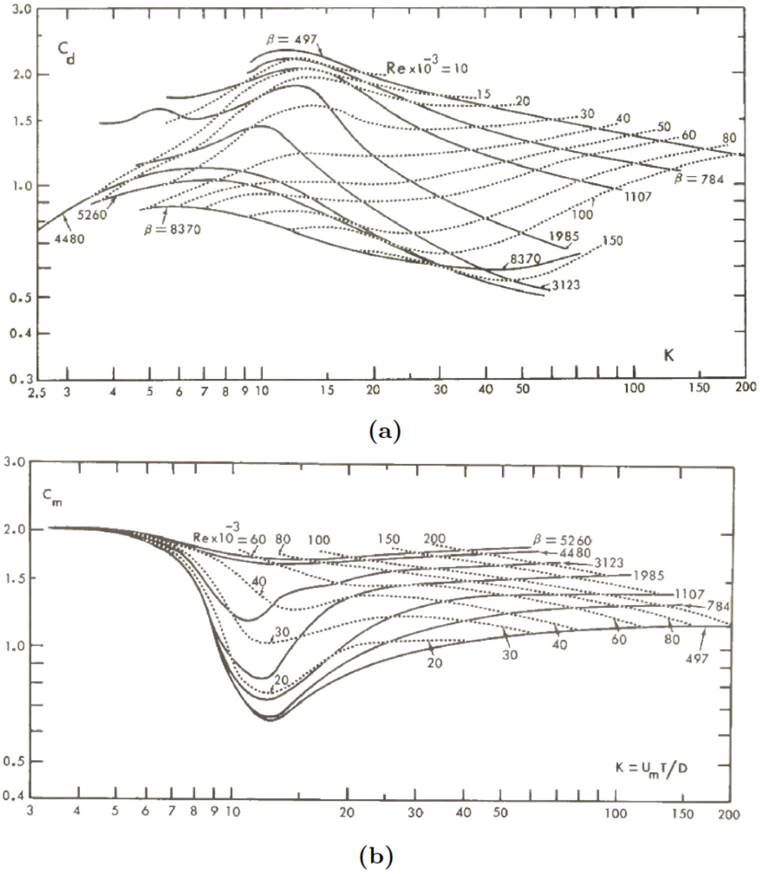

Figure 3.2: Drag (a) and mass (b) coefficients dependence on Re and KC for a smooth circular cylinder, Sarpkaya (1976)

3.2 Wave Theory

There are both linear and non-linear wave theories in use for representing waves numerically. For an area of shallow sea water, the choice of wave theory is important. With shallow waters, the effect of breaking waves will be important, Camp et al. (2003). The breaking of waves will depend on bathymetry of the site as well as the wave condition and water depth. Linear wave models can be used for simplification, however, a non-linear wave model must always be used for extreme wave calculations. Non-linear wave theory includes water surface elevation. The relations between theories are shown in Figure 3.3, provided by Camp et al. (2003).

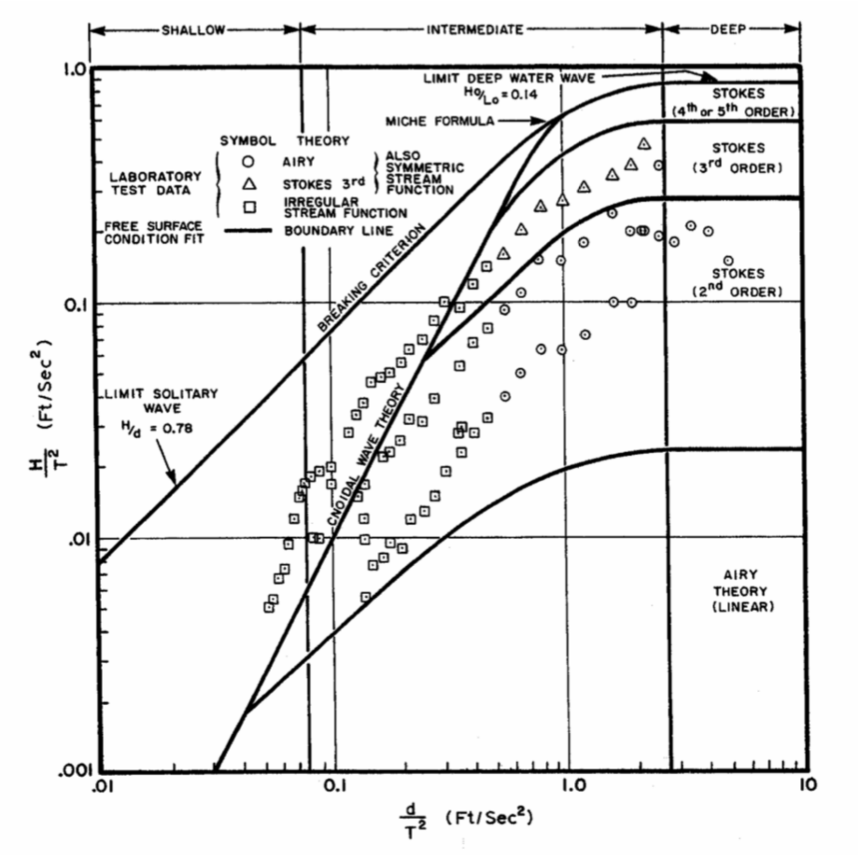

Figure 3.3: Relation between wave theories

Sum frequency loads (mean- and slowly varying loads) are important for marine structures in many contexts. Sum frequency forces are the forces from the difference or the sum of two different frequencies used in the wave spectrum, Faltinsen (1990). In most cases, the higher order forces will be smaller and less significant than the first order forces. However, in some cases, the higher order force frequency may coincide with the natural frequency of the structure, and will then be very important to account for. The response that the sum frequency force cause is often referred to as springing response according to Haver (2017). If a structure experiences transient like higher order force, the corresponding response is often referred to as ringing. If energy is distributed to higher or lower frequencies in the wave spectra, the probability of inducing higher-order forces that coincides with the natural frequency of the structure is bigger. There are different methods available for calculating non-linear forces. DNV-GL has made a list of which wave theories that can be used for representing the kinematics for different conditions. It is as follows:

- Linear wave theory for small-amplitude deep water waves
- Stokes wave theories for high waves
- Stream function theory, based on numerical methods and accurately representing the wave kinematics over a broad range of water depths
- Boussinesq higher-order theory for shallow water waves
- Solitary wave theory for waves in particularly shallow water

There are three specified wave parameters that determine which wave theory to choose. These are the wave height, period and water depth (H, T and d). According to the offshore standard from DNV-GL (2014), these define the three dimensionless parameters that determines the ranges of the different wave theories.

The wave steepness parameter is given by Equation (3.6), the shallow water parameter by Equation (3.7) and the Ursell parameter by Equation (3.8). All equations taken from the offshore standard by DNV-GL (2014).

$$S = 2\pi \frac{H}{gT^2} = \frac{H}{\lambda_0} \tag{3.6}$$

$$\mu = 2\pi \frac{d}{gT^2} = \frac{d}{\lambda_0} \tag{3.7}$$

$$U_r = \frac{H}{k_0^2 d^3} = \frac{1}{4\pi^2} \frac{S}{\mu^3} \tag{3.8}$$

DNV-GL (2014) also give the ranges of the wave theory, as presented in Table 3.1.

Table 3.1: Ranges of application of regular wave theories, taken from DNV-GL (2014)

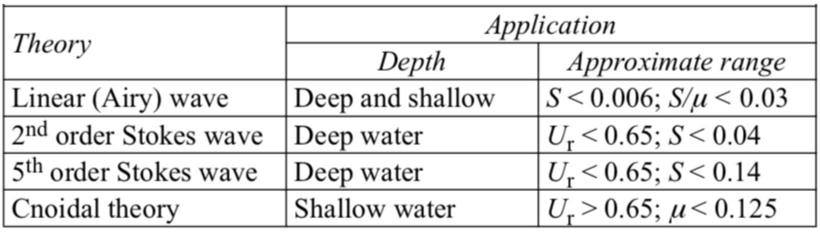

Theory	*Application*	
	Depth	*Approximate range*
Linear (Airy) wave	Deep and shallow	$S < 0.006$; $S/\mu < 0.03$
2nd order Stokes wave	Deep water	$U_r < 0.65$; $S < 0.04$
5th order Stokes wave	Deep water	$U_r < 0.65$; $S < 0.14$
Cnoidal theory	Shallow water	$U_r > 0.65$; $\mu < 0.125$

3.2.1 Cnoidal Wave Theory

Cnoidal wave theory has been developed for quite some time, and a number of various approximations have been suggested. The theory is developed for modelling complicated waves where the velocity variation over the depth is complicated and the waves show complicated behaviour, Fenton (1998). Cnoidal theory was named in 1895 when Korteweg and De Vries (1895) made an equation for propagating waves over a flat bed. This was much like the approximations done by Boussinesq and Rayleigh. However, according to Fenton (1998), *"the solution was named Cnoidal because the surface elevation is proportional to the square of the Jacobian elliptic function cn()"*. Cnoidal waves have long flat troughs and narrow crests. A possible Cnoidal wave is illustrated in Figure 3.4 with a stationary reference frame (x,z) where x is the direction of wave propagation and z is the vertical coordinate with origin on the sea bed. Cnoidal wave theory includes the effects of dispersion and non-linearity. It has therefore been demonstrated that for shallow water areas, the Cnoidal wave theory can provide much better results than linear wave theory, Isobe (1985). The Cnoidal wave theory can be used in different orders. There are proposed solutions - e.g. for 1. st order Cnoidal wave theories (Isobe (1985)) and 3. rd and 5. th order Cnoidal wave theories (Fenton (1998)). The solution of the Cnoidal wave theory is given in terms of elliptic integrals and Jacobian elliptic functions.

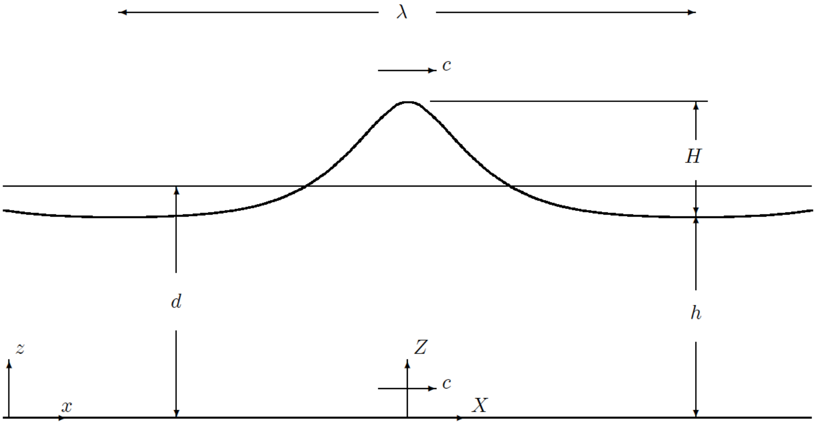

Figure 3.4: Wave train with important dimensions and coordinates, taken from Fenton (1998)

A solution of the first-order Cnoidal wave theory is given by Isobe (1985). Others have also proposed solutions of this order. The difference between them is only in the definitions of the wave celerity and the non-dimensional parameters used. The first-order solution is however independent of these definitions. The water surface elevation, η, the horizontal and vertical particle velocities, u and w, and the pressure, p, are given by Equations (3.9), (3.10), (3.11) and (3.12).

$$\eta = H[cn^2(\theta;k) - \overline{cn^2}] \tag{3.9}$$

$$u = (g/h)^{1/2}\eta \tag{3.10}$$

$$w = (g/h)^{1/2} H \frac{4Kh}{L} \frac{h+z}{h} cn(\theta;k) sn(\theta;k) dn(\theta;k) \tag{3.11}$$

$$p = \rho g(\eta - z) \tag{3.12}$$

The phase is given by θ, as shown in Equation (3.13).

$$\theta = 2K(x/L - t/T) \tag{3.13}$$

x and z are the horizontal and vertical coordinates respectively with origin at the mean water level. Table 3.2 give the meaning of the rest of the variables.

h	Mean water depth
T	Wave period
H	Wave height
t	Time
ρ	Fluid density
g	Gravitational acceleration
K	Complete elliptic integral of the first kind of modulus, k
cn, sn, dn	Jacobian elliptic functions with modulus k

Table 3.2: Overview of Cnoidal wave theory parameters

An overbar represents the average value for one cycle. All equations are taken from Isobe (1985). The average value for one cycle can be given as in Equation (3.14).

$$\overline{cn^2} = \frac{1}{2K} \int_0^{2K} cn^2(\theta;k) d\theta = \frac{E}{k^2 K} - \frac{1-k^2}{k^2} \tag{3.14}$$

Here, E is the complete elliptic integral of the second kind of modulus k. The modulus and the wavelength can be calculated if h, T and H are given by Equations (3.15) and (3.16).

$$U_s = \frac{gHT^2}{h^2} = \frac{16}{3} k^2 K^2 \tag{3.15}$$

$$c = L/T = (gh)^{1/2} \tag{3.16}$$

U_s is the Ursell parameter and c is the wave celerity. The ratio h/L should be less than around 0.2 for Cnoidal theory to be applicable. For calculation of the elliptic integrals numerically along with the elliptic functions, the power series are represented in terms on the nome, q. q is given by Equation (3.17). k and $k' = (1-k)^{0.5}$ are the modulus and complementary modulus respectively.

$$q = exp[-\pi K(k')/K(k)] \tag{3.17}$$

If U_s is bigger than approximately 10, Equation 3.15 gives k^2 bigger than 0.5. This leads to a complementary nome, q', that is smaller or equal to approximately 0.0432. This means that the terms of q' will converge rapidly, Isobe (1985). Once q' is determined, the elliptic integrals and functions can easily be calculated. This also obtains the water surface elevation and the water particle velocities. To express the integral properties in terms of

q' of Cnoidal waves, it is useful to define the two quantities given in Equations (3.18) and 3.19.

$$\lambda = (1-k^2)/k^2 = 16q'(T_{04}/T_{02})^4 \tag{3.18}$$

$$\mu = E/k^2K = [2/(-ln(q'))] - S + (T_{03})^4/(T_{02})^4 \tag{3.19}$$

According to Isobe (1985), it can be shown that the average value for the cycles can be represented as shown in Equations (3.20).

$$\overline{cn^2} = \mu - \lambda \tag{3.20a}$$

$$\overline{cn^4} = \frac{2}{3}(1-\lambda)\mu - \frac{\lambda}{3}(1-2\lambda) \tag{3.20b}$$

$$\overline{cn^6} = \frac{1}{15}(8-7\lambda+8\lambda^2)\mu - \frac{\lambda}{15}(4-3\lambda+8\lambda^2) \tag{3.20c}$$

$$\overline{cn^8} = \frac{8}{105}(6-5\lambda+5\lambda^2-6\lambda^3)\mu - \frac{\lambda}{105}(24-17\lambda+16\lambda^2-48\lambda^3 \tag{3.20d}$$

The standard deviation, σ and the skewness coefficient, β_1 and kurtosis coefficient, β_2, can be found by using the previous equations by inserting them in Equations (3.21).

$$\sigma = H[\overline{cn^4} - \overline{(cn^2)}^2] \tag{3.21a}$$

$$\beta_1 = \frac{\overline{cn^6} - 3\overline{cn^4 cn^2} + 2(\overline{cn^2})^3}{[\overline{cn^4} - (\overline{cn^2})^2]^{3/2}} \tag{3.21b}$$

$$\beta_2 = \frac{\overline{cn^8} - 4\overline{cn^6 cn^2} + 6\overline{cn^4}(\overline{cn^2})^2 - 3(\overline{cn^2})^4}{[\overline{cn^4} - (\overline{cn^2})^2]^2} \tag{3.21c}$$

The crest elevation to the wave height ratio is given by Equation 3.22.

$$\frac{\eta_c}{H} = 1 - \overline{cn^2} \tag{3.22}$$

The first-order Cnoidal solution was according to Isobe (1985) shown to yield better results than small amplitude wave theory for many practical problems. Especially in cases with low-steepness waves. A fairly accurate description of shallow water waves is possible to be obtained by the use of first-order Cnoidal wave theory. A more detailed introduction with examples is given by e.g. Isobe (1985).

3.3 Introduction to Computational Fluid Dynamics

Computational fluid dynamics is commonly referred to as CFD and is the science of finding a solution by using numerical methods to a system of partial differential equations that describes the fluid and the fluid flow, Ransau (2018). There are no analytic methods for solving the equations for viscous flow, and it has therefore been done a lot of work to develop the CFD methods. The following quantities are taken from Ransau (2018) and are necessary in order to describe the fluid phenomena:

- The velocity field: $u = [u(x, y, z, t), v(x, y, z, t), w(x, y, z, t)]^T$
- The pressure field: $p(x, y, z, t)$
- The density distribution: $\rho(x, y, z, t)$
- The temperature distribution: $T(x, y, z, t)$

An overview of the general CFD process is illustrated in Figure 3.5.

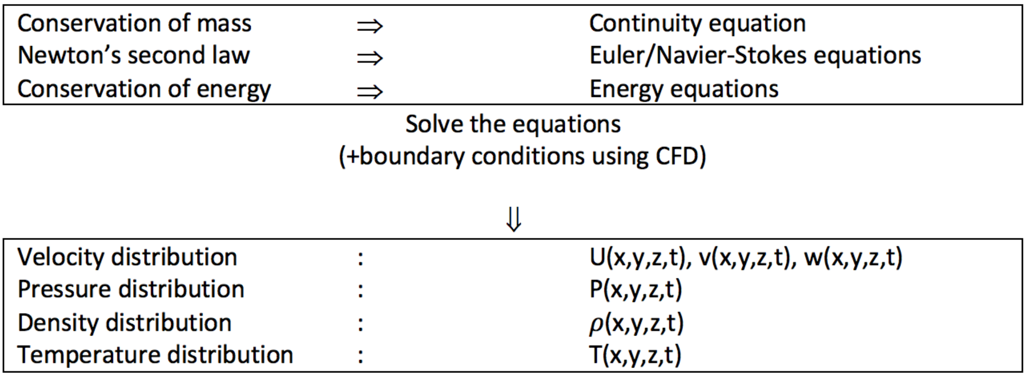

Conservation of mass ⇒ Continuity equation
Newton's second law ⇒ Euler/Navier-Stokes equations
Conservation of energy ⇒ Energy equations

Solve the equations
(+boundary conditions using CFD)

⇓

Velocity distribution : U(x,y,z,t), v(x,y,z,t), w(x,y,z,t)
Pressure distribution : P(x,y,z,t)
Density distribution : ρ(x,y,z,t)
Temperature distribution : T(x,y,z,t)

Figure 3.5: Overview of the general CFD process

When working with CFD analyses it is of extreme importance to be aware- and have knowledge of the possible pitfalls. The method that the solver in use is utilizing can strongly influence the potential errors of the solution. An investigation of the applied boundary conditions, initial conditions and the mesh is needed to ensure a good quality of the analysis. Ransau (2018) give a list of possible errors that may occur and is as follows:

- Round-off errors
- Discretization errors
- Convergence errors
- Modelling errors

Round-off errors can occur by rounding for example parameters as the kinematic viscosity. The discretization error represents the difference between the mathematical model and the exact solution. However, it can also include errors that have occurred because of an approximated geometry. When using an iterative process, convergence errors may occur. This means that if the times-steps are not fine enough or the simulation time is too short, convergence errors can be a problem. For complex situations, it can be difficult to model the problem in a good way by using the equations. This can lead to modelling errors. This may be the case when modelling turbulent flow, multiphase flow, etc. Another possible error can be an unstable CFD method where the Courant number condition is not satisfied. The Courant number will be discussed further in Section 3.3.3. Prior to this discussion it is needed to first present the differential equations of fluid flow that are to be solved.

3.3.1 Equations of Motion

The equations of motion for steady laminar flow of a viscous, incompressible, Newtonian fluid without free-surface effects are the continuity- and the Navier-Stokes equation (Equations (3.23) and (3.24) and are taken from Cengel and Cimbala (2014).

$$\vec{\nabla} \cdot \vec{V} = 0 \tag{3.23}$$

$$(\vec{V} \cdot \vec{\nabla})\vec{V} = -\frac{1}{\rho}\vec{\nabla}P' + \nu\nabla^2\vec{V} \tag{3.24}$$

The continuity equation is a conservation equation, while the Navier-Stokes equation is a transport equation. The transport of the linear momentum throughout the computational domain is represented by this equation. V is the velocity of the fluid, ρ is the density of the fluid and ν is its kinematic viscosity. P' is the modified pressure and can be utilized due to the lack of free surface effects. It also eliminates the gravity term. These equations apply only to incompressible flows which according to Cengel and Cimbala (2014) leads to the assumptions that both ρ and ν are constants. For a three-dimensional flow, there will be four coupled differential equations. These can be solved for the unknowns; u, v, w, and P'. The equations of motion for the case of a steady, incompressible, laminar flow of a Newtonian fluid with constant properties and without free-surface effects are shown in Equations (3.25a)-(3.25d).

$$\frac{\delta u}{\delta x} + \frac{\delta v}{\delta y} + \frac{\delta w}{\delta z} = 0 \tag{3.25a}$$

$$u\frac{\delta u}{\delta x} + v\frac{\delta u}{\delta y} + w\frac{\delta u}{\delta z} = -\frac{1}{\rho}\frac{\delta P'}{\delta x} + v\left(\frac{\delta^2 u}{\delta x^2} + \frac{\delta^2 u}{\delta y^2} + \frac{\delta^2 u}{\delta z^2}\right) \tag{3.25b}$$

$$u\frac{\delta v}{\delta x} + v\frac{\delta v}{\delta y} + w\frac{\delta v}{\delta z} = -\frac{1}{\rho}\frac{\delta P'}{\delta y} + v\left(\frac{\delta^2 v}{\delta x^2} + \frac{\delta^2 v}{\delta y^2} + \frac{\delta^2 v}{\delta z^2}\right) \tag{3.25c}$$

$$u\frac{\delta w}{\delta x} + v\frac{\delta w}{\delta y} + w\frac{\delta w}{\delta z} = -\frac{1}{\rho}\frac{\delta P'}{\delta z} + v\left(\frac{\delta^2 w}{\delta x^2} + \frac{\delta^2 w}{\delta y^2} + \frac{\delta^2 w}{\delta z^2}\right) \tag{3.25d}$$

Equation (3.25a) gives the continuity, (3.25b) the x-momentum, (3.25c) the y-momentum and (3.25d) the z-momentum.

Solution Procedure

In order to solve Equations (3.25a)-(3.25d) numerically, the following steps are necessary:

- Choice of computational domain along with a grid. Cells are created by dividing the domain into many small elements. These elements can either be areas or volumes depending on how many dimensions that are included in the simulation. Each cell is a discretized control volume for which the conservation equations are solved.
- Specification of boundary conditions for each edge (2D flows) or each face of the domain (3D flows).

- Specification of type of fluid and fluid properties.
- Solution algorithms and numerical parameters are selected. These are specific for each CFD code, and the default for each code can be found in the code descriptions.
- Decide initial conditions.
- Equations (3.23) and (3.24) are solved by iteration, and usually in the center of each cell. The aim of the calculation is to have the sum of the terms in Equation (3.24) equal to zero. This sum is further referred to as the residual. The residual should be zero for each cell in the domain. In reality, the residual is never identically zero, but decrease with every iteration. The residual will in this view be the deviation from the exact solution. The average residual for each transport equation is monitored, which determines when the solution converges.
- When a converged solution is obtained, post-processing is possible. Graphical illustrations can be made.
- Forces and moments acting on a body are calculated from the converged solution.

3.3.2 Mesh Quality Factors

The mesh consists of grid cells. Making sure that these cells have high quality is one of the most important stages in a CFD simulation. The quality will affect the rate of convergence and the computational time. The grid cell size and shape must be determined. Other factors that influence the mesh quality can be skewness, smoothness and aspect ratio. The total cell count is investigated in Section 4.3. There are many possible cell types that are possible to use in a CFD simulation. The selection depends on the capabilities of the solver and the problem at hand. According to Bakker (2019), the cell types are divided into 2 classes; 2-dimensional and 3-dimensional. The terminology and the two classes are illustrated in Figure 3.6 and some typical cell shapes are illustrated in Figure 3.7.

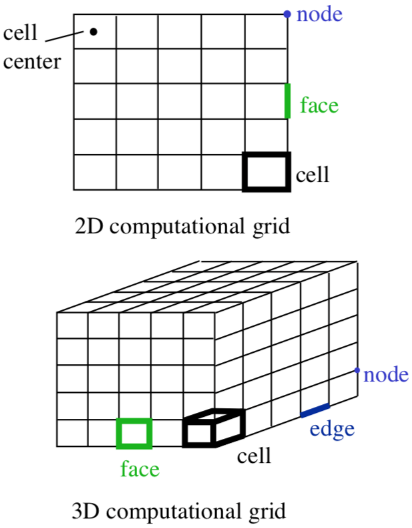

Figure 3.6: 2-dimensional and 3-dimensional computational grid, picture taken from Bakker (2019)

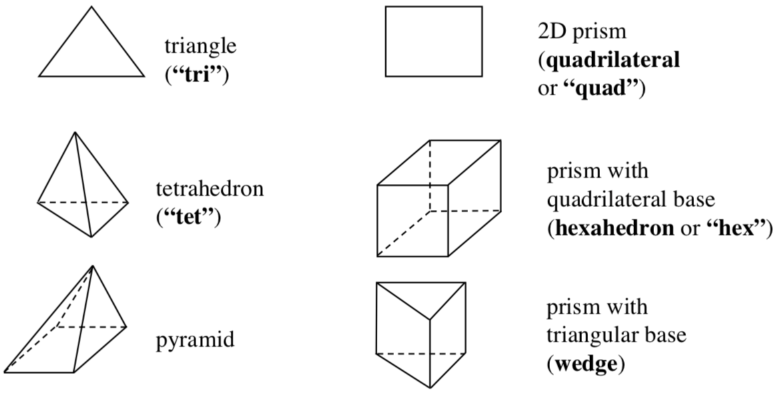

Figure 3.7: Typical cell shapes in 2D and 3D, taken from Bakker (2019)

Skewness: Skewness is the first measure of quality when it comes to grid cell quality. The aim is to have as little skewness as possible. Skewness determines how ideal a face or a cell is. The initial equations are solved be assuming equilateral cells, and highly skewed faces and cells are therefore not acceptable. Bakker (2019) recommend following skewness for different types of cells:

- Hexahedron and quadrilateral cells: Skewness should not exceed 0.85
- Triangle cells: Skewness should not exceed 0.85

- Tetrahedron cells: Skewness should not exceed 0.9

Figure 3.8 illustrates the difference between skewed and ideal shaped cells.

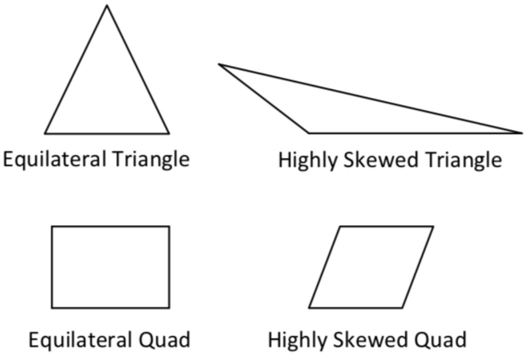

Figure 3.8: Ideal and skewed triangles and quadrilaterals, taken from Asyikin (2012)

Aspect ratio and smoothness: The change in cell size should not be abrupt. This means that nearby cells should have more or less equal size. If the cell size is increasing, it should increase gradually. The aspect ratio is the ratio of the longest edge length to the shortest edge length, Bakker (2019). An aspect ratio of 1 should be the aim of the cells. Bakker (2019) states that adjacent cells should not have a size ratio greater than 20 %. However, for a fully-developed flow quadrilateral or hexagonal cells can be stretched. This is illustrated in Figure 3.9. The aspect ratio and smoothness are illustrated in Figure 3.10.

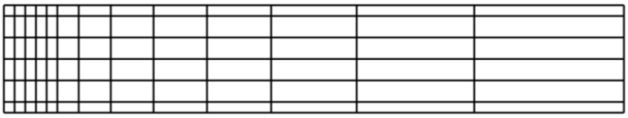

Figure 3.9: Stretched cells, taken from Bakker (2019)

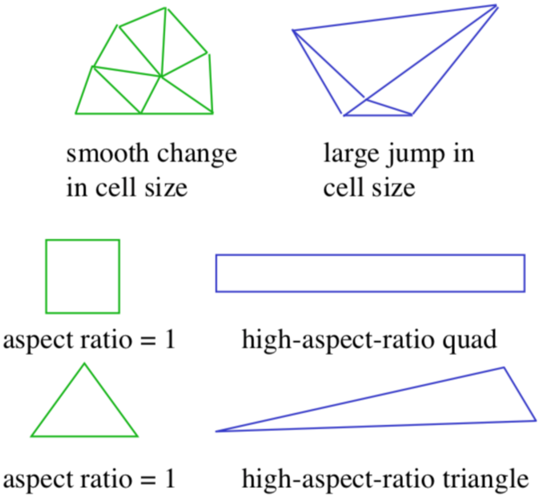

Figure 3.10: Examples of smooth vs large change in cell size and ideal vs high aspect ratio cells, taken from Bakker (2019)

Another important aspect to consider is the grid cell resolution close to the surface. If a non-slip condition is applied for a wall, the cells near the surface should be smaller near the wall region. This is illustrated in Figure 3.11.

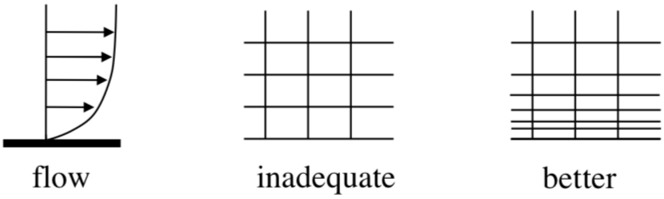

Figure 3.11: Examples of grids near wall regions, taken from Bakker (2019)

3.3.3 Courant Number

In order to describe the Courant Number (CN) it is important to have a basic understanding of how the Navier-Stokes equations can be solved. By using the differential form of the generic conservation equation in Cartesian coordinates, it will be like Equation 3.26.

$$\frac{\delta(\phi\rho)}{\delta t} + \frac{\delta(\rho u_j \phi)}{\delta x_j} = \frac{\delta}{\delta x_j}\left(\Gamma \frac{\delta \phi}{\delta x_j}\right) + q_\phi \tag{3.26}$$

Where q_ϕ is the source or sink of ϕ, ρ the density of the fluid, t is the time. x_j (j=1,2,3) are the Cartesian coordinates and u_j are the Cartesian components of the velocity vector

v. Γ is the diffusivity for the quantity ϕ. The equation can be solved by different methods. For describing the CN, an explicit Euler Method is utilized. For further reference, see Ferziger and Peric (2002). When using this method, all fluxes and sources are evaluated using known values at the time step, t_i. The only unknown at that time step will be the value at that node because the earlier time levels have already been evaluated. The new value can then be calculated for the unknown at each node. The model equation for the Navier-Stokes equation is given by Equation 3.27. This a one-dimensional version with constant velocity, constant fluid properties and no source terms, Ferziger and Peric (2002).

$$\frac{\delta\phi}{\delta t} = -u\frac{\delta\phi}{\delta x} + \frac{\Gamma}{\rho}\frac{\delta^2\phi}{\delta x^2} \tag{3.27}$$

By assuming that the spatial derivatives are approximated using a central difference scheme and uniformity in the grid in x-direction, the new variable ϕ_i^{n+1} is obtained. It is given by Equation 3.28.

$$\phi_i^{n+1} = (1-2d)\phi_i^n + (d-\frac{c}{2})\phi_{i+1}^n + (d+\frac{c}{2})\phi_{i-1}^n \tag{3.28}$$

Here, the new parameters d and c are introduced. These are given by Equations 3.29 and 3.30.

$$d = \frac{\Gamma\Delta t}{\rho(\Delta x)^2} \tag{3.29}$$

$$c = \frac{u\Delta t}{\Delta x} \tag{3.30}$$

Where d is the ratio of time step, Δt, to the characteristic diffusion time $\rho(\Delta x)^2/\Gamma$. c is the ratio of the time step compared to the characteristic convection time:

$$\frac{u}{\Delta x} \tag{3.31}$$

which is the time required for a disturbance to be convected a distance Δx. All equations are taken from Ferziger and Peric (2002). This ratio is the so-called Courant Number and is a key parameter for a successful CFD analysis (for each time the grid size is halved, the time step has to be reduced by a factor of four). If some of the ϕ_i^{n+1} terms are negative, there will be an instability problem. This instability was investigated in the 1920's by Courant and Friedrichs, and they came up with a solution that is still in use today. For convection dominated problems, the coefficient ϕ_i^{n+1} should be allowed to be negative, and the upwind differences should be used instead. The equation will then be changed to Equation (3.32).

$$\phi_i^{n+1} = (1-2d-c)\phi_i^n + d\phi_{i+1}^n + (d+c)\phi_{i-1}^n \tag{3.32}$$

The neighbor coefficient values will now always be positive and can therefore not cause an instability. However, ϕ_i^n can be negative and can create a possible problem. To fix this, and to make the coefficient always positive, the time step condition will be as in Equation (3.33).

$$\Delta t < \frac{1}{\frac{2\Gamma}{\rho(\Delta x)^2} + \frac{u}{\Delta x}} \tag{3.33}$$

This means that the Courant number should be smaller than unity, Ferziger and Peric (2002). The Courant-Friedrichs-Lewy (CFL) number is defined as in Equation (3.34).

$$CFL = \frac{u\Delta t}{\Delta x} \tag{3.34}$$

3.3.4 Boundary Conditions

In order to obtain an accurate CFD solution, it is vital to have correct boundary conditions (BC) in place. There are different types of BC, and their names will vary from one CFD software to another. Figure 3.12 illustrates where BC must be implemented. The figure is made with information from Cengel and Cimbala (2014).

Figure 3.12: Boundary conditions must be applied at all boundaries of a domain. Illustration taken from Cengel and Cimbala (2014)

Some of the available BC will here be presented in more detail. The easiest BC is the wall. As Cengel and Cimbala (2014) states; For this condition, *"the normal component of the fluid velocity is set to zero relative to the wall along a face on which the wall BC is prescribed"*. This is done to simulate the fact that fluid cannot pass through a wall. Often, this condition includes a no-slip condition as well. This means that the tangential velocity at the wall is zero as well. For a turbulence simulation, other factors such as wall roughness and wall functions may need to be specified as well. Other wall options are available as well in most CFD codes. Such options can be to have a slip condition or to have moving walls. The next BC to be discussed are the outflow and inflow conditions. These can generally be categorized as either velocity-specified conditions or pressure-specified conditions, Cengel and Cimbala (2014). For a velocity-specified condition, the velocity of the incoming flow along the inlet face or plane is decided. For a pressure inlet, the pressure along the inlet face or plane is decided. This is done in the same manner for the outlet. If the pressure is defined, the velocity cannot be defined as well since these two are coupled quantities. For a converging CFD solution, the velocity will be adjusted such that the defined pressure conditions are satisfied. Other BC that are commonly in use are the symmetry conditions, periodic conditions such as rotational conditions and periodic boundary conditions.

3.3.5 Turbulence Modelling

To model turbulence can be a challenge in the numerical world. According to Blazek (2001), high Reynolds numbers cannot be simulated by doing a direct numerical simulation (DNS) by using the time dependent Navier-Stokes equations. Other approximations are therefore being developed for the simulation of turbulent cases. The first option is to use a Large-Eddy Simulation (LES) approach. The idea behind LES is to “resolve only the large eddies accurately and to approximate the effects of the small scales by relatively simple sub-grid scale models”, Blazek (2001). LES is very computationally demanding and it is therefore taking time to developing this into a fully engineering tool. LES is however well suited for performing detailed studies of complex flow.

Another option is to use a Reynolds-Averaged Navier-Stokes equation (RANS) approach. This method is based on decomposition of the flow variables into mean parts, and then to do time or ensemble averaging, Blazek (2001). The advantage when using RANS in comparison to LES is that it is possible to use a much coarser grid, and the computational time will therefore decrease as well. A stationary mean solution can also be assumed, which also reduces the computational effort. This makes RANS more popular in the field of engineering. However, it is not possible to obtain detailed information about turbulent structures from RANS.

Other options are also available for turbulence modelling. Some of these are combinations and/or developments of earlier models. This can be for example the Reynolds-Stress Transport (RST) model and the Algebraic Reynolds-Stress (ARS) model.

When using a RANS approximation, different models can be used. Two of these will be further discussed in the next Sections. This is the k-ϵ and the k-ω model.

The $k-\epsilon$ Model

The $k-\epsilon$ turbulence model is according to Blazek (2001) based on the solution of equations for the turbulent kinetic energy and the dissipation rate. It is a two-equation model that utilizes two transport equations. One equation is for the turbulent kinetic energy, k, and the other one is for the rate of dissipation of turbulent kinetic energy, ϵ, Tawekal (2015). This model demand use of damping functions in order to be valid for the viscous layer to the wall. The damping functions aim to assure proper behaviour of the values for k and ϵ. This is described by Equations (3.35) and (3.36) which are taken from Blazek (2001).

$$k \sim y^2 \tag{3.35}$$

$$\frac{\epsilon}{k} \sim \frac{2\nu}{y^2} \tag{3.36}$$

Here y represents the coordinate normal to the wall.

The advantages and disadvantages can according to Versteeg and Malalasekera (2007) be listed as follows: **Advantages:**

- The simplest of the turbulence models since only initial and/or boundary conditions need to be defined
- Well established, the most widely validated turbulence model
- Very good performance for many industrially relevant flows

Disadvantages:

- Can be computationally demanding in comparison to other simpler turbulence models
- Does not work well with unconfined flows, flows with extra strains (for example curved boundary layers), rotating flows and flows of normal Reynolds stresses that are driven by anisotropy (for example fully developed flows in ducts with other than circular geometries)

Wall functions: As previously stated, it is necessary with a very fine grid at walls. According to Blazek (2001), the standard condition for models at low Reynolds numbers is that the first node is located at a distance of $y^+ \leq 1$ from the wall. For higher Reynolds numbers, other values are accepted in some cases in order to save computational time. Coarser grids with $10 \leq y^+ \leq 100$ are then sometimes applied, Blazek (2001). In this case, the model is applied without use of the damping functions. For such a high Reynolds number turbulence model, the distance between the first node and the wall has to be connected by wall functions. These functions give the values of K and ϵ at the first node adjacent to the wall. The turbulence equations will then not be solved at the wall or at the first nodes around the wall. More detailed information about wall functions is given in for example Blazek (2001).

The SST $k-\omega$ Model

The $k-\omega$ model achieves, according to Blazek (2001), higher numerical stability than the $k-\epsilon$ model because it does not need a damping function. The $k-\epsilon$ model has according to Versteeg and Malalasekera (2007) not been satisfactory for good wall performance for boundary layers with varying pressure gradients. They therefore state that the use of a hybrid model would be better. The suggested hybrid model would enable:

- A transformation of the $k-\epsilon$ model into a $k-\omega$ model in the near-wall region
- Use of the standard $k-\epsilon$ model far from the wall in the fully turbulent region

This is why the SST model has become this popular; It combines the best parts of two different models and use them together. The transport equation for k and ω for turbulent flows at high Reynolds numbers is given by Equation (3.37) and is taken from Versteeg and Malalasekera (2007).

$$\frac{\partial(\rho k)}{\partial t} + div(\rho k U) = div\left[\left(\mu + \frac{\mu_t}{\sigma_k}\right) grad(k)\right] + P_k - \beta \rho k \omega \tag{3.37}$$

Here, U is the fluid velocity, and P_k is given by Equation (3.38).

$$P_k = \left(2\mu_t S_{ij} \cdot S_{ij} - \frac{2}{3}\rho k \frac{\partial U_i}{\partial x_j}\delta_{ij}\right) \tag{3.38}$$

Here, S_{ij} is the components of rate of deformation in i- and j directions. The eddy viscosity, μ_t, is defined as: $\mu = \rho C_\mu \frac{k^2}{\epsilon}$, where C_μ is a dimensionless constant. σ_k is an adjustable constant, in many cases fitted to be equal to 1 for a wide range of turbulent flows. β is another constant.

Transformin the ϵ-equation into the k-ω SST model is done by the substitution in Equation (3.39).

$$\epsilon = k \cdot \omega \tag{3.39}$$

According to Versteeg and Malalasekera (2007), the transport equation for the model is as shown in Equation (3.40).

$$\begin{aligned} \frac{\partial(\rho\omega)}{\partial t} + div(\rho\omega U) = div\left[\left(\mu + \frac{\mu_t}{\sigma_{\omega,1}}\right) grad(\omega)\right] \\ +\gamma_2\left(2\rho S_{ij} \cdot S_{ij} - \frac{2}{3}\rho\omega\frac{\partial U_i}{\partial x_j}\delta_{ij}\right) - \beta_2\rho\omega^2 + 2\frac{\rho\partial k\partial\omega}{\sigma_{\omega,2}\omega\partial x_k\partial x_k} \end{aligned} \tag{3.40}$$

In a simpler form, this can according to Versteeg and Malalasekera (2007) be expressed as:

Rate of change of k or ω +	Transport of k or ω by convection =	Transport of k or ω by turbulent diffusion +	Rate of production of k or ω -	Rate of dissipation of k or ω +	Cross diffusion term which arises during the $\epsilon = k \cdot \omega$ transformation

Chapter 4

CFD Solver and Initial Set-Up

OpenFOAM (OF) is an open-source software available online. It is a Linux based software and it has a number of various solvers that can be applied to a variety of complex fluid flow problems such as heat transfer, chemical reactions and laminar and turbulent flow. The software does not have a graphical user-interface, but a plugin called ParaFOAM can visualize the data and the results. Post-processing can be done in paraView that can visualize the results. The relevant solvers for this task will be:

- **pisoFoam:** Transient solver for incompressible, turbulent flow
- **pimpleFoam:** Transient solver for incompressible, turbulent flow of Newtonian fluids on a moving mesh
- **interFoam:** Solver for two isothermal, incompressible and immiscible fluids using a volume of fluid phase-fraction based interface capturing approach. The solver Includes optional mesh motion and mesh topology changes along with adaptive remeshing

The solver pisoFoam is used for simulating the laminar conditions, while pimpleFoam is more practical to use during turbulent conditions as the Courant number (and time steps) can be adjusted during the simulation. The interFoam solver is used for the cases including waves.

OF contains many solvers, utilities and libraries that can be developed and altered after the user's wishes. Every case consists of a case folder with at least three sub-directories. This is illustrated in Figure 4.1. In the system folder, the mesh- and the control file are included. The control file, "controlDict", determines factors such as time step, run time and which output parameters that shall be written. The scheme specifications are included in the scheme file, "fvSchemes", that configures the discretization scheme. The solver specifications are included in the solution file, "fvSolution", which determines which solver to use. The constant folder contains a number of properties that needs to be decided by the user. This can be for example files for the pressure, velocity and turbulence properties. It also contains a "polyMesh" folder that contains the property of the pre-processing result.

The time directories are folders that contain results for each time step. After a simulation is done, there will be one folder for each time step that is defined in the controlDict. Before initializing a simulation, a folder named "0" must be included to set the initial conditions.

4.1 Mesh Generation

There are many opportunities for mesh generation in OF. It is also possible to make the mesh in another program with a graphic user-interface and to import this into OF. The opportunities that are built-in are the "blockMesh" and "snappyhex" plugins. The dictionary file named "blockMeshDict" is located in the system folder. The file contains a number of points, edges, blocks and patches. This is further described in Section 4.3. The terminal will read the directory by use of the command "blockMesh". This command will read the dictionary, generate the mesh, establish points, faces, cells and boundaries. According to CFD-Direct (2019a), the principle behind blockMesh is "to decompose the domain geometry into a set of 1 or more three dimensional, hexahedral blocks". Each block is defined by eight vertices, one for each corner. Each block has a local coordinate system that is right handed (x_1, x_2, x_3). An example block is illustrated in Figure 4.2.

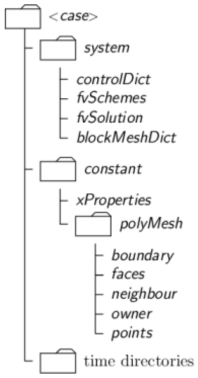

Figure 4.1: OF case directories

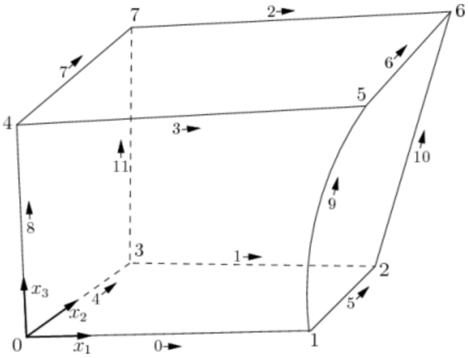

Figure 4.2: A single block, picture taken from CFD-Direct (2019a)

After making the desired geometry by combining blocks, different patches are made along with boundary conditions in the blockMesh file. This is described in further detail by CFD-Direct (2019a).

4.2 Boundary Conditions

The boundary conditions for the initial cases are given below. These cases will be the initial studies for verification of the set-up and the parameters in use. These cases are done with laminar water flow and steady current.

The boundary conditions are defined for the areas as listed below. For the pressure:

- Right - fixedValue
- Up/Down - Symmetry
- Left - zeroGradient
- Cylinder - zeroGradient

For the current velocity:

- Right - zeroGradient
- Up/Down - Symmetry
- Left - uniformFixedValue
- Cylinder - noSlip

The fixedValue boundary condition (BC) supplies a fixed value constraint, the zeroGradient BC applies a zero-gradient condition from the patch internal field onto the patch faces, the noSLip fixes the velocity to zero at walls, and uniformFixedValue provides a uniform fixed value condition. All condition definitions taken from OpenFOAM (2018).

4.3 Mesh Study

In order to get an accurate and efficient mesh that provides good results, it is necessary to conduct a mesh study. The mesh is made by the built-in blockMesh utility in OF. The program automatically solve the problem in three dimensions. However, for the first studies, a two-dimensional mesh is used by setting its thickness to a small number. The nodes and blocks are defined as shown in Figure 4.3. The backside of the mesh is equal to the front. The commands arc and patch are used for making the arcs and defining the boundaries. The mesh is mirrored by using the mirrorMesh utility in OF. By utilizing the m4 utility in OF, it is possible to easily change the points, blocks, arcs and cells.

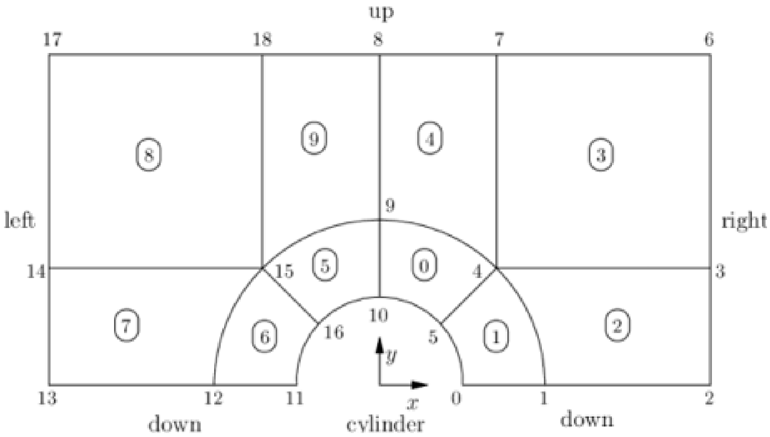

Figure 4.3: Mesh Illustration

The blockMesh file is included in the “system” folder. Also included in this folder, is the controlDict and the mirrorMeshDict. In the controlDict, the simulation time, time step and interval for writing results are included. It also includes given functions for writing results. These files can also be found in Appendix A. The case folder also includes a “0” folder with the velocity and pressure definitions, and a “constant” folder with polyMesh definition and transport and turbulence properties.

The first mesh is shown in Figure 4.4. This mesh has smallest cells close to the cylinder. The cell size is increasing with increasing distance from the cylinder. At the edge of the domain, the cells are really big. The total number of cells is 26218. The mesh is graded by use of the function "simplegrading" in the blockMesh utility.

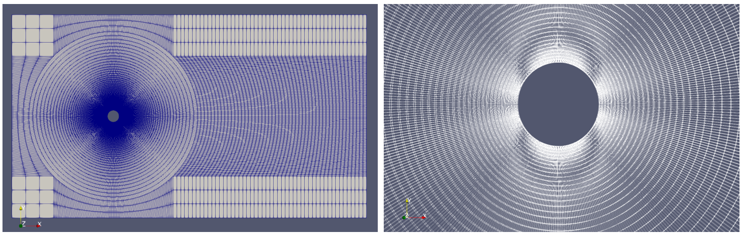

Figure 4.4: Illustration of mesh 1 with 26218 cells

The results from the simulation with mesh 1 is first investigated visually by use of the software ParaView. This has a graphic user interface that makes post-processing easier. The flow around the cylinder is illustrated in Figure 4.5. The illustrations show laminar vortex shedding.

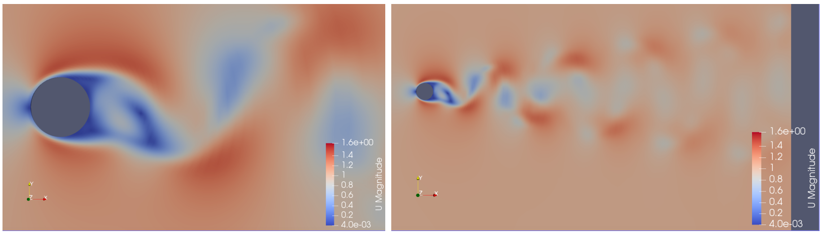

Figure 4.5: Illustration of fluid flow around the cylinder at steady state condition with a flow velocity of U=1 m/s

The second mesh is made in a similar way to the first one. The difference is the grid cell size. In this mesh, the number of cells is doubled in each direction and in each block, resulting in a total number of cells of 104872. This dramatic increase is done in order to test if the results will remain the same. The mesh and a mesh detail is shown in Figure 4.6.

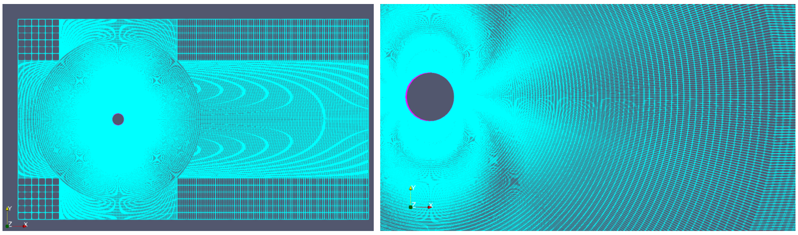

Figure 4.6: Illustration of mesh 2 with 104872 cells

The third mesh is also made in the same way as the two previous ones. The number of cells is doubled in each direction and in each block in comparison to the second mesh, resulting in a total number of cells of 419488. It is difficult to illustrate such a big number of cells since all the cell edges will cover the whole illustration. A domain illustration is given in Figure 4.7.

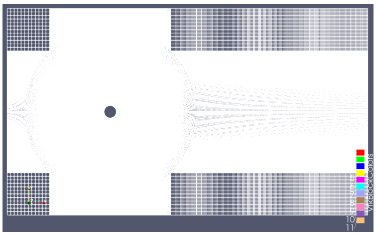

Figure 4.7: Third mesh with 419488 cells

It is important to keep track of the number of cells and to do a mesh study in order to get accurate results. The aim of the mesh study is to obtain equal results with two meshes where the first mesh has half as many cells in each direction as the second one.

4.3.1 Cell Size Study Results

Figures 4.8 and 4.9 show force coefficients from the three simulations with increasing number of cells. The CFL number is the same for all three simulations. It is visible that the third simulation with mesh 3 was run for approximately 800 time-steps. This is because such a fine grid requires a significant increase in computational time. It is also visible that the difference in the results between mesh 2 and mesh 3 are small. The mean C_D values and the C_L values are shown in Table 4.1.

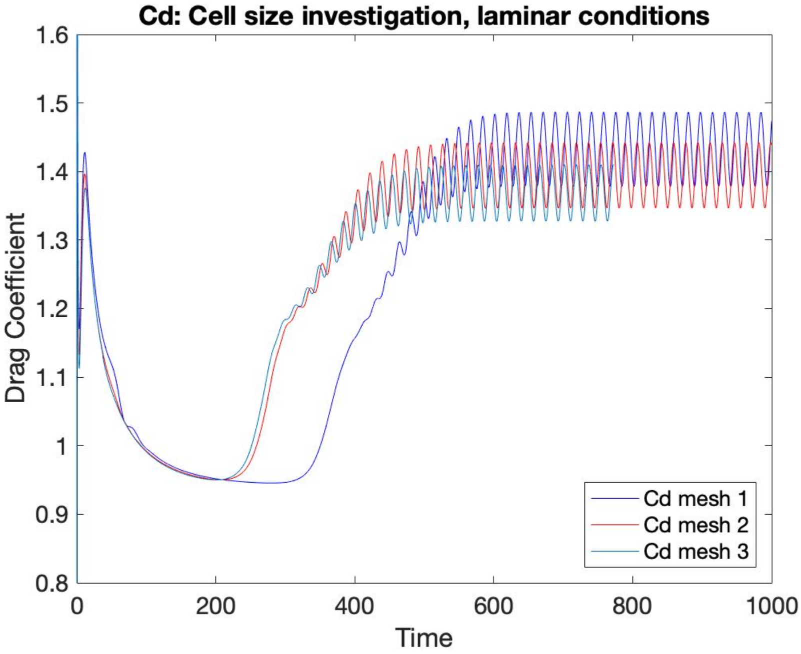

Figure 4.8: C_D values from simulations with decreasing cell size. Mesh 1 with coarsest grid.

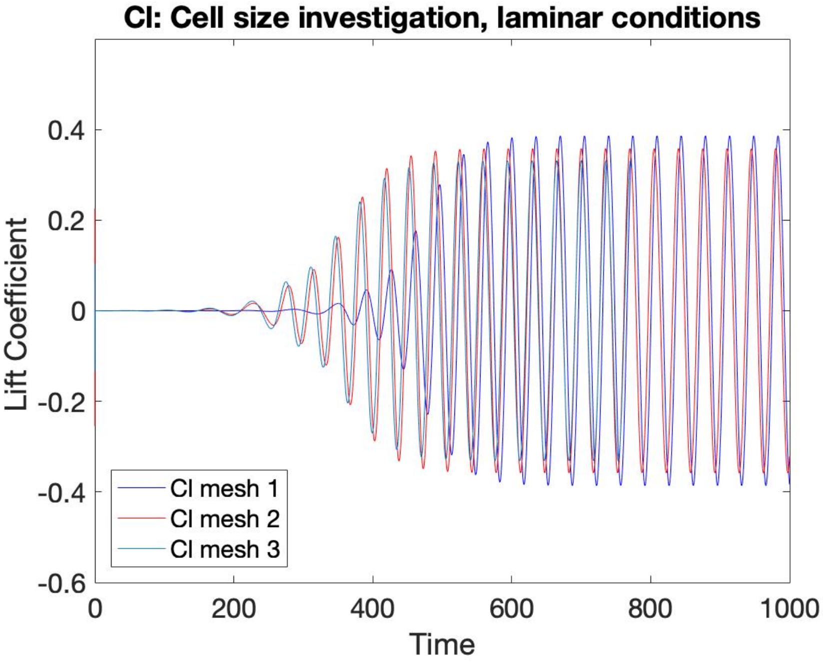

Figure 4.9: C_L values from simulations with decreasing cell size. Mesh 1 with coarsest grid.

Table 4.1: Cell size study results - C_D and C_L values

Mesh nr	Total nr of cells	Mean C_D	C_L	Decrease in mean C_D [%]
1	26218	1.433	± 0.385	
2	104872	1.395	± 0.358	-2.7
3	419488	1.369	± 0.331	-1.8

Because of the computational demand of mesh 3, this one is disregarded. Mesh 2 provides almost as accurate results and is therefore chosen for further studies. It also results in a significant decrease in computational time which is important for further simulations. Even though the results are not perfect since the results vary with decreasing grid cell size, the mesh will still be improved by investigating the domain size. The results will also possibly be improved by testing different time steps. This will be done in the following sections.

4.4 Domain size study

The aim of this study is to have no influence from the surroundings of the cylinder. If there is no influence, the results from different domain sizes are equal. This study is done in order to test how small the domain can be, but still obtain accurate results. The starting point is to have a domain size of 10 times the diameter in front of the cylinder, and 25 times the diameter in the back of the cylinder. Figure 4.10 illustrates the domain where D is the diameter of the cross-section area of the cylinder and a is a variable. It is the necessary size of a that is the wanted output from this study.

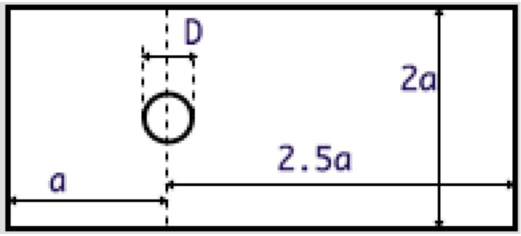

Figure 4.10: Domain Illustration and a more detailed view of the mesh

Four different domains are investigated first. The investigation is conducted with Mesh number 2 (described in Table 4.1). The domain sizes along with the results from the study are given in Table 4.2. Here a, is the domain size parameter as illustrated in Figure 4.10.

Table 4.2: Domain size study results

Domain nr	a	Mean Cd	Cl	Decrease in mean C_D [%]
1	70	1.36	±0.27	-
2	140	1.33	± 0.26	-2.2
3	280	1.30	± 0.27	-2.3
4	560	1.25	± 0.18	-3.8

The C_D and C_L values are illustrated in Figures 4.11 and 4.12. The graphs clearly show that the domain size affects the result. The smallest domain give the highest C_D and C_L -values while the largest domain gives the smallest values. The results from the studies with domain sizes 2 and 3 are quite similar. It was expected to see more of a convergence to the same results with domain sizes 3 and 4. However, it is only the domain size that is increased. It is therefore discovered that the cell size in the domain also has increased. This is not the intention of this study, as the "golden rule" is to have all other parameters unchanged while changing one of the other. Because of the definitions made in the blockMeshDict, the domain- and grid-cell sizes are closely connected. Doubling the number of cells in each direction, when doubling the parameter a, may be a better approximation as the grid cell size will almost remain constant. However, by doubling domain and number of cells for domains 2-4, the simulation is very computationally demanding and requires a smaller time step in order to run. This is because of the CFL number. Since the results in Table 4.2 show values close to the reference values in Section 4.6, it is decided to more closely investigate domain sizes between $a = 70$ and $a = 140$.

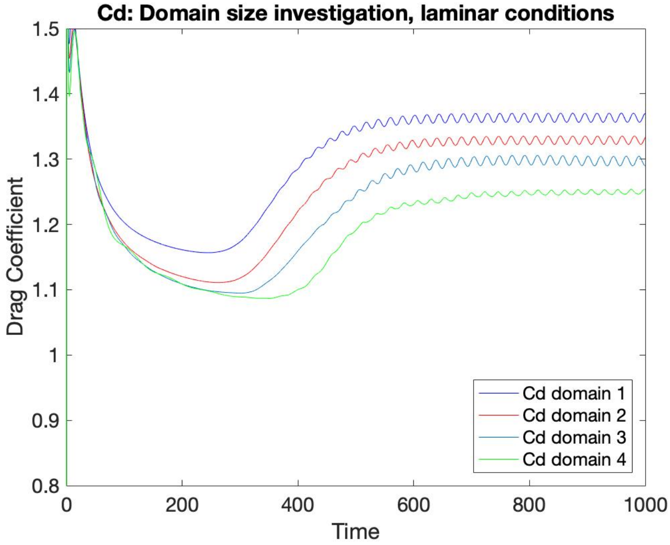

Figure 4.11: C_D results from simulations with four different domain sizes

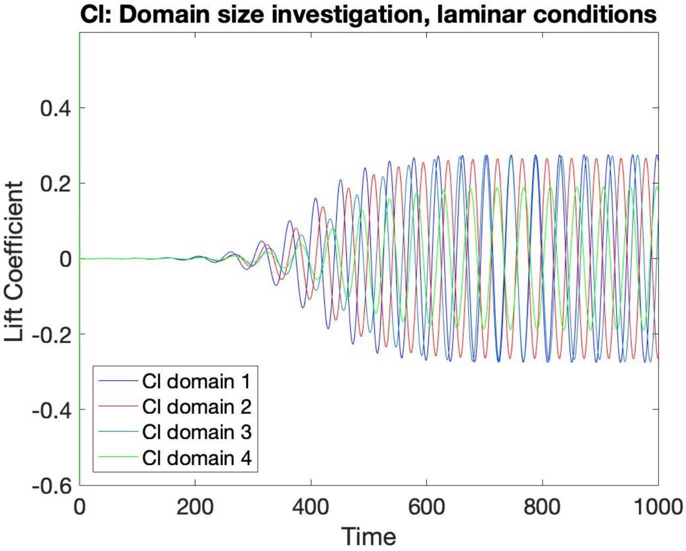

Figure 4.12: C_L results from simulations with four different domain sizes

The domains investigated are given in Table 4.3 along with the results from the simulations. It is still Mesh number 2 that is being used, and the domains increase with factors 1.2 and 1.4. The number of cells in each direction has also been increased with the same factors in order to try to keep the grid cell size unchanged.

Table 4.3: Domain size study results - second try

Domain nr	a	Mean C_D	C_L	Decrease in mean C_D [%]
1	70	1.36	±0.27	-
2	84	1.33	±0.24	-2.2
3	98	1.31	±0.20	-1.5

The C_D and C_L values are illustrated in Figures 4.13 and 4.14.

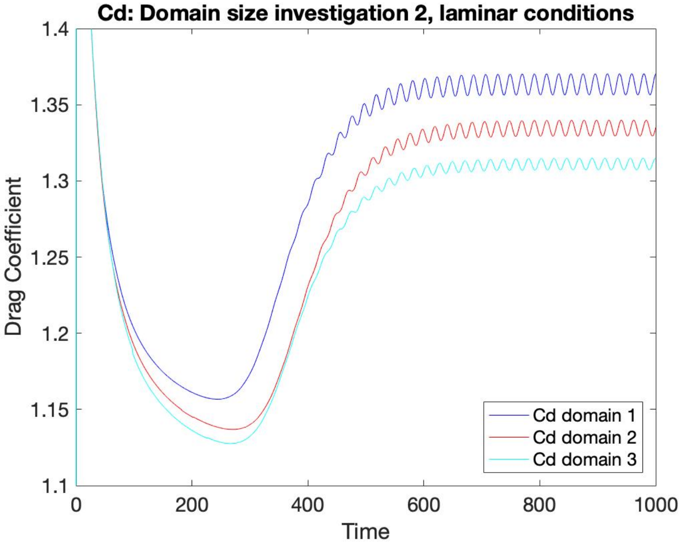

Figure 4.13: C_D results from simulations with three different domain sizes

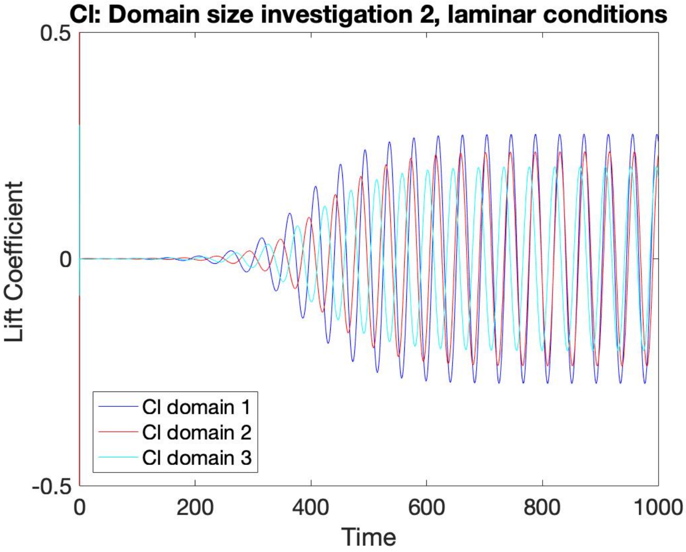

Figure 4.14: C_L results from simulations with three different domain sizes

It is clear that the results with different domains still does not converge properly. However, it is clear that the grid cell size is not sufficiently constant, and this means that the results will not be accurate. Table 4.3 show that the decrease in mean C_D -values results in less decrease between domain sizes number two and three in comparison to domain sizes one and two. It is likely that for a complete equal grid cell size, this difference between the two last domains would have been even smaller. Based on these two domain size tests, it is decided to go forward with a domain size with $a = 140$. This way, the chance of the boundaries influencing the pressure on the cylinder is very little, and the computational time is not very much increased. This is therefore considered to be a good choice for this study. The last parameter to be investigated in order to increase the simulation and its results, is the time step. This is investigated in the next section.

4.5 Time Step Study

In this study, different time steps are investigated. The other variables are held constant in order to test the sensitivity of the time steps. The chosen grid cell size will be that of mesh number 2 and the domain size will be that of domain with $a = 140$. The first time step is quite big and the simulation will therefore fail due to high Courant numbers. The last time step is very small. This makes the computational time very large, and the simulation is stopped due to large consumption time. This is visible in the illustrative graphs in Figures 4.15 and 4.16. The results from the two intermediate time steps are shown in Table 4.4.

Table 4.4: Time step, Δt, study results - C_D and C_L values

Δt	Mean C_D	C_L	Decrease in mean C_D [%]
0.1	Simulation fail	-	-
0.01	1.34	± 0.31	-
0.005	1.35	± 0.33	+0.74
0.0001	-	-	-

It is clear from the results that the force coefficients are almost identical from the results with time steps equal to 0.01 and 0.005. This means that the improvement in results in comparison to the increase in computational time is minimal from the first time step to the other. Hence, the selected time step is 0.01. This is considered to be the most relevant one, and is used for further comparison in Section 4.6 with reference values taken from previous studies.

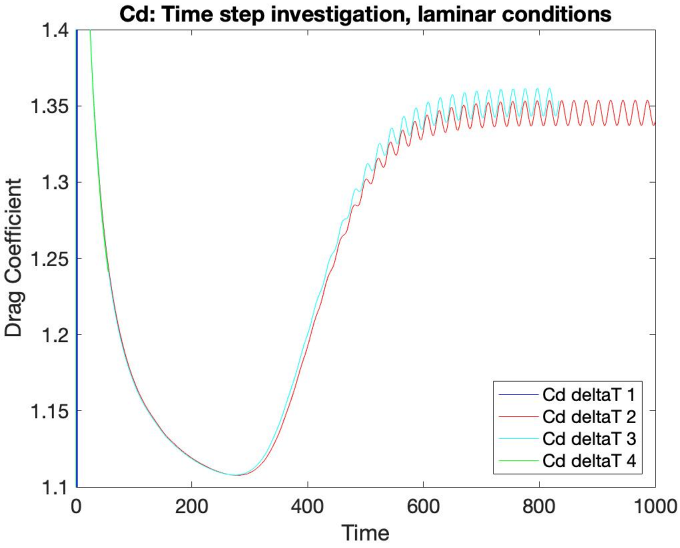

Figure 4.15: C_D results from simulations with four different time steps

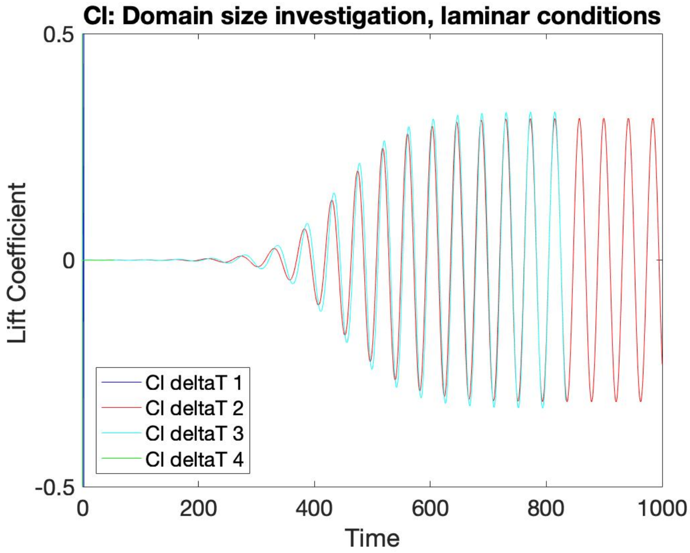

Figure 4.16: C_L results from simulations with four different time steps

4.6 Final Mesh and Verification

Based on the studies where sensitivities connected to grid size, domain size and time steps are investigated, the final mesh is chosen to be mesh number 2 with a domain size $a = 140$ and with a time step of 0.01. This choice is based on the quality of the results in combination with computational time. In order to verify the model, the results are compared to previously done studies. There have been conducted a number of studies of a circular cylinder in steady flow with Reynolds number equal to 100. Some of them are listed in Table 4.5. It is clear that the C_d values vary between 1.34 and 1.39. This can be due to grid variations, boundary conditions, etc. They are however, closely related to each other, which means that this case with a circular cylinder in laminar flow is widely verified.

Table 4.5: Reference Values for C_D and C_L for a steady current condition with Re=100

Reference	C_D	C_L
Russell and Wang (2003)	1.380 ±0.007	±0.300
Calhoun and Wang (2002)	1.350 ± 0.014	± 0.300
Braza et al. (1986)	1.386 ± 0.015	± 0.250
Choi et al. (2007)	1.340 ± 0.011	± 0.315
Lui et al. (1998)	1.350 ± 0.012	± 0.339
Guerrero (2009)	1.380 ± 0.012	± 0.333

The results obtained with the final mesh are listed in Table 4.6.

Table 4.6: Results from simulation with mesh number 2, domain size a=140 and time step=0.01

Mean C_D	C_L
1.34 ± 0.01	± 0.31

It is clear that the results obtained from this simulation are in very good coherence with the reference values. This study has been extremely important to conduct in order to test mesh sensitivities and to verify the set-up. With many variables and many possible error sources it is important to know that the basis for further work and more advanced simulations is correct. In the previous project work, the results that were obtained had some weaknesses. It was discovered during this sensitivity study that there were several minor mistakes and improvement possibilities in the previous set-up. The major learning outcomes from the evaluation are the following:

- **Cell grading:** Works well to implement a cell grading that makes the grid cells closest to the cylinder smaller than the cells far away from the cylinder. This improves the quality of the results as well as diminishes the computational time because the total number of cells will decrease in comparison to making every cell throughout the domain smaller.
- **Calculation of force coefficients:** The force coefficients are calculated by the use of a function in the controlDict. It was discovered that there were minor mistakes in this function. These are now corrected, and the coefficients are calculated more accurately.
- **Mesh transitions:** It is important to get a good transition between the different blocks in the mesh. Before the mesh got improved, it was possible to see the transition between the circular and square blocks inside the mesh. This is now corrected for, and the transitions are smooth throughout the mesh.
- **Domain size:** Domain size needs to be big enough to not interfere with the pressure around the cylinder
- **Time step:** The time step needs to be small enough for having a low CFL number. At the same time, it is too time consuming to have a very small time step.

The final mesh is illustrated in Figure 4.17. The ratio between the inner cells close to the cylinder and the cells at the outer circle is 1/10. In comparison to the original mesh, the main improving differences are in the grading of the grid cells and the domain size. There are also fewer cells further away from the cylinder in comparison to the previous set-up. This is due to the cell grading, but also because of refinements done manually.

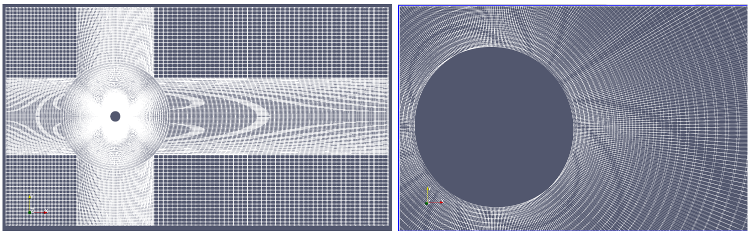

Figure 4.17: Mesh illustration - final mesh

4.7 Post-Processing

When running simulations it is also extremely important to measure desired output. This output can be different variables and can be measured at different places in the domain. The desired output variables can be force coefficients, pressure, velocity, y+ values and velocity. They can be sampled in result files. It is practical to measure these quantities in several points. This way, it is possible to extract vortex shedding frequency and do a frequency response analysis. The measurements are done by using a utility called probes. The probes are defined by points in the domain and can measure desired quantities in that point. Several probes will be located in parallel and forms a straight line in y=0. This is shown in Figure 4.18. The location and number of probes along with desired output can easily be modified in the controlDict by use of the probes function (included in Appendix A). This function is also used for measuring velocities in the vertical direction at a later stage for the simulations including waves. This is discussed further in Chapter 5.

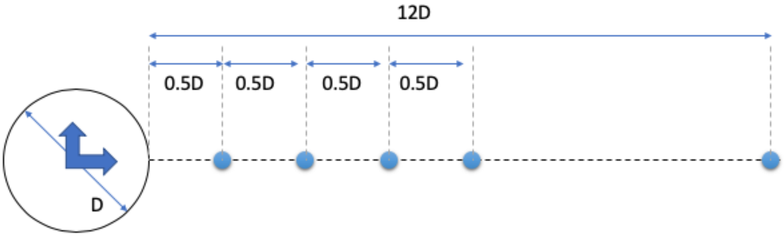

Figure 4.18: Location of the first 4 probes and the last 12th. probe

The force coefficients, C_D and C_L, are written directly by using another function in the controlDict. The visualizations of the simulations are done using the paraView utility.

Chapter 5

Wave Modelling - Waves2FOAM

To model the waves for the CFD simulations, the additional OpenFOAM package waves2FOAM is used. Waves2Foam was released as a toolbox for the generation and absorption of free surface waves, Jacobsen (2017). Extensions for the toolbox has also been developed in order to be able to model the interaction between free-surface waves and a permeable medium such as scour protection or breakwaters. The package is based on the interFoam and interDyMFoam solvers that are provided in OpenFOAM. Waves2Foam offers a good variation of wave theories that can be implemented into an OpenFOAM simulation. The manual by Jacobsen (2017) gives an introduction to how these theories are implemented. Code Fragment 4.6 defined in OpenFOAM describe the settings for Cnoidal theory, and is illustrated in Figure 5.1. It is clear from the code fragment that the necessary input is the wave height, water depth, wave period, wave directions and a ramp time (Tsoft). This ramping time should be at least one wave period. However, it is recommended to have a ramp period of at least two times the wave period.

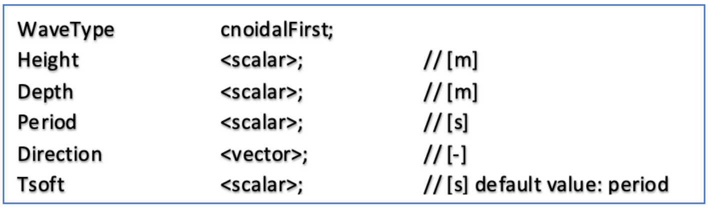

```
WaveType        cnoidalFirst;
Height          <scalar>;         // [m]
Depth           <scalar>;         // [m]
Period          <scalar>;         // [s]
Direction       <vector>;         // [-]
Tsoft           <scalar>;         // [s] default value: period
```

Figure 5.1: Code Fragment 4.6: First Order Cnoidal Theory

As discussed previously, the key parameter for Cnoidal wave theory is the parameter m. The utility setWaveParameters will therefore automatically increase the precision of m to 14 digits to ensure that the parameter is written to waveProperties as a value smaller than 1, Jacobsen (2017). A first-order Cnoidal wave theory is found in waves2Foam. It is implemented in the package after the mathematical descriptions of Svendsen and Jonsson (1976).

5.1 Volume of Fluid Method for Multiphase Flow (VOF)

In order to approximate free boundaries in finite-difference numerical simulations, there are several methods in use. One of these is the VOF method which is a simple and powerful one that is based on the concept of having a fractional volume of fluid (VOF). The VOF method can be described either by a static or dynamic mesh. It is an Eulerian method and the Navier-Stokes equations have to be solved separately. The method is developed by Hirt and Nichols (1981) and use an approximation of the interface of water and air by introducing a scalar variable, α, in the governing equations. According to Hirt and Nichols (1981), the method is shown to be more efficient and flexible than many other methods for handling complicated free boundary conditions. α represents a portion of volume of the fluids that is filled in the cells. The value of α is always between 0 and 1, where $\alpha = 1$ represents a cell filled with water while $\alpha = 0$ is a cell filled with air. The varible, α, is implemented in the Reynolds-Averaged Navier Stokes (RANS) equation for incompressible flows. The volume fraction, α, needs to satisfy Equation (5.1).

$$\frac{\partial \alpha}{\partial t} + \frac{\partial(\alpha U_i)}{\partial x_i} = 0 \tag{5.1}$$

It is necessary to have an extra compression by introducing an extra compression term, Hong-jian and De-cheng (2015). This is shown in Equation (5.2).

$$\frac{\partial \alpha}{\partial t} + \frac{\partial(\alpha U_i)}{\partial x_i} - \frac{\partial[U_{ir}\alpha(1-\alpha)]}{\partial x_i} = 0 \tag{5.2}$$

Here, the term $\alpha(1-\alpha)$ takes effect on the pressure on the interface. U_{ir} is the velocity field that is suitable to compress the interface. According to Hong-jian and De-cheng (2015), this can be obtained according to Equation (5.3).

$$U_r = n \cdot min[C_\alpha|U_i|, max(|U_i|)] \tag{5.3}$$

Here n is the unit normal vector on the interface and C_α the compression factor for controlling the strength of compression. Using a weighting function for α, the density, ρ, and the viscosity, ν, can be calculated according to Equations (5.4).

$$\rho = \alpha\rho_w + (a-\alpha)\rho_a \tag{5.4a}$$

$$\nu = \alpha\nu_w + (1-\alpha)\nu_a \tag{5.4b}$$

Here, ρ_w and ρ_a represents the density of water and air respectively, while ν_w and ν_a denote the viscosity of water and air.

5.2 Wave Generation Method

Waves2Foam is a library for use in OpenFOAM. This means that the Waves2Foam tool can be used to generate the waves into the simulation in OpenFOAM. The rest of the operations are conducted by OpenFOAM by use of the applied solvers. Waves2Foam use relaxation-zones in order to create and damp a wave. As mentioned before, the library contains a

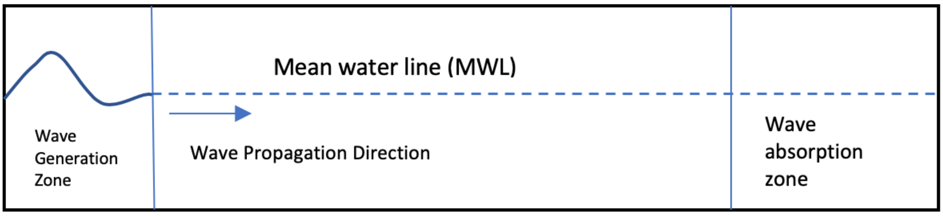

Figure 5.2: Schematic set-up of a case in Waves2Foam

multitude of wave theories, and it is also possible for the user to implement their own wave specifications and theory. Figure 5.2 illustrate a schematic case set-up in Waves2Foam with relaxation-zones for the inlet and outlet. This provide smooth transitions for the simulations and prevents wave reflection. The relaxation-zones are defined in the constant-folder along with the wave properties in the file $waveproperties.input$.

The VOF method utilize the ability of the relaxation zones to transform the analytic solution at the beginning to a fully non-linear CFD solution at the end, Khalid (2016). The outlet relaxation zone transforms the CFD solution to a no-wave (in this case constant current) condition. w is used as a weighing parameter that initially increase exponentially from 0 at the inlet. At the end of the relaxation zone it has the value 1, as shown in Figure 5.3. Similarly, w decreases exponentially from 1 to 0 during the interval between the start of the outlet relaxation zone and the end of the zone. The definitions in Figure 5.3 are:

- L_{in}^{relax} = Inlet relaxation zone
- L_{out}^{relax} = Outlet relaxation zone

Equation (5.5) show the transitions of the horizontal velocity, u, and the variable, α.

$$u = (1 - w)u_{target} + wu_{computed} \tag{5.5a}$$

$$\alpha = (1 - w)\alpha_{target} + w\alpha_{computed} \tag{5.5b}$$

5.3 2D Test Cases

Initially, a 2-dimensional test case is set-up in order to verify and check the generated waves in OpenFOAM. The domain is made in the same manner as before, only without the cylinder. This way, the domain illustrates an empty pool, and the incident waves can be measured and evaluated. The investigated domain is illustrated in Figure 5.4. The size of the domain is a very important factor as this will influence the computational time to a high degree. The size of the different three different regions is important to define in a good way. If the wave generation- and absorption zones are too small, the fluid does not have the necessary space to develop the flow properly. If the simulation region is too small, it will not be possible to investigate the wave propagation. However, if this region

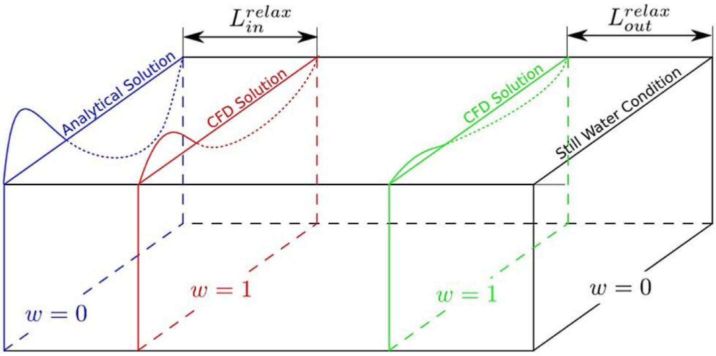

Figure 5.3: Illustration of relaxation zones, taken from Khalid (2016)

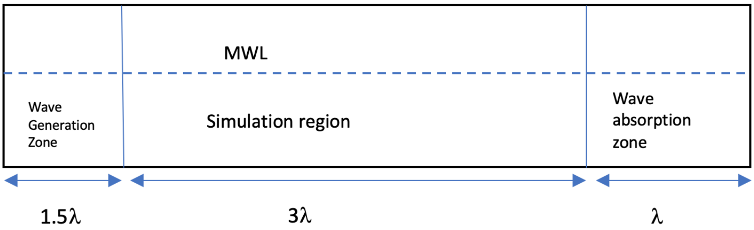

Figure 5.4: Computational Domain for the 2D test case

is very large, it will be difficult to make a good mesh and the computational time will be very large.

The same set-up is used to generate waves with different properties. The three different wave cases that are tested are listed with parameters in Table 5.1.

Table 5.1: Input parameters for the 2D wave simulation in an empty pool

Case nr	T [s]	H [m]	λ [m]
1	13	11.4	167
2	13	13.3	167
3	14	13.3	182

5.3.1 Pre-Processing

Before running the simulation, all necessary input has to be defined by the user. In addition to the files described in the mesh verification study, some files are added in order to describe the waves. The additions to the constant folder are the wave properties file that include the wave parameters and relaxation zones. The parameters in use are listed in Table 5.2. The wave gauges are placed on a line along the x-axis. The points are chosen to investigate the propagation of the waves, especially at the inlet and outlet zones. The gauges are placed at $x = -250.5, -83.5, -40, 0, 40, 100, 200, 300, 400, 417.5, 668[m]$. This way, they cover the whole length of the domain.

Table 5.2: Input parameters for the 2D wave simulation in an empty pool

Property	**Value**
Type of mesh	Static
Gravitational acceleration	9.81 $[m/s^2]$along negative y-axis
Probe definition	Wave gauges measure elevation
Type of fluid (water)	Newtonian
Viscosity of water	1e-06
Density of water	1000 kg/m^3
Type of fluid (air)	Newtonian
Viscosity of air	1.48e-05
Density of air	1 kg/m^3
Type of flow	Laminar
Wave theory	Cnoidal
Water depth	20 m
Wave period	13-14 s
Phase shift of wave	0
Wave height	11.4, 13.3 m
Wave direction	along positive x-axis

The mesh is still defined by the blockMesh-utility. The number of cells in each direction is given in Table 5.3, giving a total number of cells to be 1 000 000. A simple grading is implemented in order to have smaller cells around the mean water level. The ratio between the inner- and outer cells along the y-axis is 1/10. Running this simulation on 1 node with 16 cores takes less than 24 hours.

Table 5.3: Number of cells in each direction for the 2D wave simulation in an empty pool

Coordinate axis	**Number of cells**
x-axis	1000
y-axis	100
z-axis	1

The 0 folder includes the boundary conditions for α, the pressure and the velocity. The conditions used are listed in Table 5.4. More information about the different boundary conditions can be found in the user guides by OpenCFD (2019). The boundaries inlet, outlet, atmosphere, front, back and bottom defines the boundary conditions for the sides of the box that makes the empty pool. These boundaries are defined in the blockMeshDict, as before. This is illustrated in Figure 5.5.

Table 5.4: Boundary conditions for the 2D wave simulation in an empty pool

Boundary	α	Pressure (p_{rgh})	Velocity (U)
Inlet	waveAlpha	zeroGradient	waveVelocity
Outlet	zeroGradient	zeroGradient	fixedValue
Atmosphere	inletOutlet	totalPressure	pressureInletOutletVel
Bottom	zeroGradient	zeroGradient	slip
Front/Back	empty	empty	empty

The system folder includes the controlDict and the solver definitions. The parameters defined in the controlDict are listed in Table 5.5. The adjustableRunTime option opens for the chance for the simulation to adjust the time step along the way. This can be an effective option in some cases. However, this needs to be specified for each separate case. It can also cause the simulation to have very small time steps and thereby be too computationally demanding. If this is the case, the time step should rather be fixed.

Table 5.5: Parameters for the 2D wave simulation in an empty pool

Parameter	Value
startTime	0
endTime	100
deltaT	0.0001
writeControl	adjustableRunTime
writeInterval	0.5

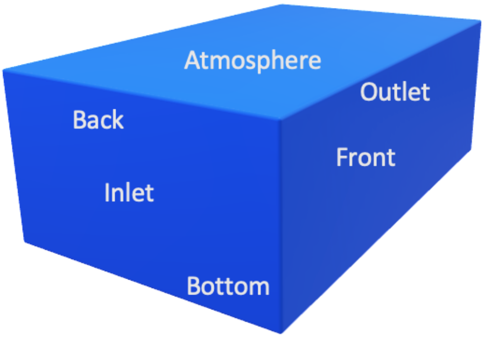

Figure 5.5: Empty pool boundaries

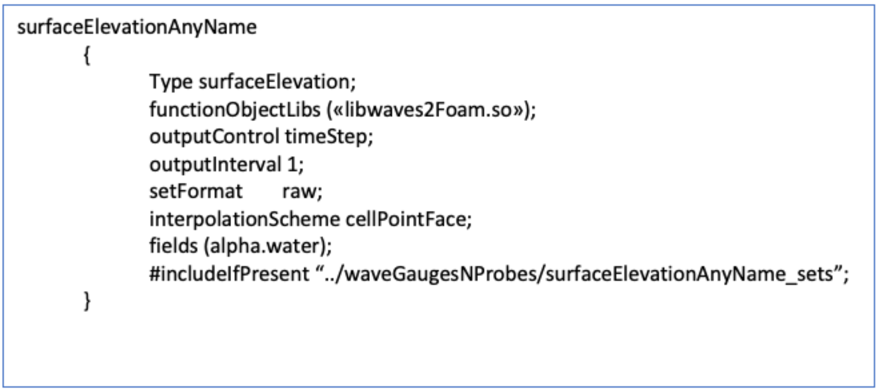

```
surfaceElevationAnyName
        {
                Type surfaceElevation;
                functionObjectLibs («libwaves2Foam.so»);
                outputControl timeStep;
                outputInterval 1;
                setFormat       raw;
                interpolationScheme cellPointFace;
                fields (alpha.water);
                #includeIfPresent “../waveGaugesNProbes/surfaceElevationAnyName_sets”;
        }
```

Figure 5.6: Surface elevation - code fraction

The wave elevation uses the alpha-coefficient to decide the wave height. Both these functions are included in the controlDict in the system-folder and the wave elevation measuring code can be seen in Figure 5.6. The surface elevation function calls another script called "probeDefinitions" that is located under the constant folder. This script contains the information about the whereabouts of the wave gauges. This code can be seen in Figure 5.7.

Solving

For solving the wave cases, there are some additional steps that needs to be included. In order to do this in an effective manner, a run script is made that will run the job in parallel. Such a script is included in Appendix A. What is included, is the commands for the execution of the four main steps of the wave generation process. These steps are illustrated in Figure 5.8. As before, the command blockMesh creates the geometry along

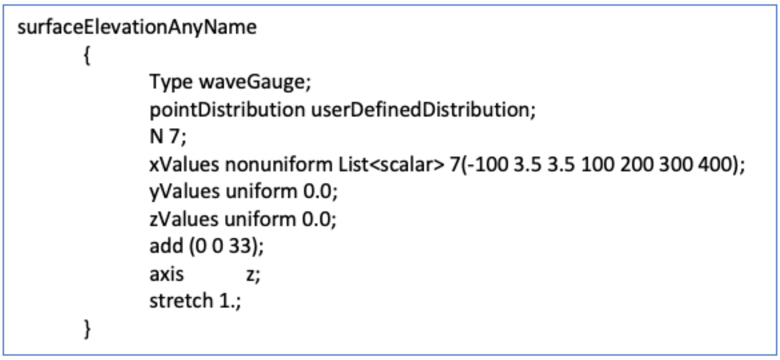

```
surfaceElevationAnyName
        {
                Type waveGauge;
                pointDistribution userDefinedDistribution;
                N 7;
                xValues nonuniform List<scalar> 7(-100 3.5 3.5 100 200 300 400);
                yValues uniform 0.0;
                zValues uniform 0.0;
                add (0 0 33);
                axis        z;
                stretch 1.;
        }
```

Figure 5.7: Wave gauges definition - code fragment

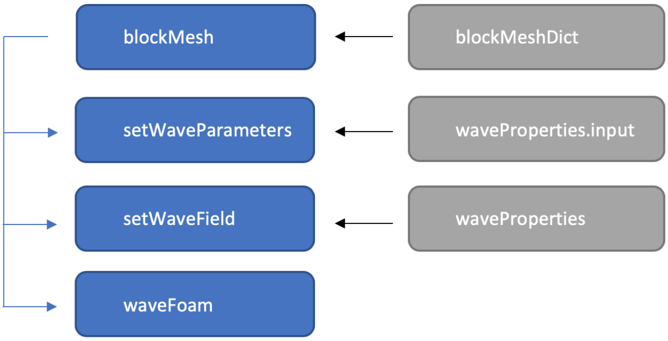

Figure 5.8: The four main steps of wave generation in OpenFOAM

with boundaries and mesh. The setWaveParameters command is used for defining the wave parameters. Waves2FOAM only need a few input parameters for defining and generating the wave for each wave theory. The rest is being calculated by the program through the specifications built in the code. This command creates a file from the waveProperties.input called waveProperties. The calculated properties in this file are the angular velocity, wave number, wave celerity, wave length and more. The setWaveField utility decides the initial condition in the computational domain. WaveFoam is a command that is used in order to start the simulation.

5.3.2 Post-Processing

ParaView is used for visualization of the waves and Matlab is used for visualizing the measured wave elevation from the wave gauges. The visualizations of the waves that were generated for the Cnoidal wave case number 1 are shown in Figures 5.9. The red is water while the blue is air. Figure 5.9a show the still water condition, while the others show the propagating waves. The waves are on the edge of breaking, and this is visible from the illustrations. The wave peak is very steep for the wave after about 40 s.

Results - 2D Case number 1

(a) T = 0s

(b) T = 30s

(c) T = 41s

(d) T = 50s

Figure 5.9: Illustrations of the first Cnoidal wave condition in 2D

The wave heights are measured at different points. It is visible that the waves are completely regular at the inlet and change to be steeper while propagating through the domain.

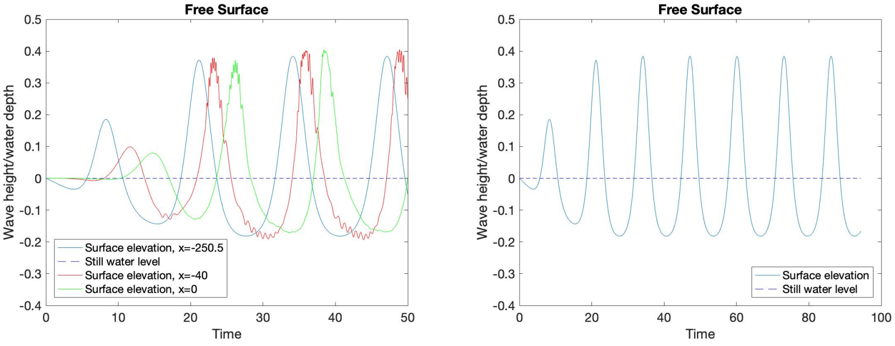

(a) Free surface, x=-250.5, x=-40 and x=0 **(b)** Free surface, x=-250.5

Figure 5.10: Time series of the waves in 2D

The free surface is measured by probes along the domain. An illustration of this is included in Figure 5.10. A more detailed plot of the wave can be seen in Figure 5.11. The wave is measured at two different points; x=-250.5 and x=0. The first point is at the inlet, and measures therefore a completely undisturbed wave. The second point is measured in x=0, namely the point that will be at the center of the cylinder in the three-dimensional simulations that are done at a later stage. It is visible that the waves have the same shape, and that the parameters have not changed significantly. The difference is that the wave measured at x=0 is a bit steeper after some propagation.

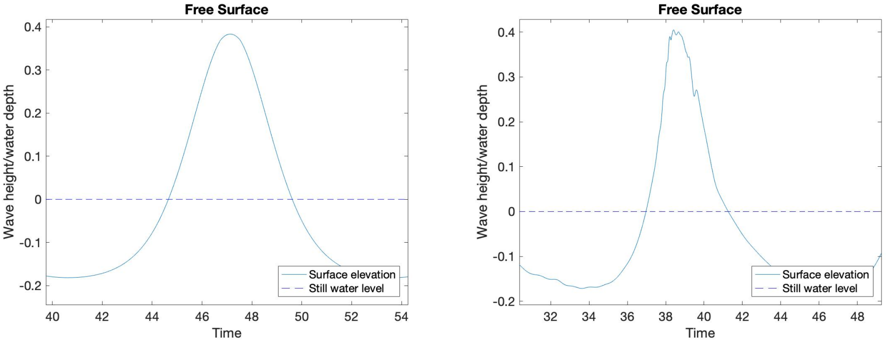

(a) One wave, x=-250.5 **(b)** One wave, x=0

Figure 5.11: One wave, measured at two different points

Results - 2D Case number 2

Visualizations of the waves for wave case number two are shown in Figure 5.12. For this wave case, the wave height is increased to be H=13.3m.

(a) T = 20s

(b) T = 30s

(c) T = 40s

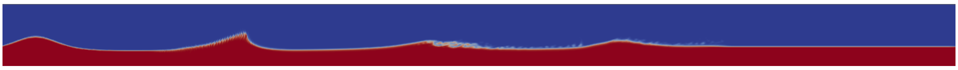

(d) T = 50s

Figure 5.12: Illustrations of the second Cnoidal wave condition in 2D

Figure 5.13 show the wave at two different points; x=0 and x=-83.5.

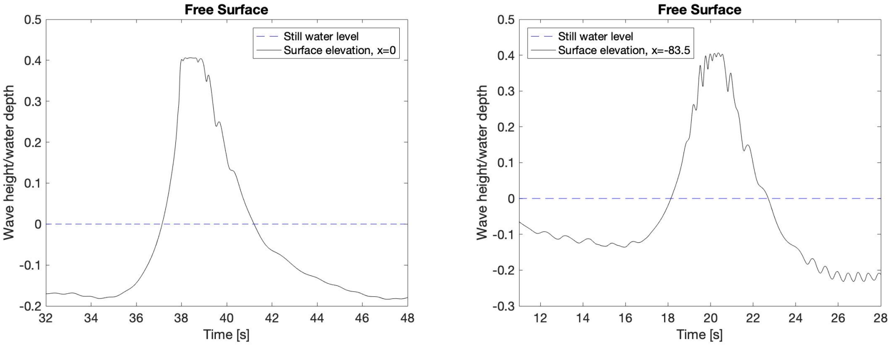

(a) One wave, x=0

(b) One wave, x=-83.5

Figure 5.13: One wave, measured at two different points

Results - 2D Case number 3

Visualizations of the waves for wave case number three are shown in Figure 5.14. For this wave case, the wave height is still 13.3 m while the period is increased to be 14s.

(a) T = 10s

(b) T = 20s

(c) T = 30s

(d) T = 40s

(e) T = 50s

Figure 5.14: Illustrations of the third Cnoidal wave condition in 2D

Figure 5.15 show time-series of the surface elevation measured in two points; x=0 m and x=-83.5 m. Figure 5.16 show the details of one wave measured at each of the points.

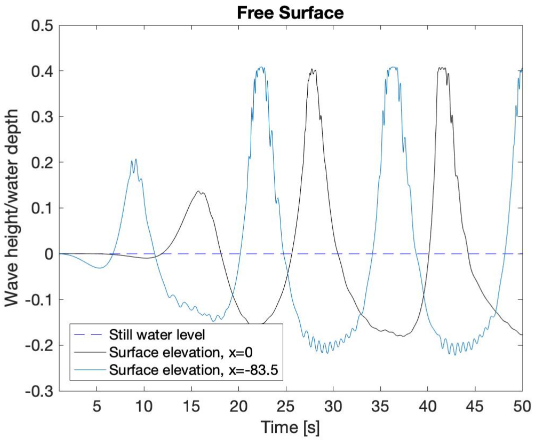

Figure 5.15: Surface elevation time-series, measured in x=0 m and x=-83.5 m

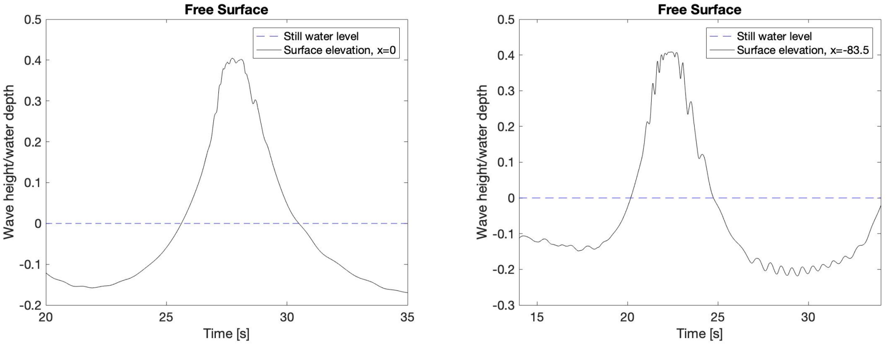

(a) One wave, x=0

(b) One wave, x=-83.5

Figure 5.16: One wave, measured at two different points

Comparison to theoretical wave propagation

The waves created by Waves2FOAM follow the first order Cnoidal wave theory as described by Svendsen and Jonsson (1976). In their description of the theory, a theoretical wave propagation illustration is included as well. This propagation is illustrated in Figure 5.17. This shows the same type of behaviour as is seen from the wave simulations.

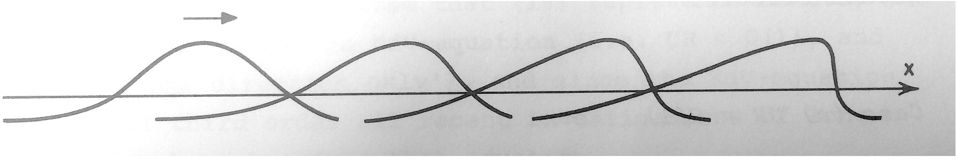

Figure 5.17: Wave propagation according to the first order Cnoidal theory

This behaviour is due to the fact that each part of the wave propagates with the speed $u = \sqrt{g(h+\eta)}$. h is the water depth and η is the wave amplitude. This means that u is dependent on the local depth of the water, and the top parts of the wave will therefore have a higher velocity and overtake the lower parts as illustrated in Figure 5.17.

5.4 Comparison to Analytic Solution

A cnoidal wave with arbitrary length and arbitrary depth can be calculated analytically by using the relative depth and steepness, along with a number of positive Fourier modes and a tolerance. The wave profile obtained in OpenFOAM is compared to the analytic wave profiles for verification. Three wave profiles are calculated to correspond to the three wave cases. The wave parameters for these are listed in Table 5.6.

Table 5.6: Waves for comparison

Case nr	λ/d	H/d
1	8.38	0.57
2	8.38	0.67
3	9.13	0.67

The most extreme waves at the site are not tested at this stage. This is due to the breaking of these waves. For the comparison, the waves that are chosen should not break in order to have a good analytic solution. The Matlab code used to generate the wave profiles is not able to compute limiting waves. It is made for computation of waves with arbitrary length for all heights up to 99% of the maximum one. The output quantities are dimensionless with scaling $\rho = g = d = 1$. The Matlab function is taken from Clamond (2018). Figures 5.18, 5.19 and 5.20 show the analytic solutions of a wave profile with the wave parameters as listed. It is clear that for case number one, the analytic and simulated waves are close to identical. The peak is a bit narrower for the simulated wave. However, the height is nearly equal, and the troughs have the same depth.

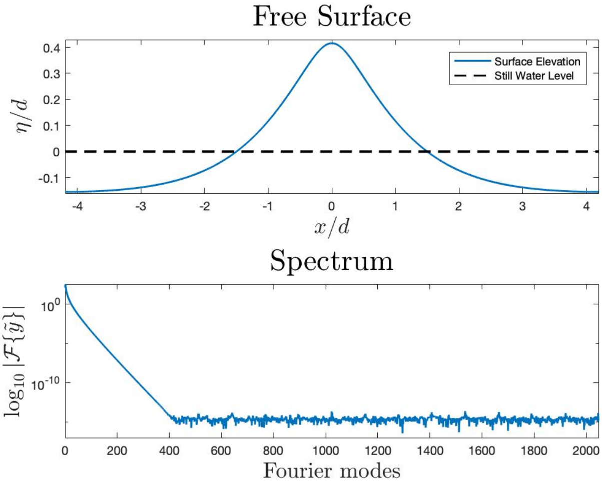

Figure 5.18: Wave profile with $\lambda/d = 167.6$ and $H/d = 0.57$. The Fourier modes show that the solution clearly converge.

Figure 5.19 shows the wave profile for wave case number two. The analytic solution indicates a narrower wave top/ a steeper wave. This wave condition is close to the limit of what the code can handle. The shape of the wave with a steep wave top is very similar to the developed waves in Figure 5.12. Figure 5.13 shows that the height/water depth is also agreeing with the analytic solution.

Figure 5.20 illustrates the analytic solution for wave case number three and is very similar to the analytic solution for wave case number two. Also for this case, the simulated

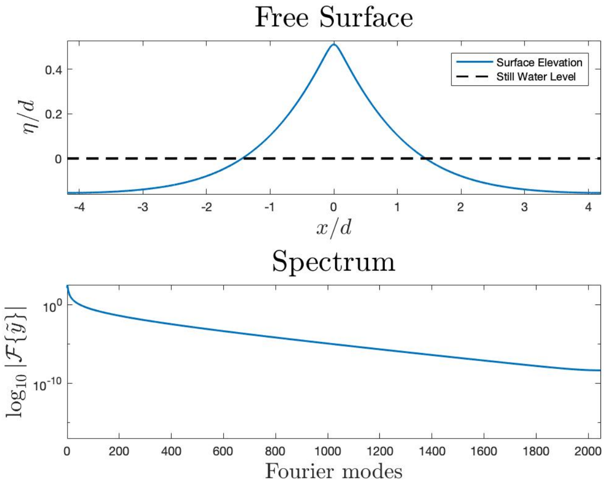

Figure 5.19: Wave profile with $\lambda/d = 8.38$ and $H/d = 0.665$. Solution converge at the last modes.

waves correspond well to the analytic solution. There are no visible deviations between the simulated and calculated wave.

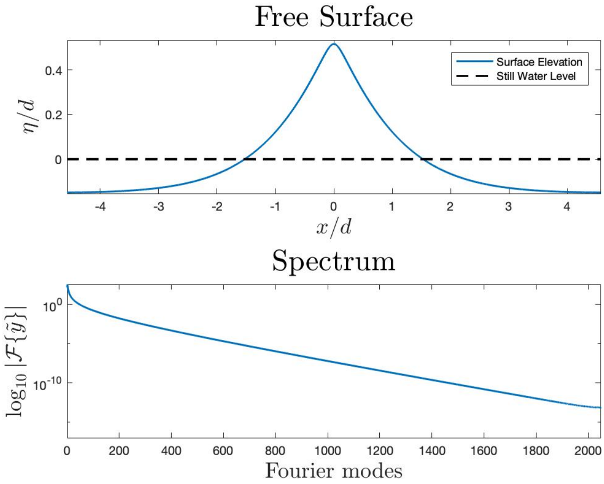

Figure 5.20: Wave profile with $\lambda/d = 9.13$ and $H/d = 0.665$. Not entirely clear whether solution converges or not.

5.5 Summary

In this Chapter, the theory, method, results and discussion about the wave implementation in OpenFOAM are given. It is discovered that the use of Waves2Foam is a good option for implementation of waves and that the library contains several wave theories. A first order Cnoidal theory is implemented and tested for three wave conditions. The results are then compared to analytic solutions of the same wave conditions. The results document almost equal solutions for the wave cases. This encourage even further use of Waves2Foam as it seems to generate well Cnoidal waves of first order.

Chapter 6

Two-Dimensional Analysis of the Cylinder in Unsteady Flow

In order to investigate the cylinder in two dimensions with conditions that are similar to the wave conditions tested in Chapter 5, a case is set up with the same system as described in Chapter 4. It is domain size number two that is in use. In order to get a wave condition in two dimensions with flow around the cylinder, a function is inserted for the flow velocity. The flow is characterized by the changing velocities in the Cnoidal waves. The velocities in the wave change with time in addition to changing with the relative water depth. This means that the function for the water current velocities must have changing velocities with time in order to represent the waves in a good manner. Therefore, the velocities in the wave are measured in time for different heights (z-coordinates). Further investigation is carried out for the selected z-coordinates by doing one simulation for each of them. This is further described in the next section. Since the KC numbers for the wave conditions at site are relatively large, the flow can separate.

6.1 Unsteady Boundary Condition Set-Up

The set-up of the cases with varying flow velocity is done with the same method as described in Chapter 4. However, some changes are done in order to get appropriate CFL numbers and a converged solution. Domain size number two is used along with a small time step. The time step is set to $\Delta T = 0.0005$. Mesh size number two is initially in use, but the number of cells is increased in order to get a good quality of the results. The flow velocity, U, is inserted as a list of different velocities according to time. These lists of velocities are taken from the two-dimensional wave simulations where the velocities are measured by use of probes. The probes are placed at different heights (z-values), but at the same x-coordinate. The top of the wave have a different velocity than the bottom of the wave. The time series of the velocities are implemented in the simulations by the use of an unsteady boundary condition. This boundary condition includes a table for the different velocities. This way, the original wave can be mimicked by the use of several two-dimensional simulations. The results are later used for representing the forces on the cylinder at different heights of the wave. These can then be integrated to three dimensions and compared to the results from the three-dimensional simulations. This integration is further described in Section 6.3. The relation between the wave height and wave speed is shown in Figure 6.1. It is clear from these illustrations that the wave velocity is highest at the wave crest. The free surface has the value (z-20)=20 [m] on the x-axis. The crest height is approximately 7 [m], and the velocity peaks are located at around (z-20)=27 [m]. It is also clear that the velocity profiles are varying strongly with time. The stream velocity varies between approximately 0 [m/s] and 8 [m/s].

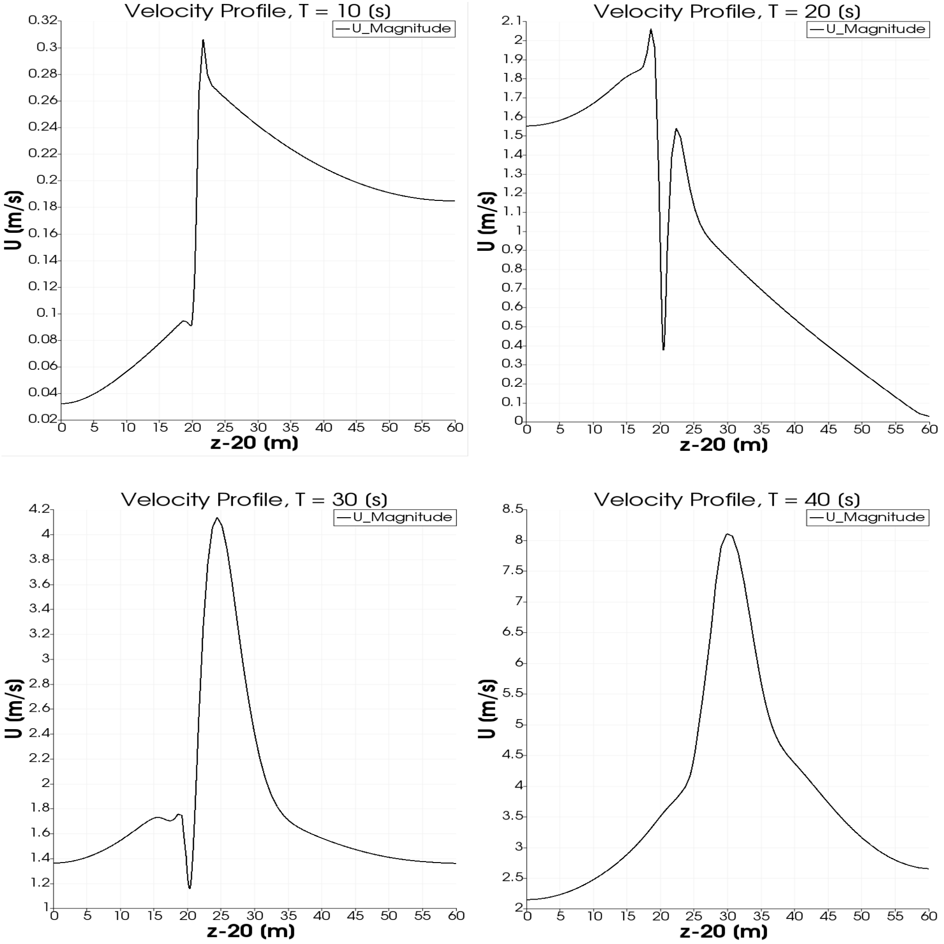

Figure 6.1: The time varying relation between the water particle velocity in the wave at different heights

It is worth to take notice that the two first illustrations in Figure 6.1 are in the ramp period for the wave that lasts 26 [s]. It is therefore assumed that this is the reason for the abrupt changes and jumps that are seen in these two figures. The two last illustrations taken at times T=30 [s] and T=40 [s] show a more even transition from lower to higher velocities. The illustration from T=50 [s] is nearly identical to the one for T=40 [s] and is therefore not included here.

The free surface varies with time according to the wave. Probes along the x-axis have measured the elevation and the probe located in x=0 [m] show the surface elevation illustrated in Figure 6.2b. In comparison, Figure 6.2a show the measured elevation from probes in x=-250 [m] and x=-40 [m]. They show the free surface in the time between 30 [s] and 50 [s]. This is because this interval will be used later for integration. The initial phase includes a ramp function of 26 [s] (two times the wave period), and the results from this phase are not included in an attempt to achieve better accuracy.

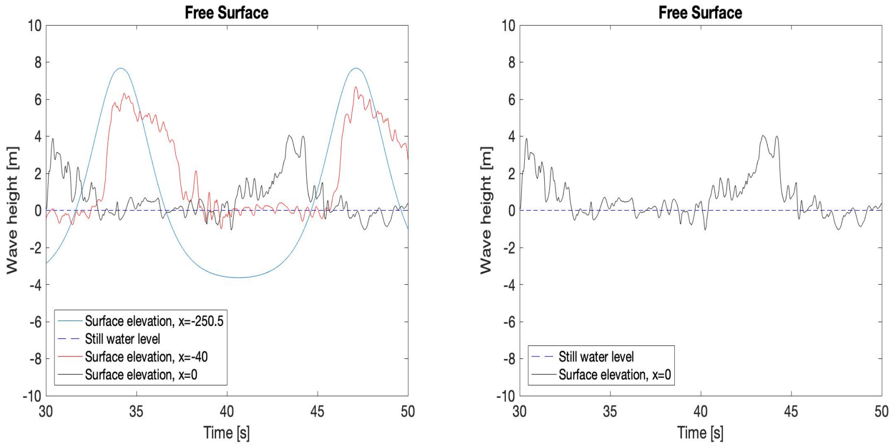

(a) Free surface at x=-250, x=-40, x=0 [m]

(b) Free surface measured at x=0 [m]

Figure 6.2: Free surface measurements in the time span 30 [s] - 50 [s]

The file for the flow velocity found in the folder "0" is altered to include the code for the time varying fluid flow at the inlet (left). This is included by use of the code in Figure 6.3. The Figure also show the code fraction in use for calculating the force components and writing these to an output file. The table for the different velocities include the velocity in all three directions for every half time step. The simulations are run for about 100 time steps (a bit more for the simulations with the lowest velocities).

These first simulations with time varying flow input are done in laminar conditions and no turbulence model is included. They are done for a number of different z-coordinates; -3, -2, -1, 0, 1, 2, 3, 4, 5, 6, 7 and 7.4. An overview of the process can be seen in Figure 6.4. The results and the integration (step 3) is presented and described in the next sections.

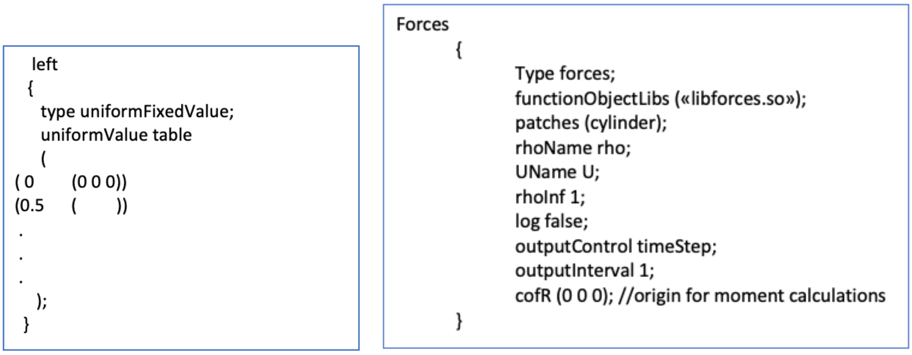

```
 left
{
  type uniformFixedValue;
  uniformValue table
  (
( 0      (0 0 0))
(0.5     (       ))
.
.
.
  );
}
```

```
Forces
      {
              Type forces;
              functionObjectLibs («libforces.so»);
              patches (cylinder);
              rhoName rho;
              UName U;
              rhoInf 1;
              log false;
              outputControl timeStep;
              outputInterval 1;
              cofR (0 0 0); //origin for moment calculations
      }
```

Figure 6.3: Code fractions used for making a time varying flow input and for calculation of the force components

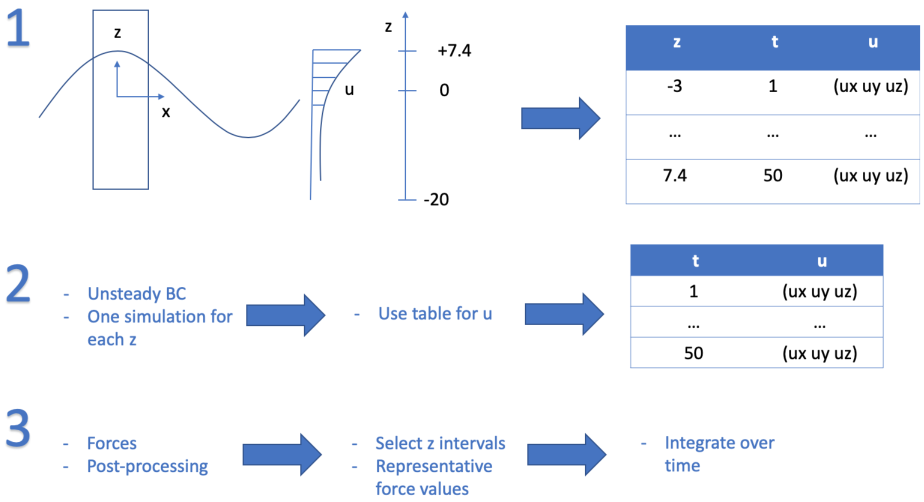

z	t	u
-3	1	(ux uy uz)
...	...	...
7.4	50	(ux uy uz)

t	u
1	(ux uy uz)
...	...
50	(ux uy uz)

Figure 6.4: Overview of procedure for the unsteady boundary condition simulations

6.2 Results - Laminar Time-Varying Fluid Velocity

Depending on the incoming fluid velocity, the flow can separate behind the cylinder. Illustrations below in Figure 6.5 show the flow features around the cylinder with incoming stream velocity according to measurements from the wave at z=0 [m].

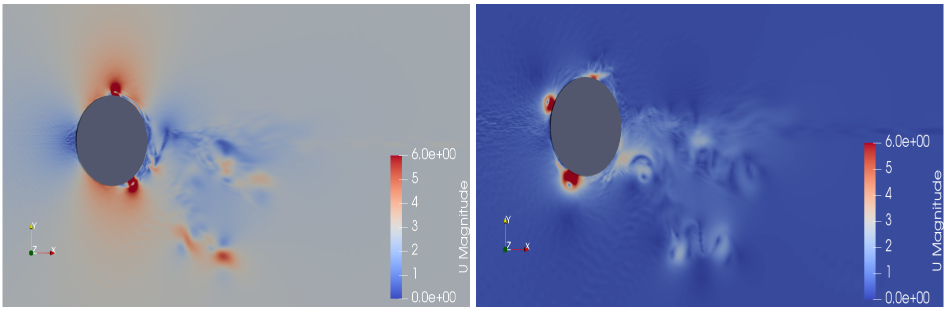

(a) t=40 [s] **(b)** t=42 [s]

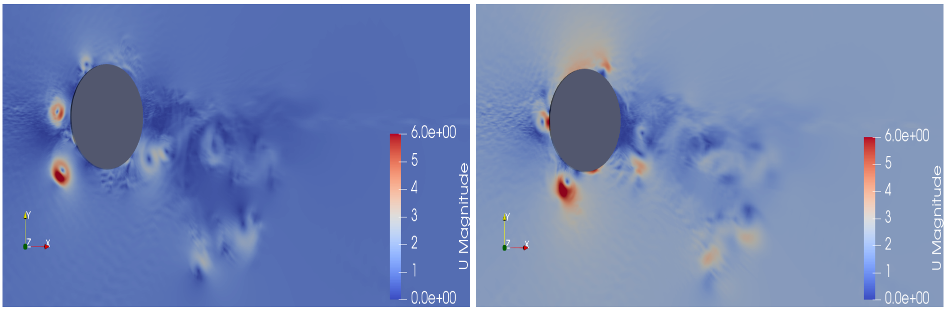

(c) t=44 [s] **(d)** t=46 [s]

Figure 6.5: Illustrations of the water flow around the cylinder. Pictures taken at different time steps in the simulation at z=0 [m]

Based on the illustration the degree of separation is not clear. Hence, the case is further investigated by measuring the lift-forces. The forces are measured at the cylinder. The forces in x-direction represent the drag forces while the forces in y-direction represent the lift forces. The measurements of the lift forces show clear separation effect. The vortex shedding frequency was not completely constant as the velocities in the simulations are constantly changing for every time step. Figure 6.6 show the measurements of the lift force from simulations z=-3 [m] and z=6 [m]. It is clear that the forces are higher when the velocities are higher. The higher speed occur in the highest level of the wave - e.g. the lift forces are higher for the simulation at z=6 [m]. This is also illustrated in Figure 6.7 where the drag forces from two different simulations are included in order to illustrate the difference in the drag components at different heights. In this figure it is clear to see that a higher z-coordinate concludes in a rise in the drag-forces as well. The rest of the results from the simulations can be found in Appendix B.

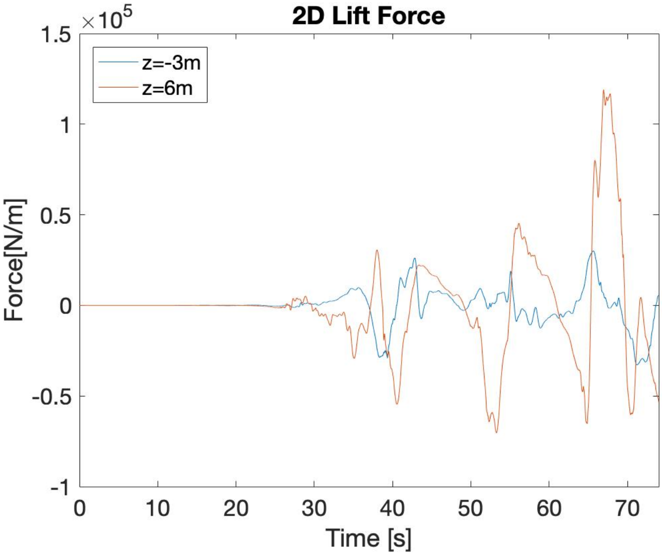

Figure 6.6: Lift forces taken from 2D simulations with z= -3 [m] and z=6 [m]

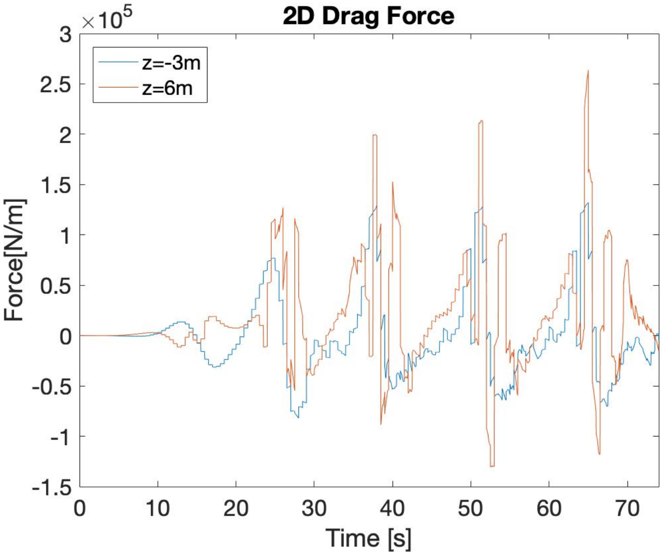

Figure 6.7: Drag forces taken from 2D simulations with z= -3 [m] and z=6 [m]

Measurements of the drag- and lift forces from the simulation at z=0 [m] are illustrated in Figure 6.8. Also included in the figure is the wave height and the stream velocities at the same time step. This is done in order to compare if the maximum force follows the wave crest or if they are out of phase. Prior to simulation it was expected that they would be in phase because of the Cnoidal wave theory stating that the wave crest will have the highest wave velocity. It would therefore be logical to assume that higher velocities will give higher forces. Comparing to the results, this assumption fit well as the results give highest forces at the wave crests where it is also visible that the highest velocities are found.

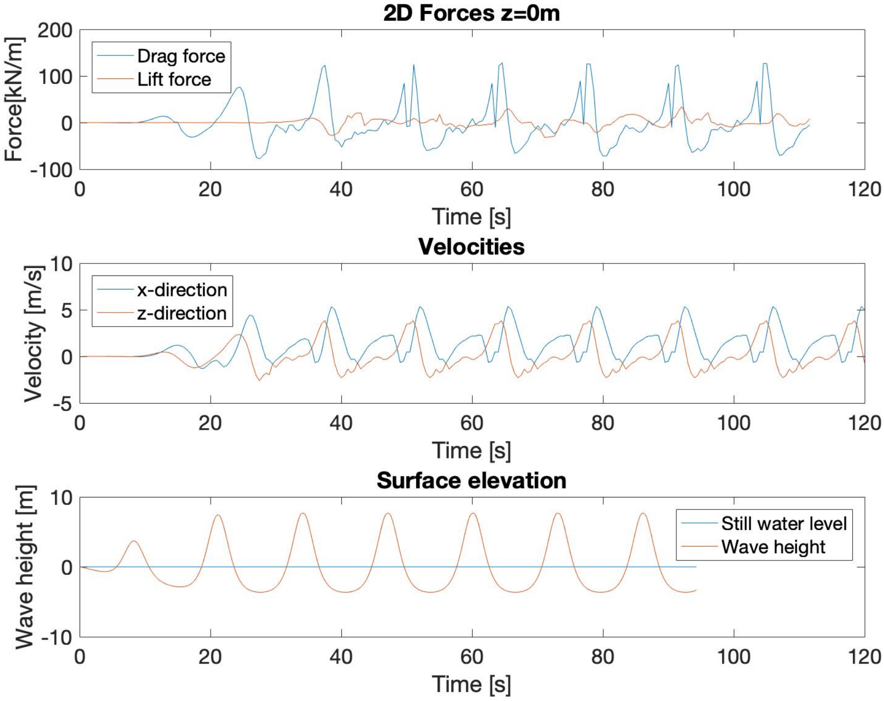

Figure 6.8: Forces, water velocity and corresponding surface elevation from 2D simulation at z=0 [m] (still water level)

Each of the simulations create time series for the force components. All figures are included in Appendix B. These time series are used for integration in the next Section. The drag-force results show that the forces are highest near the wave crest, at z=7 [m]. At the same time step, t, it appears that the magnitude of the forces can vary more than 50 [kN] from one z-coordinate to another. This is because of the variation in the stream velocity depending on where in the wave the velocity measurements are taken from.

6.3 Integration of Two-Dimensional Results

The results for each height in the wave are used to integrate over the cylinder height to get an estimated 3D result of the drag- and lift forces. Each result is used for one meter of the cylinder. This method is often called "strip theory" as the geometry that is investigated is

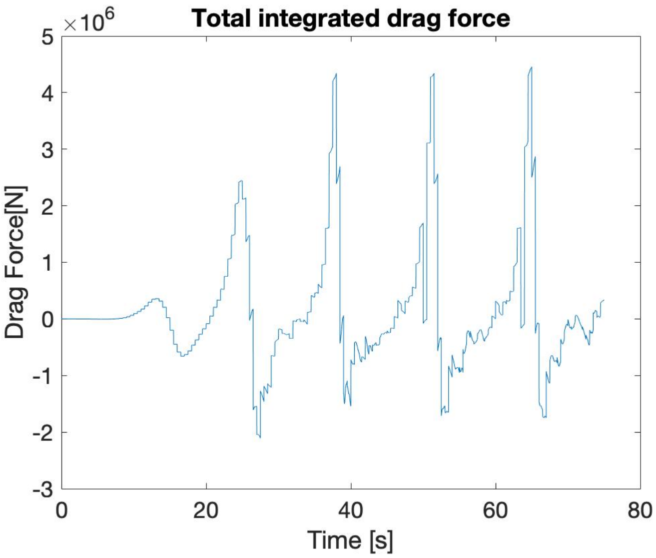

Figure 6.10: Total integrated 3D drag force over time

divided into "strips" that is considered isolated from the rest of the geometry in a 2D flow, Pettersen (2018). A typical strip is illustrated in Figure 6.9.

In this case, the length of each strip is 1 [m]. The extra simulations for z=5.5 [m] and 7.4 [m] did not give results that deviated much from the results at 5 [m] and 7 [m] and will therefore not be included in the integration. Hence, the results are integrated from z=-3 [m] to z=7 [m]. z=7 [m] represents the wave crest and the results from z=-3 [m] are used for the rest of the lower parts of the cylinder down to the bottom at z=-20 [m]. The cylinder diameter, D=7 [m], is constant for the entire domain and is equal for all the simulations.

The total integrated forces in 3D are illustrated over time in Figures 6.10 and 6.11. The forces are close to zero until the ramp period is over. This lasts 26 [s]. After this, the first wave hits the cylinder. The waves are visible by the peaks in the drag force. The figure only includes the time interval between 30 [s] and 80 [s], because at 30 [s] the ramp period is over. It is not clear for all the simulations whether a steady state is obtained for the lift forces, which is also seen by the variations in the illustration of the lift time-series. This will be discussed further in Chapter 7 when comparing to the 3D results.

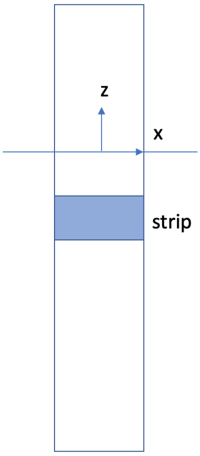

Figure 6.9: Partition of the cylinder geometry by use of strips

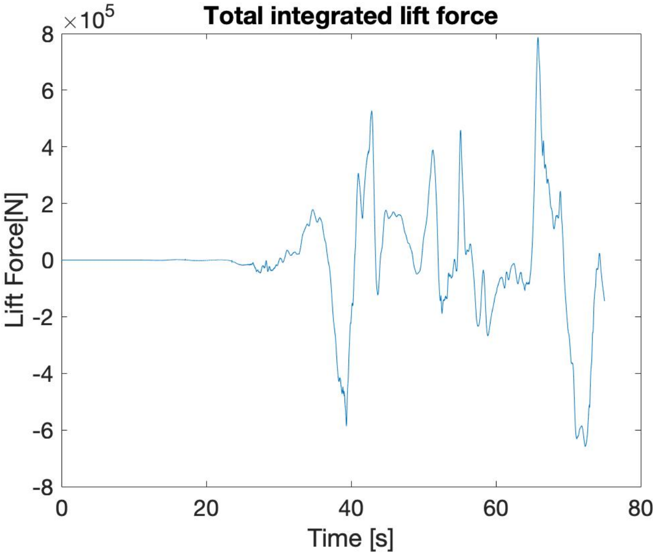

Figure 6.11: Total integrated 3D lift force over time

6.4 Discussion and Error Sources

The ramp period of $2T$ is excluded from further investigation as
the forces in this period are not representatives for the wave state. During this period, the program is generating the wave. After this period the waves are developed and the results for the integration are therefore taken from the time slot between t=30 [s] - t=80 [s].

For these simulations, the parts of the cylinder that are being investigated are assumed to be under water at all times, i.e. deviating from the 3D simulations where the wet surface area will vary according to the wave. Other possible error sources can be:

- **Cell size:** Cell size too big around the cylinder, i.e. measuring of forces is not accurate.
- **Inlet boundary condition:** Measurements show that the inlet velocity fit quite well to the desired velocity given in the function. However, there is a small delay since it takes some time before that velocity reaches the cylinder, while the measured velocity for the wave is taken at the center of the cylinder.
- **Boundary Conditions:** The boundary conditions for this case are difficult to determine because of the rapidly varying inflow.

The first point, cell size, should not have a big influence as the mesh is refined in a way where the cells closest to the cylinder are smaller than the cells further out. Such refinement should make the measurements at the cylinder to be quite accurate. It was also discovered during the initial mesh study that further refinement of the mesh did not show a substantial improvement of the results. The mentioned delay can be of significance

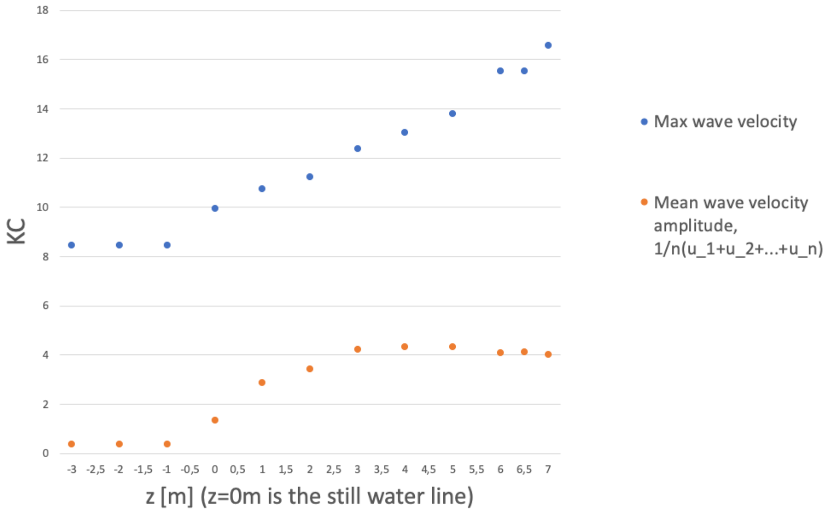

Figure 6.12: KC for max and mean wave velocity amplitudes at different z

because it may cause the solution to reach steady state at a later time step. The other boundary conditions are kept as the ones also used in Chapter 4. It is seen during post-processing that the pressure is showing some unexpected behaviour. This may be caused by a reference cell defined in the solution scheme where the solver steps are defined. It is also tested to change the outlet boundary condition for the pressure from fixedValue to zeroGradient. This do not work for this case. The outflow condition for the velocity has also been tested; Instead of zeroGradient it is tested to use an "inflowoutflow" condition. This does not work either for this case. It is decided that the boundary conditions are kept as they are and that the pressure error may be caused by either the rapid changes in the inflow or by the reference cell. It is suggested for further work to look further into the possibility of changing this reference cell to a cell further away from the cylinder. This can be found under the "system" folder in the "fvSolution" file.

The speed variations for the different locations (z-coordinates) in the wave give fluctuating KC numbers for the different simulations. An overview of these KC numbers is given in Figure 6.12. The lowest KC numbers (0-4) will in theory not give any vortexes behind the cylinder. For $KC > 8$, vortexes appear and separation can occur. For $KC > 26$ the flow is recognized by complete vortex separation behind the cylinder, Pettersen (2018). This is illustrated in Figure 6.13.

When comparing the theoretical flow picture for different KC numbers to the results from the simulations, they show to some extent similar behaviour. For the parts of the simulations that have KC numbers between 8 and 18, the vortex shedding frequency from the lift forces results in the same type of behaviour that is illustrated in the figure. The flow picture is further discussed in Chapter 7. For the parts of the simulations where the KC numbers are small, the lift forces are also small, hence it also correspond well with theory. The increased speed higher up in the wave give higher KC numbers but also higher lift forces, resulting in higher loads at this part of this cylinder. The higher loads may cause

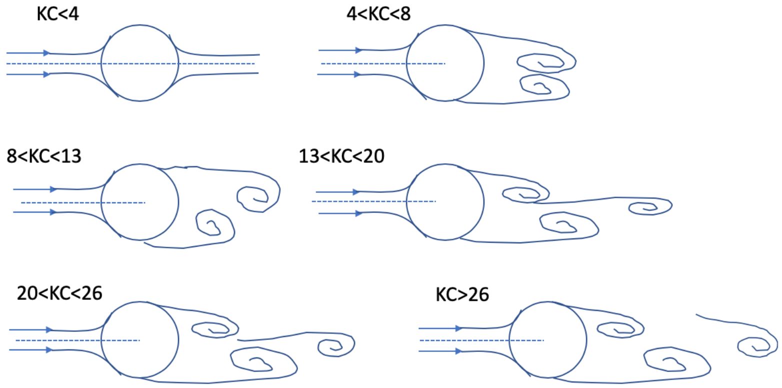

Figure 6.13: Flow picture around the cylinder at different KC numbers

a moment on the foundation in the transverse direction compared to the waves. The wind direction is for most conditions aligned with the waves. This means that the damping from the turbine acts in the same direction as the waves and wind. If a big moment occurs in the transverse direction due to high lift forces, such case needs to be damped in another manner and to be looked further into.

The water velocities from the wave and the measured forces showed to be in-phase. This was an expected result since according to Morison's equation (Equation (6.1)) the forces on a structure depend on the incoming stream velocity and its acceleration, Faltinsen (1990). The drag-force on a strip should according to this theory have its maximum value when there is a wave crest or a wave trough (absolute value). Such conclusion fits well with these results as they gave highest absolute values for the highest z-values; 7.4 [m], 7 [m] and 6 [m]. 7.4 [m] is at the top of the wave crest, and 7 [m] will also be by the wave crest. These two simulations give similar drag-forces and the highest values.

$$dF = \rho\frac{\pi D^2}{4}dzC_M a_1 + \frac{\rho}{2}C_D D dz|u|u \tag{6.1}$$

The flow features from these 2D simulations with unsteady inlet boundary condition are further investigated and presented in the comparison to the 3D simulations in Section 7.3.

6.4.1 Turbulent vs Laminar Models - 2D

For the main part of the simulations in this project, no turbulence model is included. This is due to limited time and a complicated problem to model. Because of the shallow waters, higher order wave theory and big domain size, the problem is difficult to simulate. The optimum is to include a turbulence model into all the simulations in order to get a closer-to-reality solution. However, it is also of interest to investigate the differences between a laminar and a turbulent solution.

There are a limited amount of experiments executed with high Reynolds numbers around a circular cylinder. Some numerical results done with by the use of URANS (Unsteady Reynolds-Averaged Navier-Stokes) and LES simulations. Ong et al. (2009) use an URANS approach including a $k - \epsilon$ model for modelling the turbulence. Their C_D results are presented in Table 6.1. The limited amount of studies on this is due to the complexity of the flow in this supercritical to upper-transition flow regime.

Table 6.1: Numerical and experimental results at Re=$1 \cdot 10^6$ and $3.6 \cdot 10^6$

Re		C_D
$1 \cdot 10^6$	Ong et al. (2009)	0.5174
	Catalano et al. (2003) (3D LES)	0.31
	Catalano et al. (2003) (URANS)	0.41
	Singh and Mittal (2005) (2D LES)	0.591
$3.6 \cdot 10^6$	Ong et al. (2009)	0.4573
	Catalano et al. (2003)	0.46

The C_D-values from the simulations done for this project vary strongly with the velocities in the wave. Taking the 2D simulations for z=0 [m] as an example, the velocities vary between 0 and 5 [m/s]. The forces are measured for every time step and the drag coefficient can therefore be calculated by using Equation (6.2).

$$C_D = \frac{F_D}{0.5 \rho A U^2} \tag{6.2}$$

Excluding the velocities approximately equal to zero in the wave, the time series of C_D-values for one wave period are shown in Figure 6.14 for the 2D simulation done at z=0 [m]. Even though the mean value is very close to the reference values presented in Table 6.1, the values in the time series vary a lot and it is therefore not sure how much influence a turbulence model would have given on the results presented in this thesis.

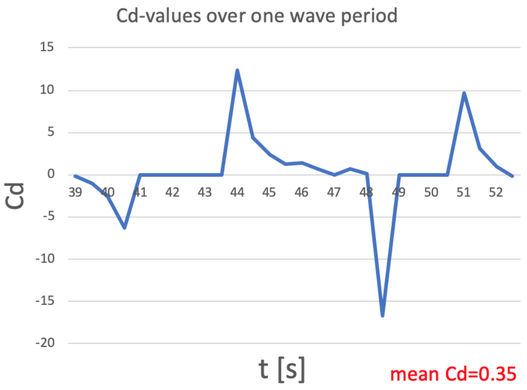

Figure 6.14: C_D-values as function of time from 2D simulation at z=0 [m]

In order to investigate this further, a turbulent simulation is executed for this wave condition in 2D for z=0 [m]. Doing this, a RAS simulation with a $k-\omega$ model is included in the set-up with an unsteady boundary condition at the inlet. The turbulence parameters are found by use of the conversion calculator by Online (2018), and the turbulence intensity is set to 1% and the turbulence length scale to 3 [m]. The choice of these parameters are further discussed by Younis (2010). It is discovered that the conditions at site are difficult to simulate with the above-mentioned turbulence parameters. The simulation with the parameters as listed in Table 6.2 had to be somewhat modified in order to run properly with appropriate CFL numbers. This forced the number of cells in each direction down.

Table 6.2: Input parameters and variables, turbulent 2D simulation

Tu	TuL	U	ΔT	Modifiable Run-time
1%	3 [m]	list for z=0 [m] from WC 1	0.0005	no

Figures 6.15 and 6.16 show the differences in the results between the simulation at z=0 [m] with- and without a turbulence model. It is visible that both the drag- and lift forces are over-predicted by the laminar model in comparison to the turbulent simulation. However, it is not perfectly clear how accurate the turbulent results in reality are since the number of cells had to be decreased in order for the simulation to run. In conclusion it is safe to say that including a turbulence model makes a difference in the results. How much this difference matters is still unsure and it is necessary to test the turbulent simulations further and to verify the turbulence model. Also, the comparison between the 2D- and 3D results should not have been very much affected by this since both are done in laminar conditions.

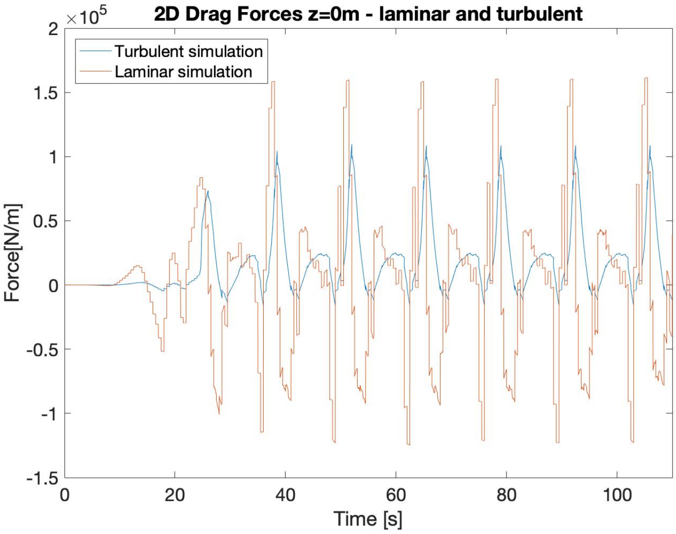

Figure 6.15: Comparison of drag forces between 2D simulation in laminar- and turbulent conditions

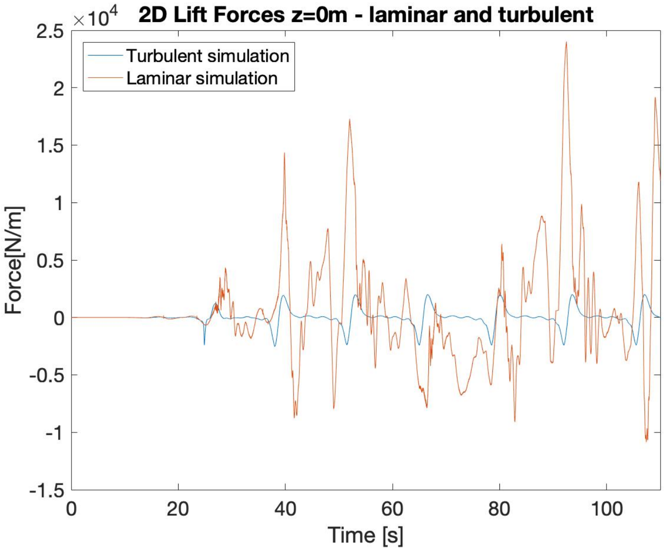

Figure 6.16: Comparison of lift forces between 2D simulation in laminar- and turbulent conditions

6.5 Summary

In this chapter, the set-up and method for simulations with unsteady inlet boundary conditions are described. The results are presented and tested towards theory. The results give highest forces for the highest velocities. The results from all the simulations are used for integrating the forces into 3D. This is done by using the principle of "strip theory". The conclusion of this integration is that time series of drag- and lift- forces are obtained and can then be used for comparison to results from a 3D simulation. This way, it is possible to study three-dimensionality and compare flow features. This is described and discussed further with the 3D simulations and their set-up in the next Chapter. One 2D case is tested with turbulent conditions. The 2D turbulent case give results varying relative to the corresponding laminar 2D case. Some discrepancies are visible including more steady-state behaviour and a lower magnitude of both drag- and lift forces.

Chapter 7

Three-Dimensional Simulations in Extreme Conditions

This Chapter includes the set-up, description and method in use for the three-dimensional simulations in OpenFOAM. These are executed with the aim of being able to compare the results with the integrated two-dimensional results. Because of the extension of the domain and the challenging wave conditions, only a few cases are tested due to limited amount of resources. Wave case 1 (WC 1) has the same conditions as for the 2D simulations with unsteady inlet boundary condition and is used for the comparison. WC 2 and WC 3 (described later in this chapter) are the same conditions as tested earlier for the wave simulations in an empty pool in Chapter 5. In addition, one simulation is executed with practically zero viscosity but else with the same conditions as in WC 1. This is done in order to be able to do a comparison. Last, a turbulent simulation of WC 1 is executed in order to see the difference in terms of flow behaviour and to test the difference.

7.1 Case Set-Up

The case set-up is the same as the ones used before. The difference is that the simulations done in Chapter 6 are extended in the z-direction to make them three dimensional. In addition, the waves from Chapter 5 are included in the simulation by the use of Waves2FOAM. It is also necessary to change the initial mesh set-up. This was discovered due to the fact that the previous mesh required the same cell size in between the different blocks in the blockmeshDict. This is not very efficient for the 3D simulation because the number of cells will increase dramatically if the cells around the cylinder are going to be very small. Since the simulation will not work in a good manner by having few cells, it is necessary to build the mesh in a new way. This is described in the next section.

7.1.1 Three-Dimensional Mesh and Initial Domain

The new 3D mesh is built by use of the OpenFOAM utility snappyHexMesh. This utility automatically generate a 3D mesh that contains split-hexahedra and hexahedra cells from surface geometries, CFD-Direct (2019b). The geometry is imported from a CAD (computer aided design) program in either Stereolithography (STL) or Wavefront Object (OBJ) format. For this case, the geometry of the cylinder is made in the free 3D creation program Blender, BlenderFoundation (2019), and imported into a STL file. The big advantage with using snappyHexMesh for this project is that it is very easy to define areas where it is possible to specify mesh refinement levels. According to CFD-Direct (2019b) it uses a robust surface handling with a final mesh quality that can be pre-specified by the user. The mesh generation process includes three main steps:

- Generate geometry file(s) and place them in the *"constant/triSurface"* sub-directory
- Generate a background mesh that the geometry will be placed unto.
- Write a *snappyHexMeshDict* dictionary and place it in the *system* sub-directory of the case

The background mesh can have a coarse grid. For this case, the background mesh is made in by the blockMesh utility and is made as a 3D box with the right dimensions for the entire domain. The dimensions for the domain is the same as for the 2D wave case described before in Section 5.3. The *snappyHexMeshDict* dictionary includes possibilities for control of all the stages of the meshing process including refinements, smoothing, correction factors, etc. A complete overview of all the entries in the *snappyHexMeshDict* can be found in the manual by CFD-Direct (2019b).

Figure 7.1 shows the new mesh. The difference from the previous mesh set-up is that the mesh refinement areas are only around the cylinder, at the inlet, and from the wave crest area and down to the bottom. This enables a more efficient mesh. The refinement factors are increased a bit further from what is shown and the refinement area around the cylinder has a diameter of 40 [m]. The additional input files necessary to run the case; snappyHexMeshDict and surfaceFeatureExtractDict are included in Appendix C.

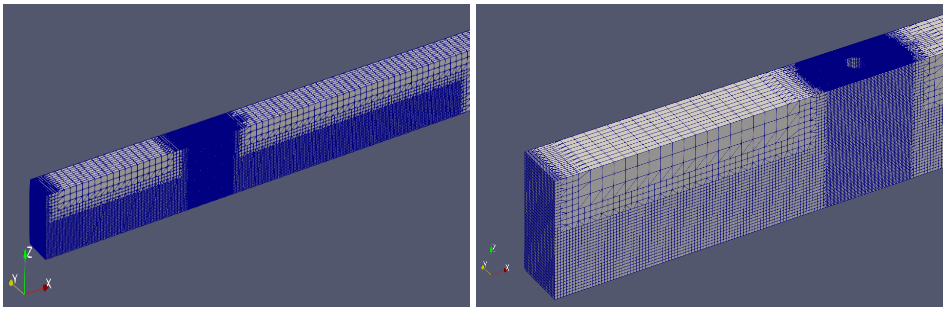

(a) 3D Mesh **(b)** 3D mesh - smaller cells close to the cylinder

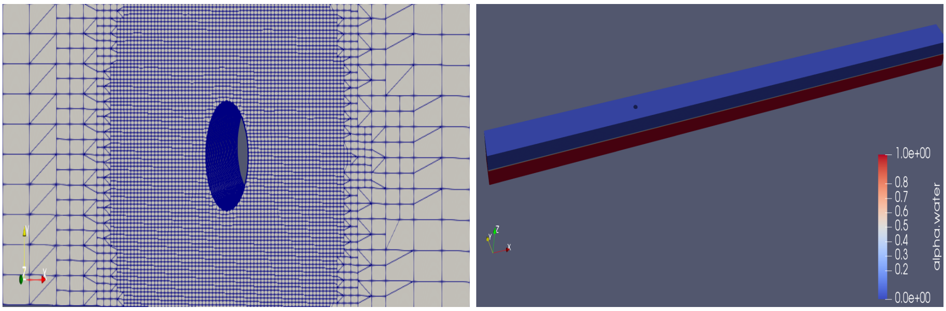

(c) 3D mesh - detailed view around the cylinder **(d)** Initial time step with water and air

Figure 7.1: 3D Mesh

7.1.2 Wave Cases and Input Parameters

The wave cases (WC's) are the same as for the 2D cases. The parameters used are listed in Table 7.1. The same parameters are used for the specifications of water and air (Table 5.2). The simulations are done with laminar conditions (in order to match the 2D simulations) and no turbulence model is included.

Table 7.1: Input parameters and variables, 3D simulations

Case nr	H [m]	T [s]	ΔT	Number of cells	Modifiable Run-time	Tsoft[s]
1	11.4	13	0.0005	≈1315000	no	26
2	13.3	13	0.0005	≈402100	no	26
3	13.3	14	0.0005	≈481500	no	26

The boundaries are the same (inlet, outlet, front, back, bottom and atmosphere), but in addition there is one more boundary for the cylinder. Table 7.2 show an overview of the boundary conditions in use for the 3D simulations.

Table 7.2: Boundary conditions for the 3D wave simulations with the cylinder

Boundary	α	Pressure (p_{rgh})	Velocity (U)
Inlet	zeroGradient	zeroGradient	zeroGradient
Outlet	zeroGradient	zeroGradient	zeroGradient
Atmosphere	inletOutlet	totalPressure	pressureInletOut*
Bottom	zeroGradient	zeroGradient	slip
Front/Back	zeroGradient	zeroGradient	slip
Cylinder	zeroGradient	fixedFluxPressure	movingWallVel

(*pressureInletOutletVelocity)

The functions used for measuring the forces and the wave elevations are still kept in the controlDict. The force function is now measuring the forces and not the force coefficients, similarly as for the simulations in Chapter 6, and the code for the force measuring is found in Figure 6.3. For the wave elevation a similar wave gauge method as for Chapter 5 is in use.

7.1.3 Turbulence Model

The three wave cases are simulated using a laminar model. A fourth simulation is thereafter done including a turbulence model for wave case number one. This is done in order to test how much difference it makes and to investigate the difference in the flow and wake around- and after the cylinder. The turbulence model in use is a RAS model with $k - omega$ constants. The constants are decided by use of the converter by Online (2018) and are listed in Table 7.3.

Table 7.3: Boundary conditions for the 3D turbulent wave simulations with the cylinder

Boundary	k	omega
Inlet	0.0027735	fixedValue
Outlet	zeroGradient	zeroGradient
Atmosphere	zeroGradient	zeroGradient
Bottom	zeroGradient	zeroGradient
Front/Back	zeroGradient	zeroGradient
Cylinder	kqRWallFunction - uniform value	omegaWallFunction - internalField: 0.0175546

The input values, wave parameters, mesh and other boundary conditions are the same as for wave case number one and the turbulence intensity is set to 1% and the turbulence length scale is set to 3 m.

7.2 Results

The mesh is successfully refined around important areas such as the cylinder, inlet and free surface. The final mesh result is illustrated in Figures 7.2 and 7.3. The illustrations clearly show a good structure of the mesh and a gradually refinement closer to the critical areas. All three wave cases use the same mesh set-up and refinement. The only variation is the number of cells in x-direction of the background mesh made in blockMesh.

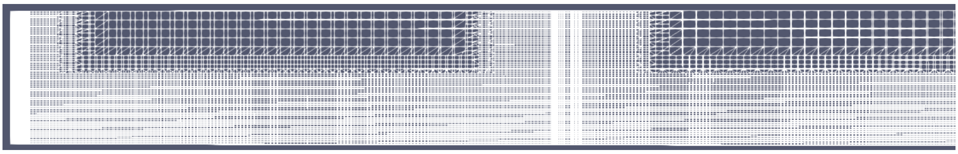

Figure 7.2: 3D mesh details near inlet and cylinder

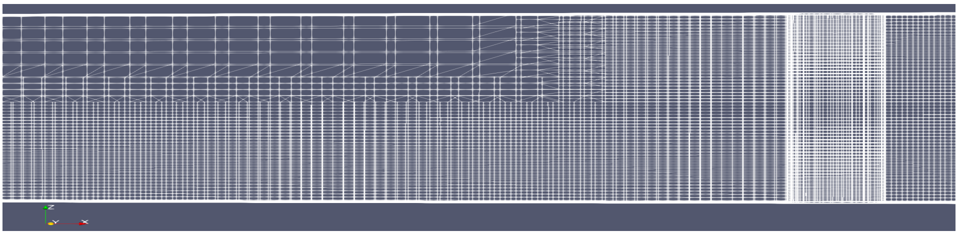

Figure 7.3: 3D mesh details near cylinder

The incoming waves in the domain for the first wave case are illustrated in Figure 7.4. The visualizations of the case show promising results with pressure- and wave behaviour as expected. In order to further validate the wave elevation, a comparison to the 2D generated waves is done in Section 7.3.2. What is common for all three wave cases, is that they all show the expected behaviour with regards to pressure, wave elevation and stream velocity.

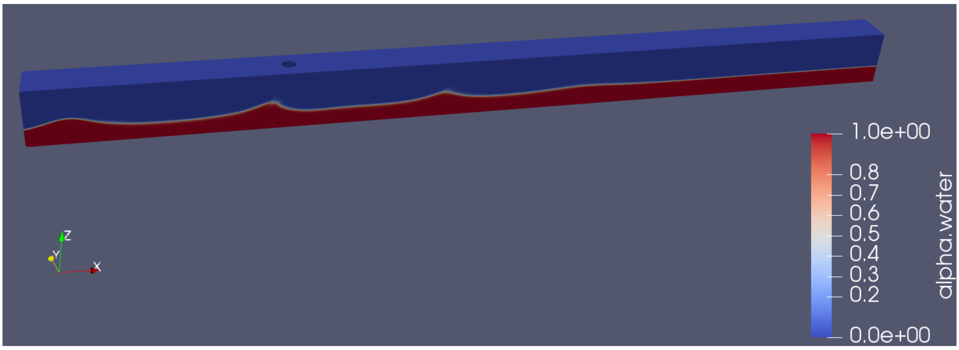

Figure 7.4: Incoming waves at time step 50s for wave case number 1

7.2.1 Wave Case Number 1

The simulated waves for this wave case are illustrated in Figure 7.5 and the measured drag- and lift forces are presented in Figures 7.6 and 7.7. The wave elevation illustrations clearly show the propagation and development of the Cnoidal waves. It is visible that the wave crest travels faster than the trough. The drag forces are in the order of 20000 [kN]. It is visible from Figure 7.6 that steady state is obtained after about 30 time steps. This is the same as for the 2D simulations with unsteady boundary conditions at the inlet. The lift forces are in the order of 100 [kN]. However, it is not clear from Figure 7.7 whether the lift has reached a steady state yet. This was also seen from the 2D simulations. Because of varying inlet velocities, it is not sure how many time steps that would be necessary to simulate in order to see a pattern in the behaviour of the lift forces. It is however visible to see that lift forces are present and are acting on the structure in the transverse wave direction. The magnitude of the forces is compared to the integrated 2D forces in Section 7.3.3.

(a) T = 30s

(b) T = 40s

(c) T = 50s

(d) T = 55s

Figure 7.5: Illustrations of the first Cnoidal wave condition in 3D

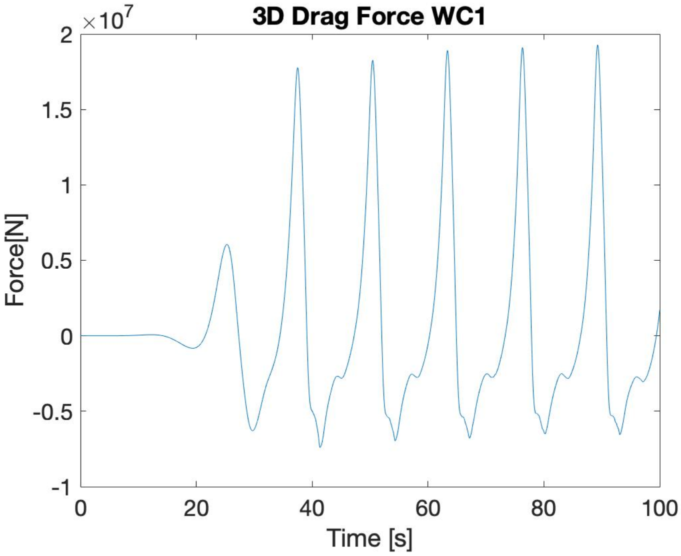

Figure 7.6: Drag force time series from 3D simulation of wave case number 1

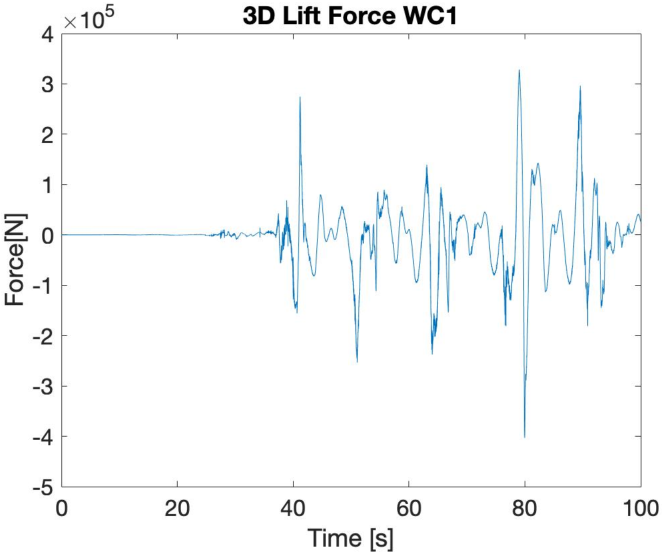

Figure 7.7: Lift force time series from 3D simulation of wave case number 1

7.2.2 Wave Case Number 2

The simulated waves for this wave case are illustrated in Figure 7.8 and the measured drag- and lift forces are presented in Figures 7.9 and 7.10. It is visible from the figures that the waves are a bit steeper than for wave case number 1 and the lift- and drag forces are of approximately the same magnitude. This is with the exception of the largest negative peak in the lift-forces. This simulation is run for 100 time steps in order to investigate whether it is possible to see a clear pattern of the lift force and determine whether a steady state is reached or not. This is still not possible and it is therefore unknown for how long the simulation needs to be run for this to happen.

(a) T = 30s

(b) T = 40s

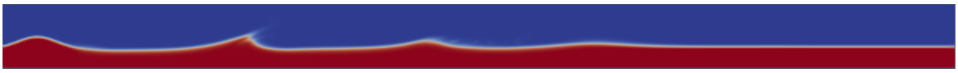

(c) T = 50s

(d) T = 60s

Figure 7.8: Illustrations of the second Cnoidal wave condition in 3D

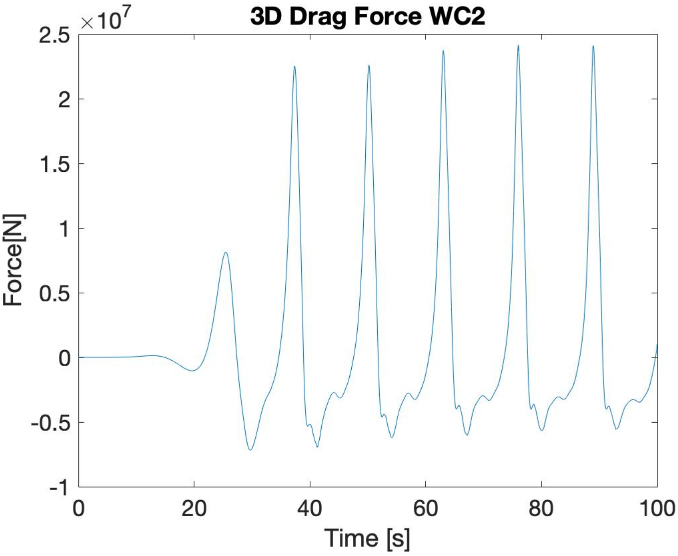

Figure 7.9: Drag force time series from 3D simulation of wave case number 2

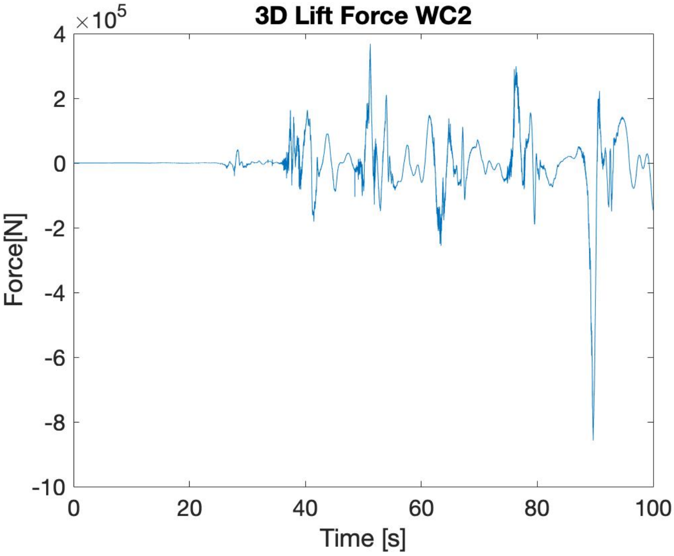

Figure 7.10: Lift force time series from 3D simulation of wave case number 2

7.2.3 Wave Case Number 3

The simulated waves for this wave case are illustrated in Figure 7.11 and the measured drag- and lift forces are presented in Figures 7.12 and 7.13. The first thing to notice about the wave elevation illustrations is that the peaks are a bit steeper than for wave case number 1 as they are on the verge of breaking. This is as expected due to the fact that both wave case number 2 and 3 both have the same relative steepness of $H/d = 0.67$ which is higher than for wave case number 1 where $H/d = 0.57$. The drag-forces have peaks of the order 25000 [kN] and have also reached steady state at about 30 time steps. The lift forces are maximum $\pm$ 100-250 [kN]. There are major variations in the magnitude of the lift forces, and it is not possible to say anything about the state with this limited number of time steps. It is however visible that the initial phase is over after about 30 time steps for the lift forces as well. It is not sure how many time steps that are necessary to achieve a steady state.

(a) T = 30s

(b) T = 40s

(c) T = 50s

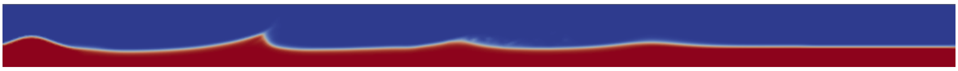

(d) T = 55s

Figure 7.11: Illustrations of the third Cnoidal wave condition in 3D

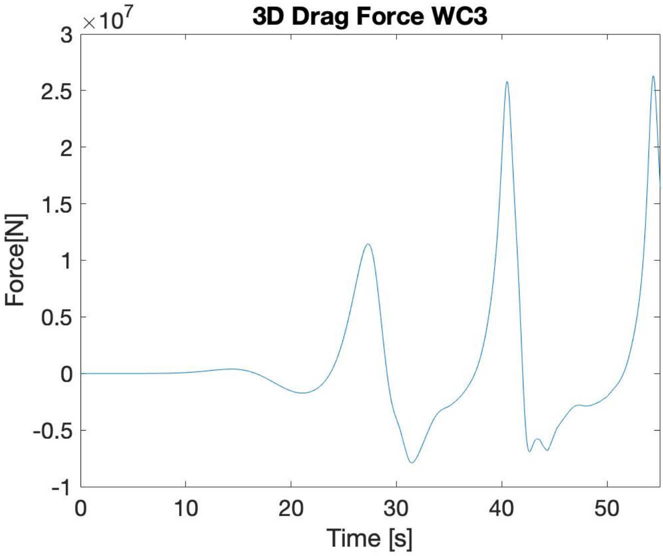

Figure 7.12: Drag force time series from 3D simulation of wave case number 3

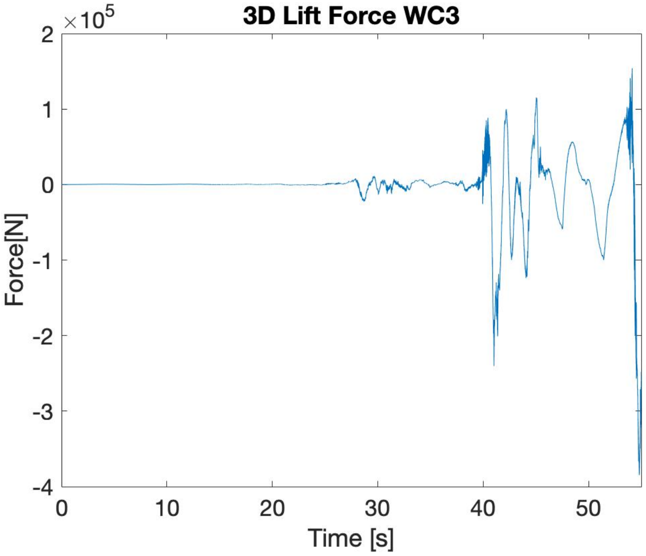

Figure 7.13: Lift force time series from 3D simulation of wave case number 3

7.2.4 Practically Zero-Viscosity Case

Figure 7.14 show the results from the 3D simulation of WC 1 with practically zero viscosity (100 times decrease in viscosity in comparison to the real viscosity). This is the only change done for this simulation. The differences in the results between zero- and normal viscosity are further presented and discussed in Section 7.3.1.

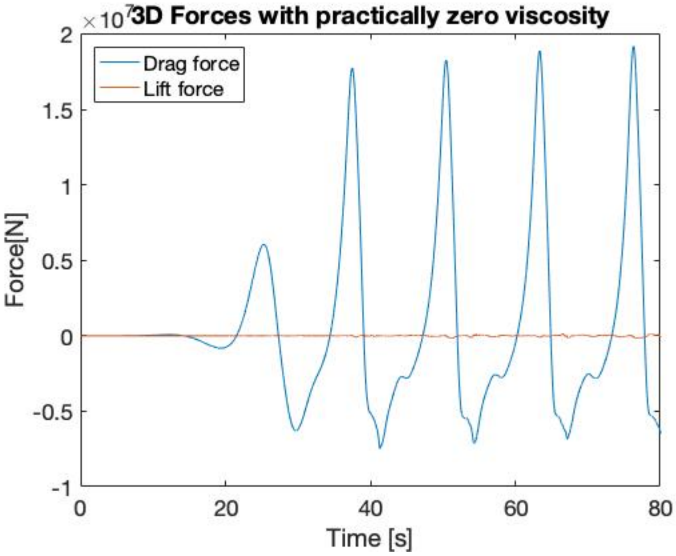

Figure 7.14: Drag- and lift force from 3D simulation of WC 1 with practically zero viscosity

7.2.5 Wave case 1 - Turbulent Simulation

The simulated waves for this wave case are illustrated in Figure 7.15 and the measured drag- and lift forces are presented in Figures 7.16 and 7.17. It is clear from Figure 7.15 that the turbulence model strongly affect the wave propagation. The wave is not propagating in the same way as for the laminar condition, as it is forming a steeper wave top and then decreasing in size. This can be a type of breaking behaviour and results in lower waves passing the cylinder. The waves are illustrated at T = 35, 38 and 40 [s] in order to illustrate what is happening with one wave as the same behaviour occurs for all the waves generated at the inlet zone. The forces presented in Figures 7.16 and 7.17 are further discussed along with the flow features in Section 7.3.6.

(a) T = 35 [s]

(b) T = 38 [s]

(c) T = 40 [s]

(d) T = 50 [s]

Figure 7.15: Illustrations of the first Cnoidal wave condition in 3D including turbulence model

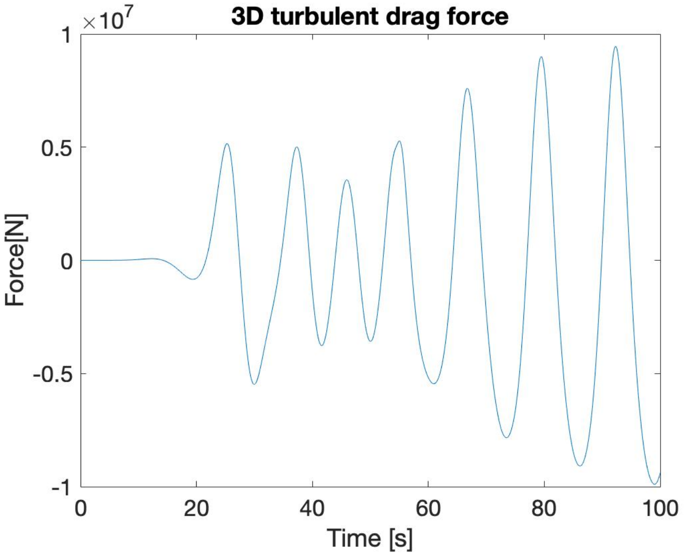

Figure 7.16: Drag force time series from 3D simulation of wave case number 1 including turbulence model

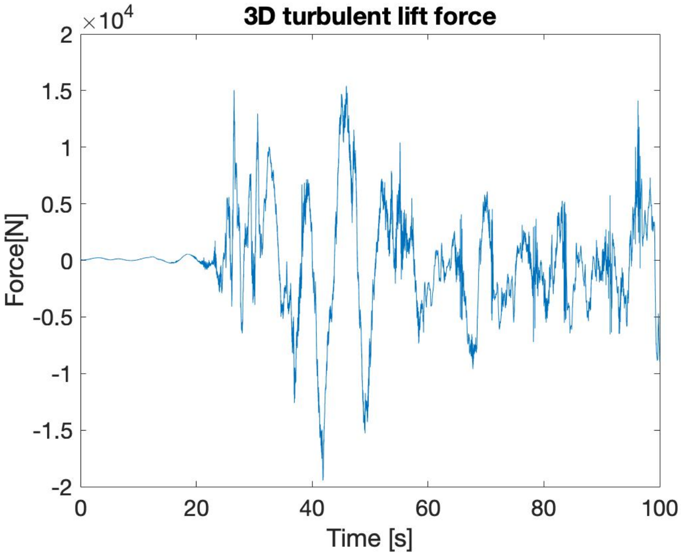

Figure 7.17: Lift force time series from 3D simulation of wave case number 1 including turbulence model

7.3 Discussion

The cell sizes in use for these simulations are not properly investigated and a convergence test is not executed due to limited available time. In order to properly test the set-up including domain size, inlet- and outlet zones, cell size and refinement sizes, a sensitivity analysis should be done for each one of the parameters in order to optimize the set-up. This way, more accurate results can be obtained or computational time can be saved. However, it takes a lot of time to discover how to best optimize the set-up for each individual case. The quality of these 3D results is therefore evaluated based on references and the comparison to the 2D results.

7.3.1 Comparison Between Practically Zero- and Real Viscosity

Figures 7.18 and 7.19 show the variations in the results with different viscosities; the real viscosity and a practically zero viscosity. It is visible that the viscosity influence the lift forces. Decreased viscosity means decreased lift force. This fits well with results from other studies even though these other studies are a bit different and focus on other aspects than this thesis. See for example the work of Williams et al. (1996) where they also found an increase in the lift for increasing viscosity.

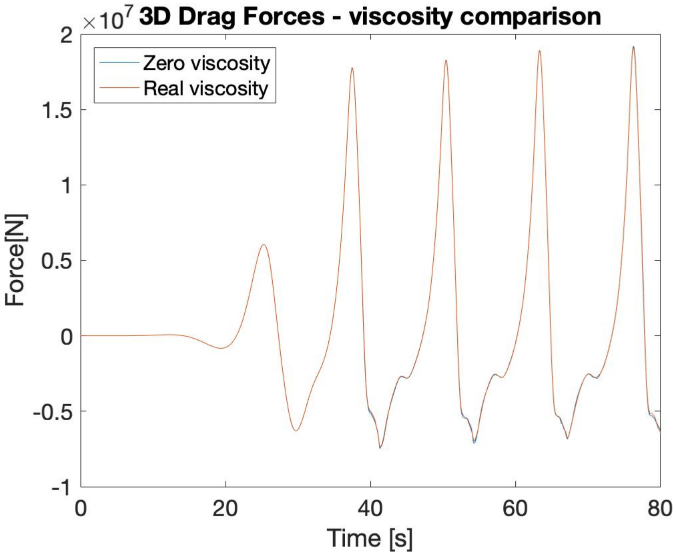

Figure 7.18: Drag comparison between different viscosities

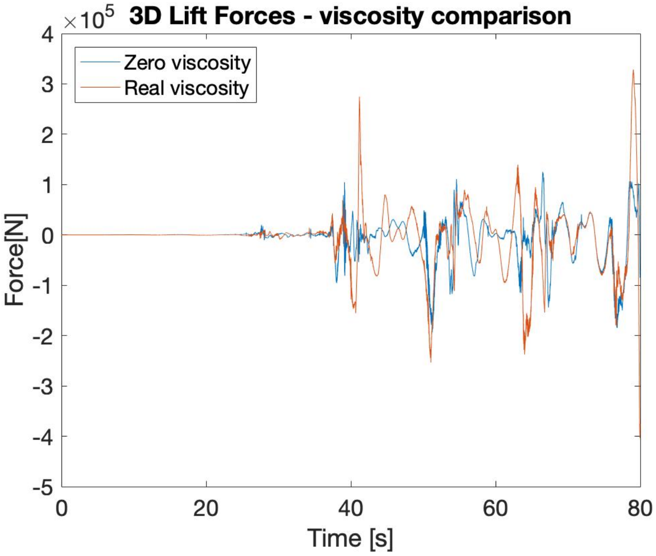

Figure 7.19: Lift comparison between different viscosities

It is more difficult to sight the differences in the drag results. A more detailed view is provided in Figure 7.20. Note that the forces are scaled to [MN]. Scaling to this for the lift forces as well, they turn out as illustrated in Figure 7.21. Now it is more clear that the differences are of the same significance and that both the drag- and lift forces decrease with decreasing viscosity. The decrease is however minimal (< 3%).

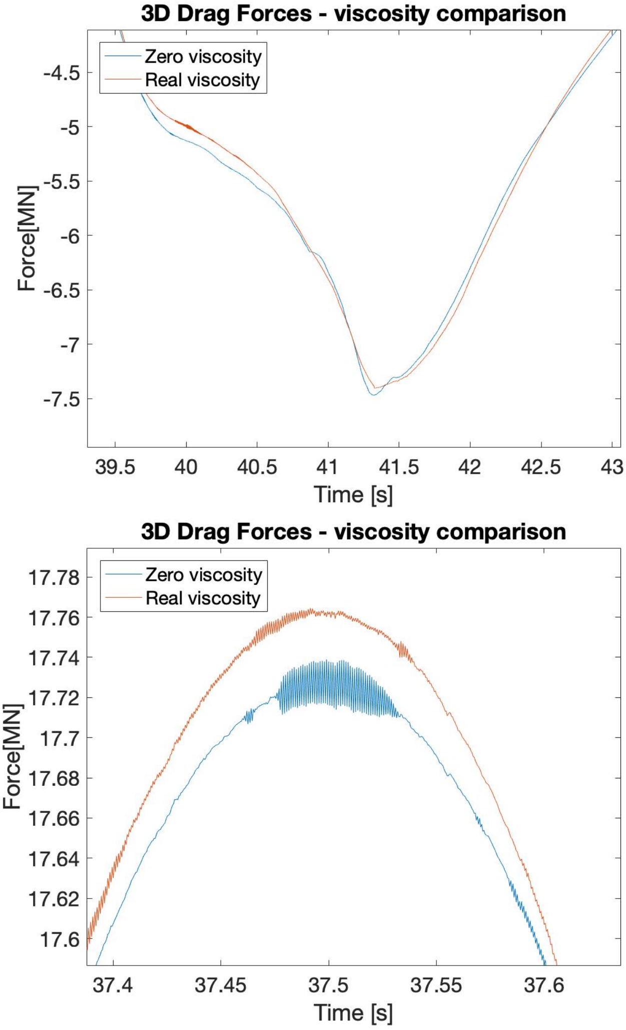

Figure 7.20: Details - Drag comparison between different viscosities

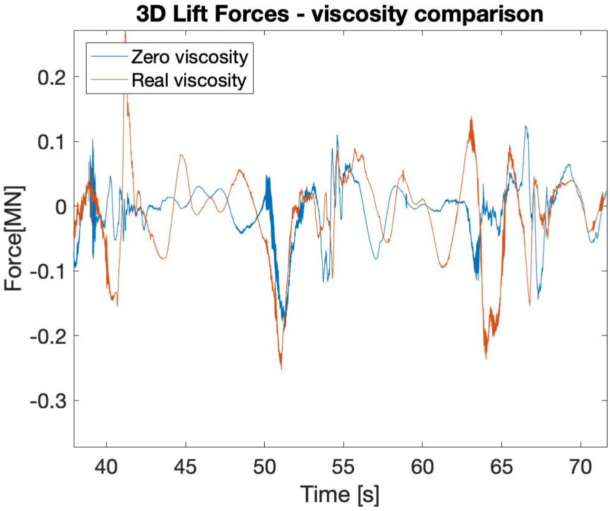

Figure 7.21: Details - Lift comparison between different viscosities

Figure 7.22 show the viscous contribution to the total force in x- and y- directions for the two viscosity cases. It is visible that the decrease in total force comes from the decrease in the viscous components. Also notice the scaling in this figure as the forces are in [N], and therefore correspond well to the decrease in total force.

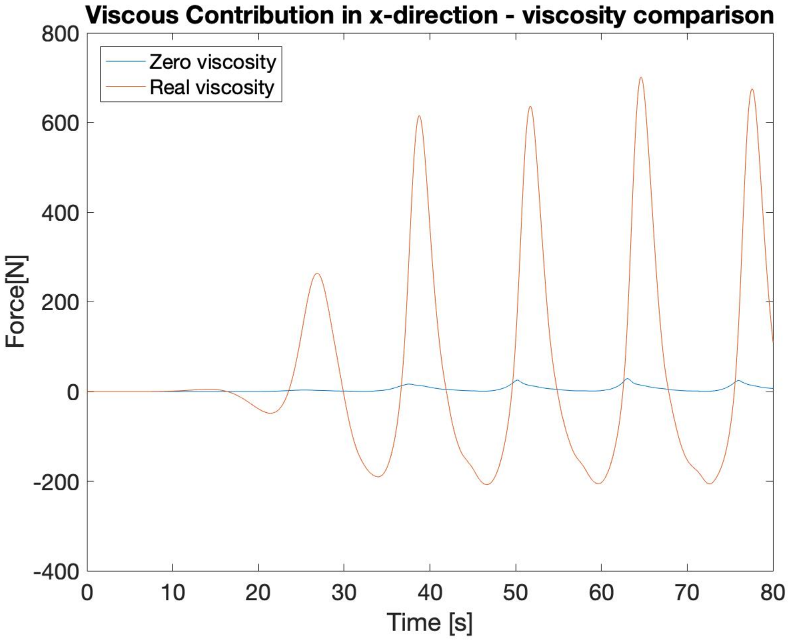

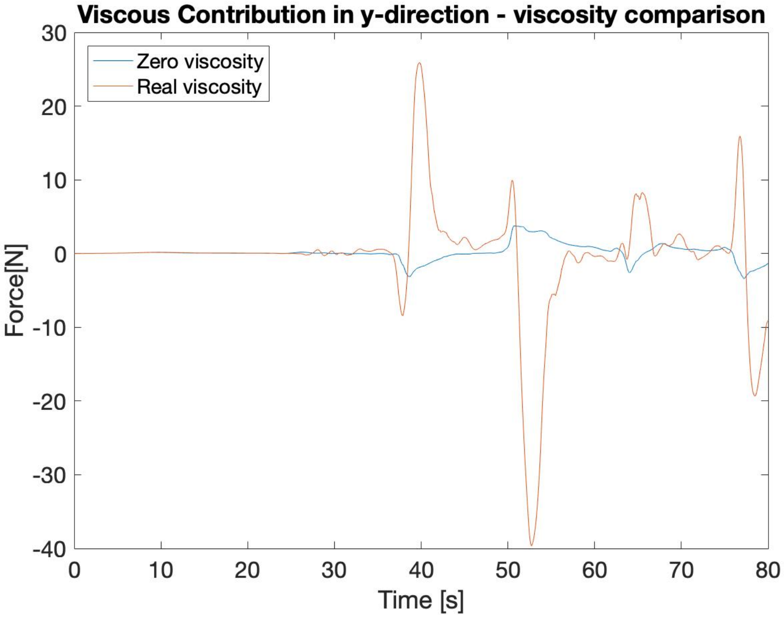

Figure 7.22: The viscous contribution to the forces

7.3.2 Wave Comparison Between 2D- and 3D Simulations

The waves generated in the 3D simulations have the same wave conditions as for the 2D simulations. It is therefore of interest to check whether the two simulation types creates the same wave elevation. The 2D waves were successfully compared and verified to theoretical estimations of Cnoidal waves. The aim for the 3D waves is therefor to be as similar as possible to the 2D waves. Figure 7.23 show waves generated by the 3D simulation with wave condition number 1. Figure 7.24 show the same wave condition generated with a 2D simulation. The two figures are quite similar, but it seems like the 2D waves have developed a bit more and are a bit closer to breaking than in the 3D simulation.

Figure 7.23: Wave elevation at time step 50s - 3D simulation, seen from the side

Figure 7.24: Wave elevation at time step 50s - 2D simulation

The expected result is to have identical wave profiles. The input into the wave-generating functions is the same, and the program uses the same solvers for doing both types of simulations. However the cell size and the build-up of the grid is different for the 3D simulations in comparison to the ones in 2D. In 2D, the cell size is smaller because of the possibility to have more cells in x-direction while still have much less cells in total, because there is one dimension less. This means that the cells can capture more of the "real" conditions, and it may be that the 3D solution miss something because of use of bigger cells. However, the wave results are quite similar and as previously stated, also similar to the analytic wave solution. It is therefore safe to say that the program successfully generates Cnoidal wave conditions.

7.3.3 Comparison to Integrated 2D Results

Figures 7.25 and 7.26 show the drag- and lift forces from the integrated 2D result and the 3D result together. As clearly seen from the Figure 7.25, the 3D simulations give higher drag forces than the integrated 2D simulations. The drag peaks are approximately four times higher which can be seen as a significant difference. When it comes to the lift forces it is the other way around. The integrated 2D simulations give higher results. The peaks are significantly higher in magnitude (two to four times higher approximately). The jumps in the time series from the integration are large and the results show a big degree of variation. It was expected to have results that were more equal in magnitude. The patterns are the same in both figures as for where the peaks are. This is due to the fact that the forces peak during a wave crest and a wave trough (negative peaks). However, it seems like the 2D simulations miss out on some aspect of capturing everything of the 3-dimensionality.

Other errors may also have occurred for these 2D simulations, as previously discussed in Section 6.4. The difference in the flow around the cylinder can also give more information about the equalitites and difference in the simulations. This is addressed next.

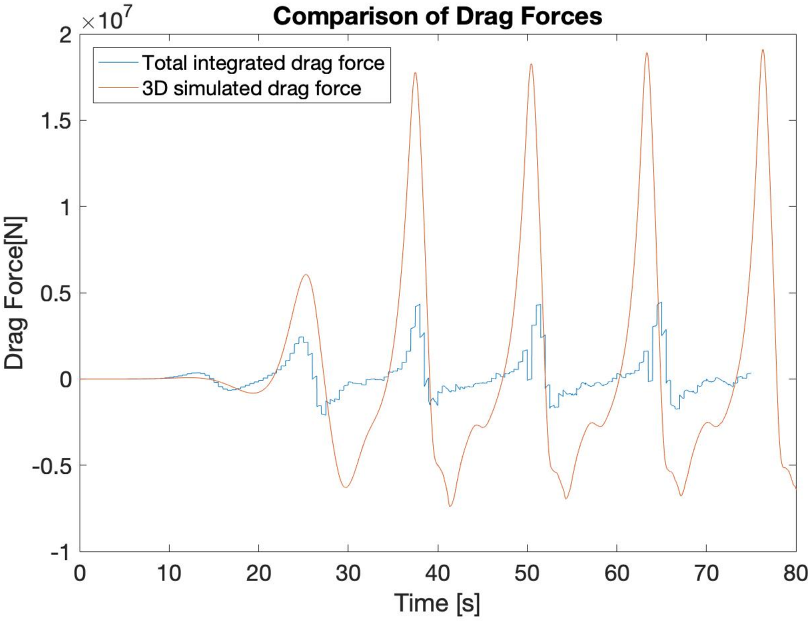

Figure 7.25: Comparison of drag forces between integrated 2D results and simulated 3D results

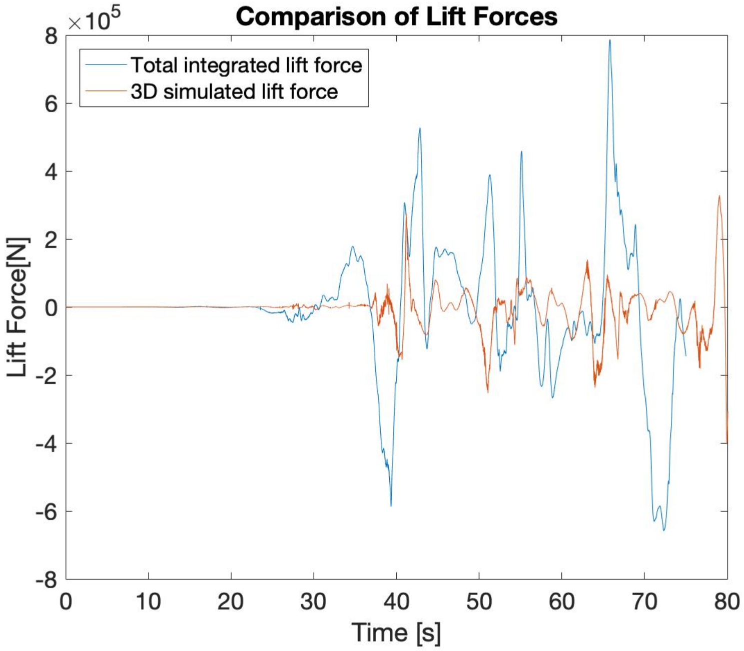

Figure 7.26: Comparison of lift forces between integrated 2D results and simulated 3D results

Flow features: From the visualizations of both the 2D- and 3D simulations it is not possible to see clear separation behaviour. This way, the flow features are not influenced significantly by three-dimensionality. There are lift forces present in both simulation types, but they do not show steady state behaviour. This means, that at a later stage in the simulations it can be possible to see separation. Typically, this can happen after running the simulations for a much longer period of time. Visualizations of the stream velocity in the waves in the 3D simulations are illustrated in Figure 7.27.

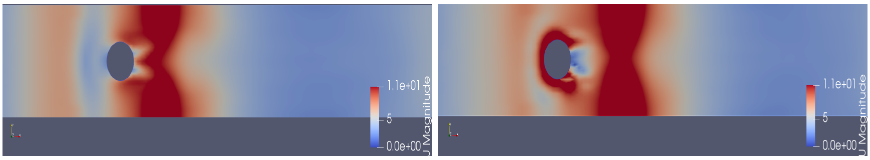

(a) t=39 [s] **(b)** t=40 [s]

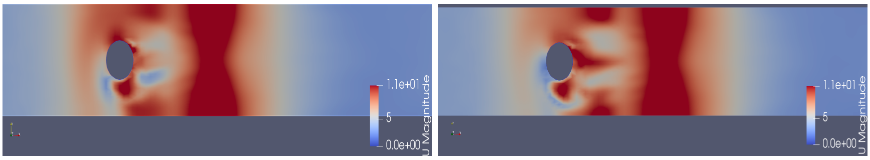

(c) t=41 [s] **(d)** t=41.5 [s]

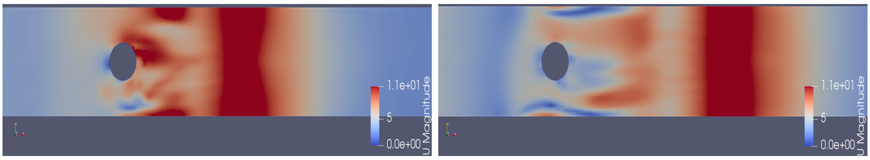

(e) t=42 [s] **(f)** t=44 [s]

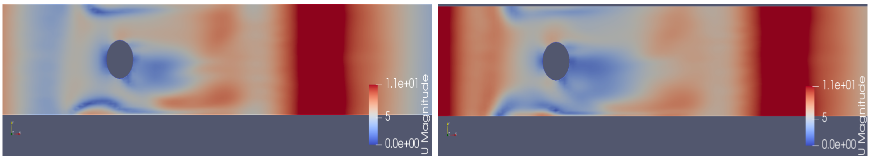

(g) t=45 [s] **(h)** t=46 [s]

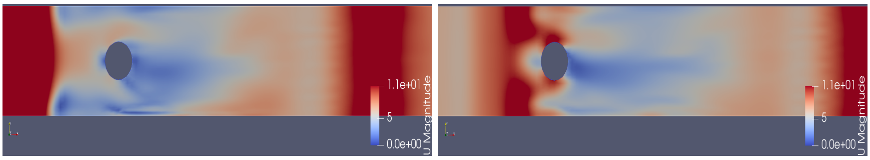

(i) t=47 [s] **(j)** t=49 [s]

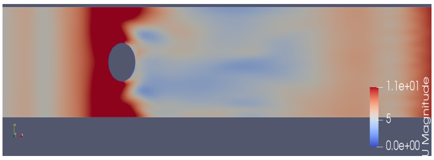

(k) t=50 [s]

Figure 7.27: Water flow around the cylinder in the xy-plane - taken from the 3D simulation with WC1

Figure 7.27 show the flow at the cross-section for one wave period. This same period is illustrated for the 2D simulation at z=0 [m] in Figure 7.28.

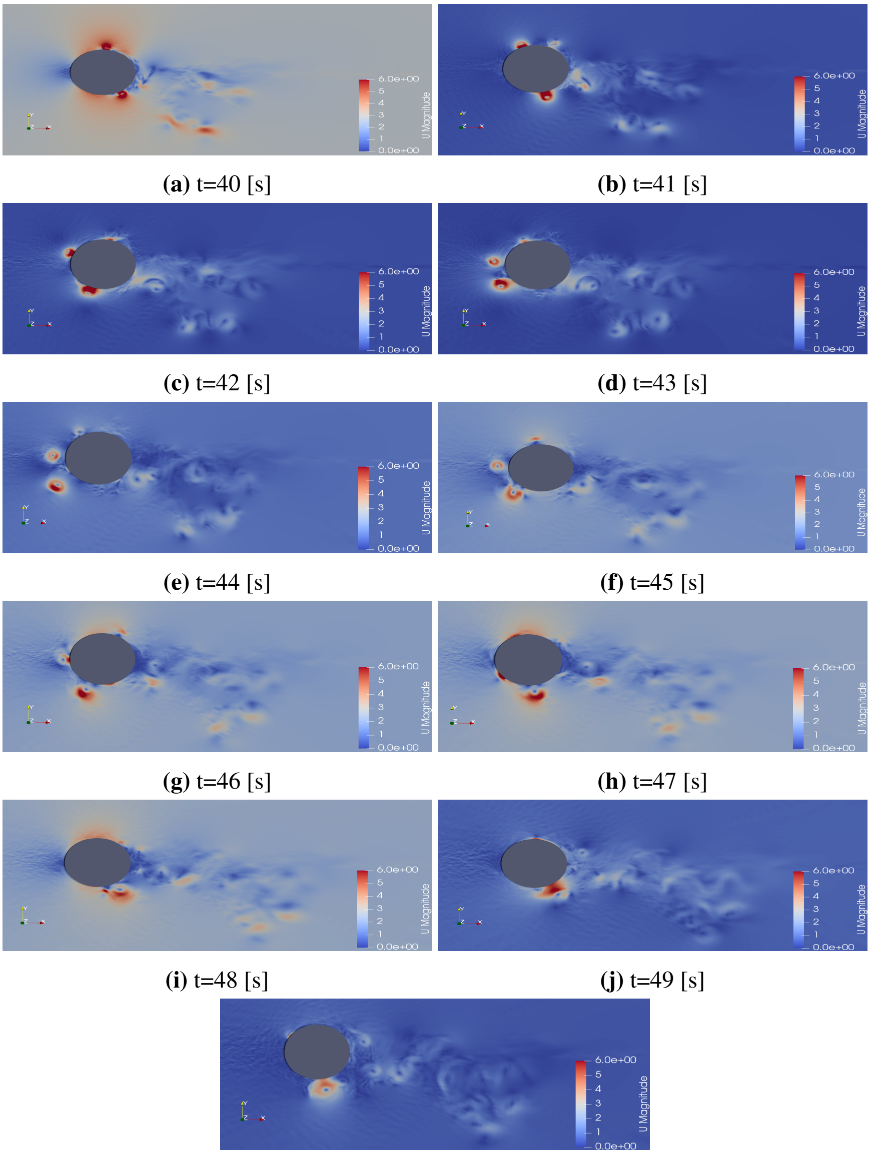

(a) t=40 [s] **(b)** t=41 [s]

(c) t=42 [s] **(d)** t=43 [s]

(e) t=44 [s] **(f)** t=45 [s]

(g) t=46 [s] **(h)** t=47 [s]

(i) t=48 [s] **(j)** t=49 [s]

(k) t=50 [s]

Figure 7.28: Water flow around the cylinder in the xy-plane - taken from the 2D simulation at z=0 [m]

It is visible that the flow around the cylinder in the 2D simulation have more vortexes but it does not separate evenly from side to side. It seems like the flow separates more from one side than the other. The flow picture in the 3D simulation is different in a way that it is symmetric across the cylinder and it is possible to see the beginning of a flow separation pattern. The abnormal behaviour in the 2D simulation may be caused by the unexpected pressure differences and the very high pressures in the simulation as shown in Figure 7.29. The pressure vary strongly for every time step while in 3D the pressure follows the wave. Figure 7.30 show that the pressure in the 2D simulation is a lot higher than in 3D, here shown in x-direction. As mentioned before, this may be caused by the use of a wrong solver or scheme. It is therefore recommended to investigate further the use of different schemes, solvers and boundary conditions in order to improve the quality of the 2D results with unsteady boundary condition at the inlet.

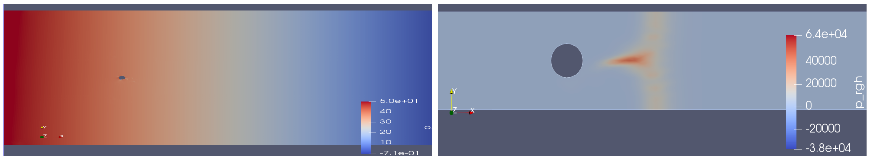

(a) 2D, t=42 [s] **(b)** 3D, t=41 [s]

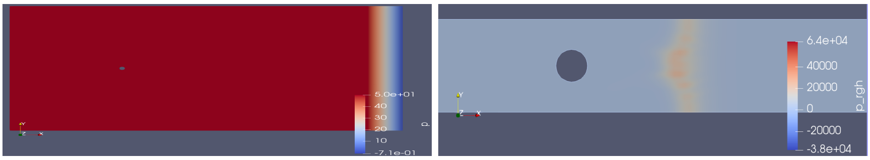

(c) 2D, t=44 [s] **(d)** 3D, t=43 [s]

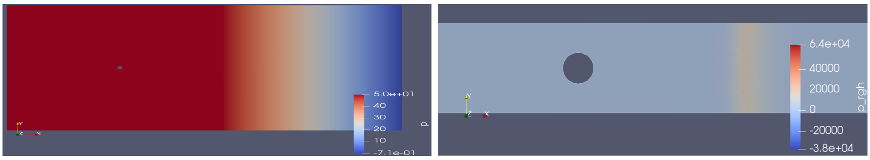

(e) 2D, t=47.5 [s] **(f)** 3D, t=44 [s]

Figure 7.29: Pressure around the cylinder - a comparison between the 2D and 3D simulations

CPU time and number of cells: The CPU (central processing unit) time is a lot shorter for the 2D simulations with unsteady boundary condition. For most of these simulations it is sufficient with a simulation time of around 6-12 hours (depending on the number of cells) while the full 3D simulations require at least 30 hours for a number of cells above 1000000. For simulating around 100 time steps for the 3D simulations, the number of cells is decreased approximately 50%, resulting in only 15 hours (approximately) simulation time (this of course depends also on the number of cores in use). In the end, it is clear that the simulation time is strongly dependent on the number of cells both in terms of capturing the problem at hand and when it comes to the necessary time step. A big number of cells requires a smaller time step meaning that the simulation time will increase. Running a 2D simulation requires less than half of the number of cells in comparison to an equivalent 3D simulation, meaning that the CPU time also reduces dramatically.

It is difficult to certainly state the accuracy of the 2D simulations in comparison to the 3D ones. There are some errors in the 2D simulations when it comes to the water level on the cylinder. Here, the cylinder is constant submerged in water while in reality this is not

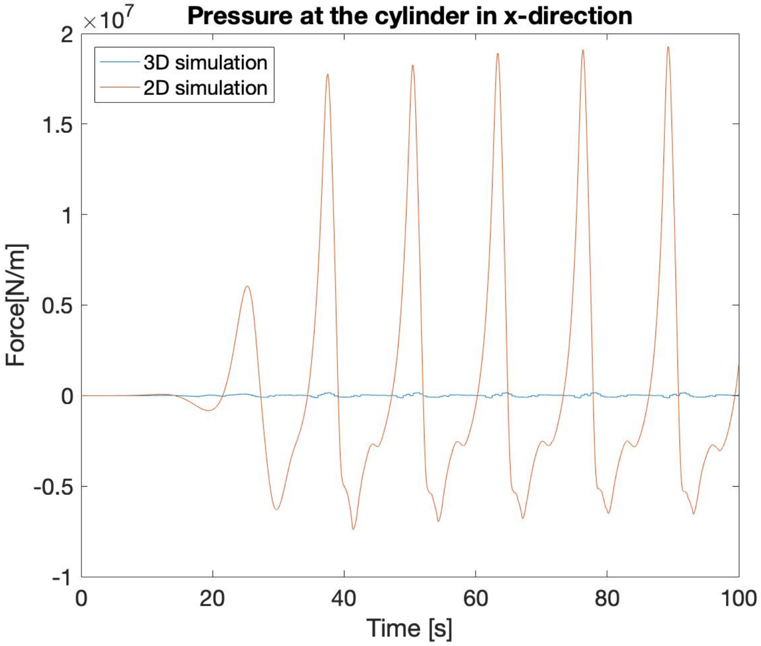

Figure 7.30: Pressure in x-direction plotted over time

the case as the wet surface varies with the wave. However, the simulation in itself should be more accurate for the 2D cases, as the grid is much finer. If the set-up is improved in terms of schemes and boundary conditions it would be more efficient to run several of this type instead of running a full 3D simulation. Since a convergence study has not been performed for the 3D case it is not possible to say anything about how much difference this makes, but the number of cells in x-direction is more than two times higher for the 2D simulations in comparison to the finest 3D simulation.

7.3.4 Wave Run-Up Around the Cylinder

As mentioned earlier, Kristiansen and Faltinsen (2017) studied higher wave loads on a cylinder in finite water depth experimentally. In their study they find that their theoretical FNV model do not describe discrepancies that occur in the experiments with very steep waves. Here they find a distinct wave run-up at the rear of the cylinder. They also perform a 2D simulation in order to test whether this is visible and to qualitatively explain this local run-up. With this thesis also investigating steep waves in shallow water it was also expected to find some of the same higher order behaviour. And as can be seen in Figure 7.32 this is actually the case. In Figure 7.32c and 7.32e this rear run-up is visible. This occur for steep waves with long wavelengths according to the experiment of Kristiansen and Faltinsen (2017). This fits well with the 3D numerical experiments conducted in this thesis. High pressure locally at the rear of the cylinder can be the explanation for the local rear run-up. Figure 7.29b show this locally observed pressure in the back of the cylinder in the beginning of the wave period (wave period starts at t=39 [s]). This pressure can be due to vortical structures that comes from flow separation. This was also observed by Kristiansen and Faltinsen (2017) by doing a 2D LES simulation of a cylinder. The alpha coefficient scale in use for the wave-run up illustrations is seen in Figure 7.31 and the illustrations are taken by making a contour plot and contouring by the alpha coefficient with a value range of 0.5 (still water level).

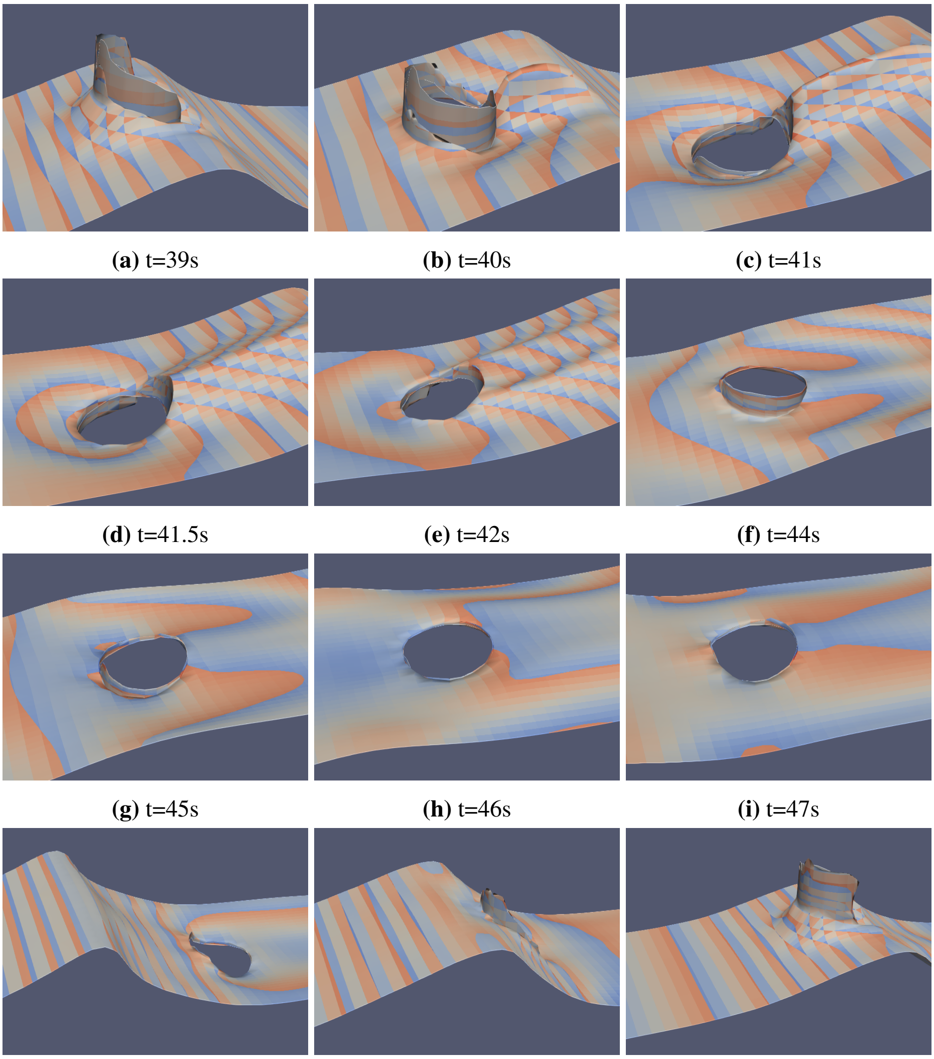

(a) t=39s **(b)** t=40s **(c)** t=41s

(d) t=41.5s **(e)** t=42s **(f)** t=44s

(g) t=45s **(h)** t=46s **(i)** t=47s

(j) t=49s **(k)** t=50.5s **(l)** t=52s

Figure 7.32: Wave run up in front and in back of the cylinder - taken from 3D simulation with WC1

7.3.5 Domain- and Cell Size

The mesh in use for the 3D simulations is made specifically to match this wave case. The length of the domain is made in order to fit the wave lengths. The inlet- and outlet areas have dimensions specified to include $1 \cdot \lambda$ and $1 \cdot \lambda$. This is assumed to be sufficient as the model has proven to be able to generate and absorb the waves without difficulties. It has also been documented that having a smaller outlet zone has also been sufficient for some cases. This was tested by for example Arreba (2017) and Khalid (2016) where they used one wavelength for both the inlet and outlet. The domain size in z-direction is also assumed to be of an adequate size, as the water level and water depth is chosen to be equal to the actual water depth at site. The domain left for the air is chosen to be $2 \cdot h$ and should be more than enough space for the free surface and to not influence the solution. The domain breadth is chosen somehow arbitrarily. It was important to not have a very wide domain in order to save computational time. On the other hand, the side walls of the domain should not influence the wave propagation and the solution. This way, the breadth had to be much wider than the cylinder. The boundary conditions at the front and back boundaries are also changed to slip for this simulation and should let the waves propagate without interfering.

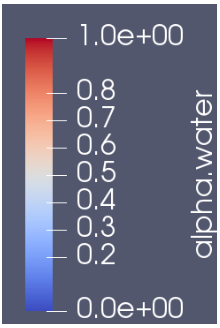

Figure 7.31: Alpha coefficient scale

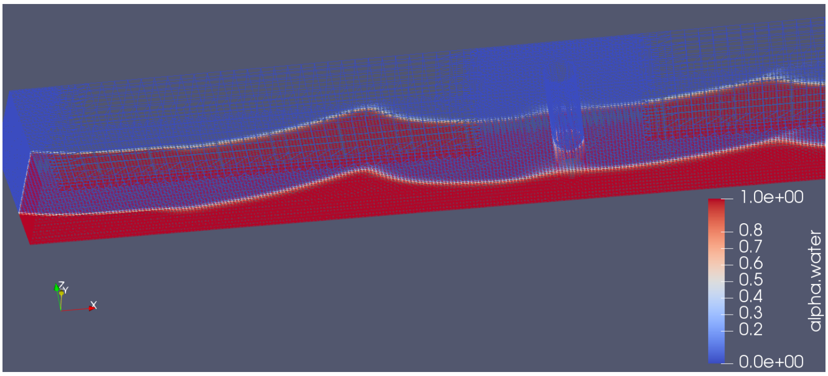

Figure 7.33: Illustration of wave elevation including the grid cell size

The cell size and refinement level around the inlet, cylinder and free surfaces are all very important factors to consider. Since sensitivities have not been tested, some comparisons to other studies are made. In the work done by Khalid (2016), a mesh without any refinements is used for a 3D case. To have a fine grid throughout the mesh gives a high number of cells. In his study, more than 3.3 million cells are used for a domain with cell sizes 2 x 1.25 x 1.75 [m]. This gives in x-direction a number of 156 cells per wavelength in his case. In comparison for this study, there is about 55 cells per wavelength. This is a much smaller number and it may be that a test should have been carried out to check for result-differences by use of increased number of cells. The number of cells in z-direction is important for the results in relation to the wave height and measurements of the velocities in the waves. In a study conducted by Wang et al. (2018), multi-directional wave simulations are carried out. In their experiments, several tests are conducted with the same wave condition but with varying cell size. They find that the cell size affect the significant wave height, but to a limited degree. Simulations with a grid where the cell size, dx, measure $3dx = H_s$ give good results. This means that there are three cells to measure the wave height. For the 3D cases investigated in this paper, there are approximately 4 cells to measure the wave height, $4dx = H_s$. According to this, the number of cells in z-direction should be sufficient. According to the study by Wang et al. (2018), they use the same cell size in every direction for good results. This is a bit different from what is done in this thesis, as the breadth is smaller than the depth in the domain. This concludes in more cells in y-direction than in z-direction and the amount in y-direction is therefore assumed to also be sufficient.

7.3.6 Turbulent vs Laminar Models - 3D

Figure 7.34 show the flow around the cylinder in the xy-plane for one wave period in time. It is seen that the water stream velocity, U, is much smaller than for the laminar 3D simulation with the same condition. This is due to the smaller propagating waves as shown earlier. This makes for no visible separation as the lift forces are quite small. The difference in the forces are shown in Figures 7.35 and 7.36. The smaller magnitude in the lift confirms the absence of the separation of the flow. The diminishing of the drag force can also be seen as a result of the smaller wave impact due to the strange wave behaviour in this case. To the knowledge of the author, there are no other public cases done in OpenFOAM that include both generation of waves by waves2FOAM and turbulent conditions. It was therefore unsure what result to expect. The choice of turbulence parameters and turbulence model can also have influenced the results as it may be that they should have been adjusted to better fit the wave condition. It is recommended to further investigate the behaviour of the propagation of waves in turbulent conditions numerically and to verify a model based on comparisons to experiments of the same weather condition.

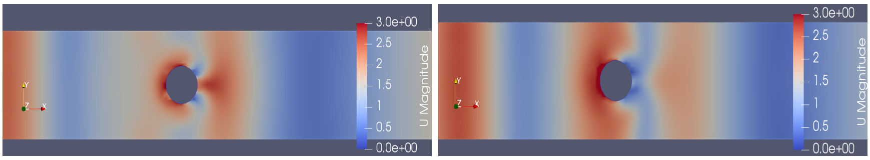

(a) t=39 [s] **(b)** t=40 [s]

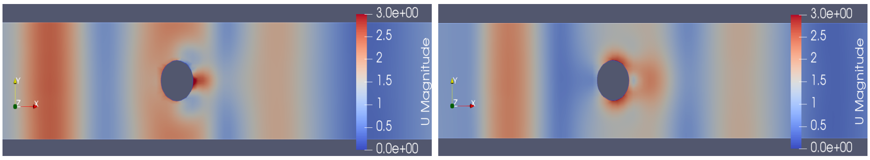

(c) t=41 [s] **(d)** t=42 [s]

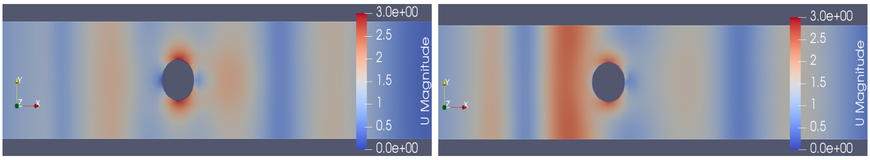

(e) t=43 [s] **(f)** t=44 [s]

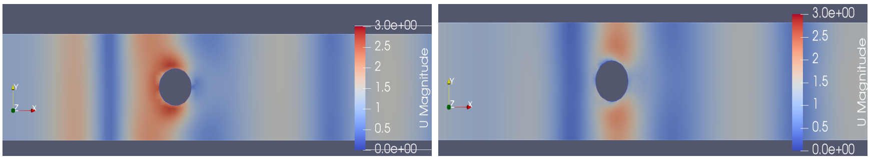

(g) t=45 [s] **(h)** t=46 [s]

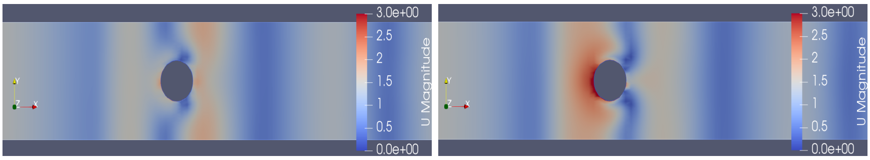

(i) t=47 [s] **(j)** t=48 [s]

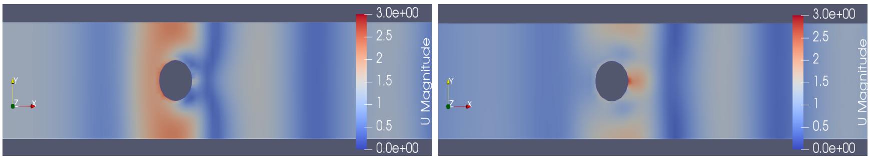

(k) t=49 [s] **(l)** t=50 [s]

Figure 7.34: Water flow around the cylinder in the xy-plane - taken from the 3D simulation with WC1 and turbulent conditions

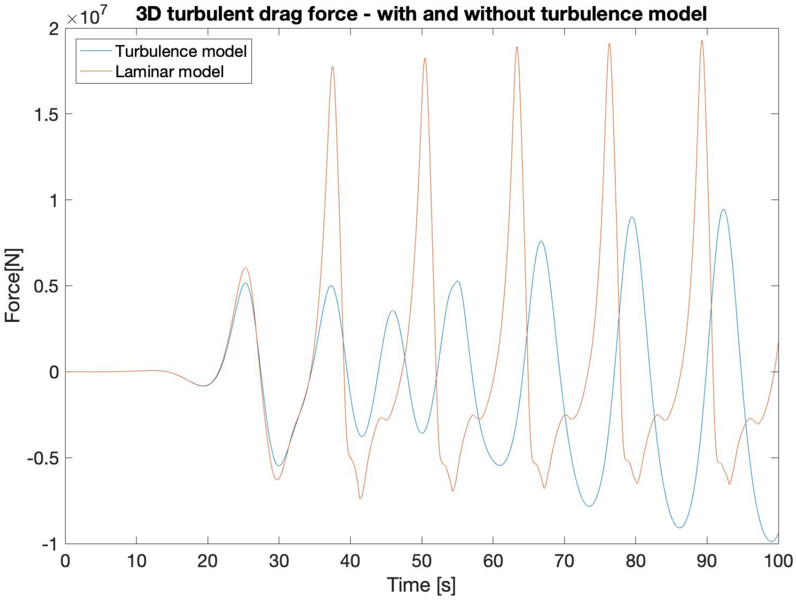

Figure 7.35: Laminar and turbulent drag force from 3D simulation with WC 1

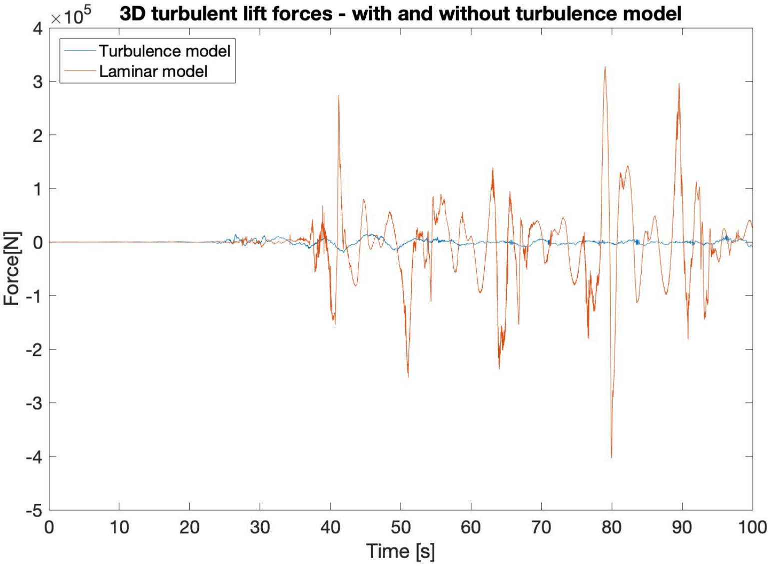

Figure 7.36: Laminar and turbulent lift force from 3D simulation with WC 1

7.3.7 General Discussion

Structural matters: When testing a marine structure for impacts under extreme condition it is often natural to check for coherence with natural periods and such. Also, as mentioned before, there will be transverse moments from the lift force. It is therefore necessary to investigate further additional damping than that from the WT. This is outside of the scope for this thesis, but is of interest for further work with this type of structure.

Computational time and power: These simulations are all run in parallel by a supercomputer, hence the computational time is less than what is the case for many others. Running the cases on 48 nodes enables efficiency while at the same time obtaining the accuracy. For the industry this means that there are demands for the computational power that needs to be available when doing especially 3D simulations. However, computational power is becoming more and more available and many can even have in-house computers solving these tasks. This makes the world of CFD more open and available to more people and makes for a good condition for further development of software and models.

Short-crested waves: The wave heading measurements from site show that the main heading of the waves is west-southwest, and the extreme events occur with west to northwest directions. Only including one direction in the extreme wave conditions meant for this simulation to only include long-crested waves. Short-crested waves are therefore not included, but can be of interest to investigate at a later stage.

7.4 Summary

In this chapter, the set-up, method, results and some discussion sections concerning the 3D simulations in OpenFOAM are included. The simulation required a new mesh with several refined areas with smaller cells in order to work. This new mesh is made with the mesh utility snappyhexMesh. Else, the set-up from the previous simulations done in Chapter 5 and 6 are combined and extended to include a full 3D simulation including both waves and the cylindrical structure that represents the monopile for the wind turbine. The conditions are kept as they are on the actual site with accurate water depth (20 [m]) and actual extreme wave conditions. This made the simulations complicated. The wave formation concur well with the 2D waves generated in an empty pool. The results document to some extent conformity with the integrated 2D results. However, in general the loads appear to be increased in the 3D simulations and the flow patterns around the cylinder show distinctive behaviour. In addition, wave run-up is detected for the 3D simulations. The CPU time and the cell sizes in comparison to the 2D simulations is higher and bigger. Laminar conditions are used for the majority of the simulations. One 3D case is tested with turbulent conditions. The 3D turbulent case give results varying relative to the corresponding laminar 3D case. Some discrepancies are visible including less lift-force and no vortex shedding. The wave profiles are quite different as the turbulent waves show more of a breaking pattern and the waves reaching the cylinder are therefore of smaller heights.

Chapter 8

Conclusion

This thesis presents the work done to fulfill the objective of investigating a bottom-fixed monopile wind turbine interacting with shallow water waves. The basis of the work is made by conducting a literature study and documenting previously done work. The problem is defined by the wind turbine's geometry and a suitable location. The environmental parameters at the site are presented and define the scope of the project. In this sense, the state of the art of the problem is defined and the range of relevant parameters is discussed and summarized to be meteorological variables (such as wind), water- and sea bed- related variables and joint characteristics. A deterministic wave-modelling is selected and use a Cnoidal wave theory to represent the waves. Three main wave conditions are chosen for further investigation. All three wave cases are typical waves that can be described by Cnoidal wave theory. In order to proceed with the project work, the necessary background theory is investigated and documented.

The numerical method selected is a CFD approach and the solver in use is OpenFOAM. The tool and its basic assumptions are investigated and documented. Different types of simulations are carried out; verification studies of the initial mesh and set-up, 2D simulations with waves and without the cylinder, 2D simulations without waves and with the cylinder, and 3D simulations with both waves and the cylinder. Three dimensional flow and three dimensional effects are investigated by comparing a 3D simulation to integrated 2D simulations. The drag- and lift forces show discrepancies with the 3D drag forces being approximately four times higher than the integrated 2D drag forces. It is shown by investigating the flow features around the cross-section of the cylinder that the pressure in the 2D simulations show strange behaviour that needs to be investigated further and may cause some error in the results. The 3D simulations also demonstrates wave run-up at the rear of the cylinder as can be caused by steep and long waves in shallow waters. The viscosity investigation give a small decrease in the forces with practically zero viscosity implemented into the simulation. The decrease is very small ($< 3\%$) and is due to the decrease in the viscous force components.

The turbulent simulation in 3D give a different wave profile than for the other 3D cases. The waves seem to form a steeper peak and thereby diminish in height as they propagate towards the cylinder. This give smaller magnitude of both drag- and lift force and no vortex shedding. Using shallow water wave theory prove to work efficiently and the waves generated in the simulations are almost identical to the theoretical waves with equal wave parameters. Using this wave theory in comparison to a regular wave theory is more difficult to simulate in terms of shallow water conditions. These conditions make it harder for the solver to find converged solutions. However, it is efficient and doable to take higher order wave theories into OpenFOAM and into CFD analyses. The discussions aim to answer the research questions presented in the Introduction of this thesis in order to fulfill the objective: Investigation of a bottom-fixed monopile WT interacting with shallow water waves and to assess the relevance of three-dimensional flow, turbulence and viscosity. The main results to answer and fulfill the objective are in short the following:

- There are many available sites for the implementation of OWT's. One relevant site in the North Sea is selected and the environmental parameters defined. Wave measurements give the extreme conditions that are picked for further investigations.
- The initial domain, mesh and set-up are successfully tested and verified by comparing the results with other previously done studies
- A Cnoidal wave theory is implemented into the CFD solver in a good manner and the generated wave profiles from 2D simulations without the cylinder are tested and compared against analytic solutions for the wave profiles. The results agree well with each other.
- Using an unsteady boundary condition at the inlet for several 2D simulations to represent different cross-sections of the monopile show great potential to work well. The results are integrated using strip theory. Some improvement points are pointed out.
- 3D simulations of the monopile in waves are difficult to conduct as there are many variables and possible error sources. However, they show promising results and ability to model even higher order behaviour and near-breaking waves in a good way.
- Comparing the 3D results to the integrated 2D results give higher drag forces for the 3D results (approximately four times higher peaks) and lower lift forces. It is concluded that the reasons for this difference are due to pressure errors in the 2D simulations.
- The relevance of viscosity is presented and assessed and show the importance of the viscous components in the total force working on the cylinder.
- The turbulent simulation in 2D show steady state behaviour and lower magnitude of the forces. The 3D turbulent simulation show different wave behaviour and also a lower magnitude in both lift- and drag forces. This is concluded to be caused by the much smaller waves hitting the cylinder as the measured water flow velocities are also of a smaller magnitude than the corresponding laminar case.

- Difficult surroundings and wave conditions make it hard to conduct a turbulent simulation. Time limited this work, and it is only conducted one 2D turbulent case and one 3D turbulent case.

The field of CFD is in constantly improvement and can be developed for use in the industry. The results obtained from tests are produced in a reasonable amount of time. However, this is partly because the simulations are carried out by a supercomputer with the possibility to run the simulation in parallel on several nodes. But with increasing computational power getting more available it is no problem to do these types of simulations without the accessibility of a supercomputer. The most time-consuming part of doing CFD simulations is to get the mesh and general set-up in order.

8.1 Further Work

For continuation of this project, there are some aspects that are of interest to investigate. Suggestions are the following points.

- **Improve 2D simulations with unsteady boundary condition inlet:** Change reference cell for the solution in the solver files. Improve the solver files in the system folder and try using different solvers to test for differences in the solution.
- **Convergence study for 3D simulations:** During this study, there was no time to do a proper convergence study for the domain size, grid size and time step for the 3D simulations. It is of interest to optimize all parameters for these simulations as more accurate results could be achieved, and computational time could be saved going forward with studies of this geometry.
- **Longer simulations:** A steady state for the lift forces was not obtained in the 2D simulations with unsteady inlet BC and neither for the 3D simulations. It is of interest to run both of these simulations for a longer time to test if the results change over time.
- **Verify turbulence model:** Do convergence testing and verify against other turbulent cases for the 2D turbulence set-up with unsteady boundary conditions.
- **Turbulence:** A turbulence model can be verified by use of experiments with similar conditions. Choice of turbulence model and turbulence parameters should then be investigated further.
- **Soil interaction effects:** It would have been of interest to investigate how much damping and/or challenges the soil interaction would provide at the relevant site.
- **Bottom slope:** Investigate further possible bottom conditions and the impact this has for the force and the structure.
- **Short-crested waves:** Check for possible impacts of having short-crested waves and an irregular wave spectra.

Bibliography

Arreba, I. R., 06 2017. Computation of nonlinear wave loads on floating structures. Master thesis, NTNU, Trondheim, Norway.

Asyikin, M. T., 06 2012. Cfd simulation of vortex induced vibration. Master thesis, Norwegian University of Science and Technology, Trondheim, Norway.

Bachynski, E. E., Kristiansen, T., Thys, M., 2017. Experimental and numerical investigations of monopile ringing in irregular finite-depth water waves. Applied Ocean Research 68, 154 – 170.
URL `http://www.sciencedirect.com/science/article/pii/S0141118716305284`

Bailey, B., 2016. 3 - wind resources for offshore wind farms: Characteristics and assessment. In: Ng, C., Ran, L. (Eds.), Offshore Wind Farms. Woodhead Publishing, pp. 29 – 58.
URL `http://www.sciencedirect.com/science/article/pii/B9780081007792000039`

Bakker, A., 02 2019. Applied computational fluid dynamics: turbulence models.
URL `http://www.bakker.org/dartmouth06/engs150/07-mesh.pdf`

Blazek, J., 2001. Computational fluid dynamics: principles and applications. Elsevier.

BlenderFoundation, 05 2019. About blender.
URL `https://www.blender.org/about/`

Bouzid, D. A., 2018. Numerical investigation of large-diameter monopiles in sands: Critical review and evaluation of both api and newly proposed p-y curves. International Journal of Geomechanics 18 (11).

Braza, M., Chassaing, P., Hinh, H., 1986. Numerical study and physical analysis of the pressure and velocity fields in the near wake of a circular cylinder. Journal of Fluid Mechanics 165, 79 – 130.

Calhoun, D., Wang, Z., 2002. A cartesian grid method for solving the two-dimensional streamfunction-vorticity equations in irregular regions. Journal of Computational Physics 176, 231 – 275.

Camp, T. R., Morris, M. J., Rooij, R. v., Tempel, J. v. d., Zaaijer, M., Henderson, A., Argyriadis, K., Schwarts, S., Just, H., Grainger, W., Pearce, D., 2003. Design methods for offshore wind turbines at exposed sites. Tech. rep., EU Joule III Project JOR3-CT95-0284.

Catalano, P., Wang, M., Laccarino, G., Moin, P., 2003. Numerical simulation of the flow around a circular cylinder at high reynolds numbers. Int J Heat Fluid Flow 24, 463 – 469.

Cengel, Y. A., Cimbala, J. M., 2014. Fluid Mechanics. Mc Graw Hill Education.

CFD-Direct, 02 2019a. Mesh generation with blockmesh.
URL `https://cfd.direct/openfoam/user-guide/v6-blockmesh/`

CFD-Direct, 05 2019b. Mesh generation with snappyhexmesh.
URL `https://cfd.direct/openfoam/user-guide/v6-snappyhexmesh/`

Choi, J., Oberoi, R., Edwards, J., Rosati, J., 2007. An immersed boundary method for complex incompressible flows. Journal of Computational Physics 224, 757 – 784.

Clamond, D., 05 2018. Surface gravity waves.
URL `https://se.mathworks.com/matlabcentral/fileexchange/61499-surface-gravity-waves?focused=7218242&tab=function`

de Ridder, E. J., Aalberts, P., van den Berg, J., Buchner, B., Peeringa, J., 2011. The dynamic response of an offshore wind turbine with realistic flexibility to breaking wave impact. ASME 2011 30th International Conference on Ocean, Offshore and Arctic Engineering OMAE2011-49563.

de Vos, L., Frigaard, P., de Rouck, J., 2007. Wave run-up on cylindrical and cone shaped foundations for offshore wind turbines. Coast. Eng. 54, 17–29.

DNV-GL, 10 2010. Position Mooring. Offshore Standard, DNV-OS-E301.

DNV-GL, 05 2014. Design of Offshore Wind Turbine Structures. Offshore Standard.

DNV-GL, 2018. Energy Transition Outlook 2018. DNV-GL.

Equinor, 09 2018. Hywind.
URL `https://www.equinor.com/en/what-we-do/hywind-where-the-wind-takes-us.html`

Faltinsen, O. M., 1990. Sea Loads on Ships and Offshore Structures. Cambridge University Press.

Fenton, J. D., 1988. The numerical solution of steady water wave problems. Computational Geoscience 14, 357 – 368.

Fenton, J. D., 1998. The cnoidal theory of water waves. Developments in Offshore Engineering 2.

Ferziger, J. H., Peric, M., 2002. Computational Methods for Fluid Dynamics. Springer Berlin Heidelberg.

GmbHm, R. . D. C. F. K., 02 2019. Fino3.
URL `https://www.fino3.de`

Guerrero, J., 2009. Numerical simulation of the unsteady aerodynamics of flapping flight. PhD Thesis, University of Genoa 139.

Haver, S., 05 2017. Metocean Modelling and Prediction of Extremes. University in Stavanger and NTNU, Stavanger, 1st Edition.

Hirt, C., Nichols, B., 1981. Volume of fluid (vof) method for the dynamics of free boundaries. Journal of Computational Physics 39 (1), 201 – 225.
URL `http://www.sciencedirect.com/science/article/pii/0021999181901455`

Hong-jian, C., De-cheng, W., 2015. Rans-vof solver for solitary wave run-up on a circular cylinder. China Ocean Engineering 29 (2), 183 – 196.

Isobe, M., 1985. Calculation and application of first-order cnoidal wave theory. Coastal engineering 9, 309 – 325.

Jacobsen, N. G., 2017. waves2Foam Manual. Published digitally.

Khalid, M. N., 06 2016. Design optimization of tendons of snorre a tension leg platform (tlp) for extreme wave event. Master thesis, University of Stavanger, Stavanger, Norway.

Kristiansen, T., Faltinsen, O. M., 11 2017. Higher harmonic wave loads on a vertical cylinder in finite water depth. Fluid Mech. 833 (1), 773–805.

Li, L., Gao, Z., Moan, T., 2013. Joint environmental data at five european offshore sites for design of combined wind and wave energy devices. OMAE2013-10156.

Lui, C., Zheng, X., Sung, C., 1998. Preconditioned multigrid methods for unsteady incompressible flows. Journal of Computational Physics 139, 33 – 57.

Merz, K. O., Moe, G., Gudmestad, O. T., 2009. A review of hydrodynamic effects on bottom-fixed offshore wind turbines. Ocean, Offshore and Arctic Engineering, OMAE 1.

Morison, J. R., O'Brian, M. P., Johnson, J. W., Schaaf, S. A., 1950. The force exerted by surface waves on piles. Pet. Trans 189, 149 – 154.

Nielsen, A. W., Schlutter, F., Sørensen, J. V. T., Bredmose, H., 2013. Wave loads on a monopile in 3d waves. ASME 2012 31st International Conference on Ocean, Offshore and Arctic Engineering OMAE2012-83533.

Ong, M. C., Utnes, T., Holmedal, L. E., Myrhaug, D., Pettersen, B., 2009. Numerical simulation of flow around a smooth circular cylinder at very high reynolds numbers. Marine Structures 22, 142 – 153.

Online, C., December 2018. Turbulence properties, conversions & boundary estimations. URL `https://www.cfd-online.com/Tools/turbulence.php`

OpenCFD, 05 2019. Standard boundary conditions. URL `https://www.openfoam.com/documentation/user-guide/standard-boundaryconditions.php`

OpenFOAM, November 2018. Standard boundary conditions. URL `https://www.openfoam.com/documentation/user-guide/standard-boundaryconditions.php#x35-138000A.4`

Paulsen, B. T., Bredmose, H., Bingham, H. B., Jacobsen, N. G., 2014. Forcing of a bottom-mounted circular cylinder by steep regular water waves at finite depth. Journal of Fluid Mechanics 755, 1–34.

Pettersen, B., 2018. Marin Teknikk 3 - Hydrodynamikk. NTNU and Akademika.

Ransau, S., 2018. Numerical Methods in Marine Hydrodynamics.

Rosenlund, E., 06 2013. Nonlinear hydrodynamic effects for bottom-fixed wind turbines. Master thesis, Norwegian University of Science and Technology, Trondheim.

Russell, D., Wang, Z., 2003. A cartesian grid method for modelling multiple moving objects in 2d incompressible viscous flow. Journal of Computational Physics 191, 231 – 275.

Sarpkaya, T., 1976. Vortex shedding and resistance in harmonic flow about smooth and rough circular cylinders at high reynolds numbers. Tech. rep., Naval Postgraduate School Monterey Ca.

Schloer, S., Bredmose, H., Mikkelsen, R. F., 2013. Fatigue and extreme wave loads on bottom fixed offshore wind turbines. effects from fully nonlinear wave forcing on the structural dynamics. DTU Wind Energy PhD 0017.

Singh, S., Mittal, S., 2005. Flow past a cylinder: shear layer instability and drag crisis. Int J Numer Meth Fluids 47, 75 – 98.

Svendsen, I. A., Jonsson, I. G., 1976. Hydrodynamics of coastal regions. Den private ingeniørfond, Technical university of Denmark.

Tawekal, J. R., 06 2015. Cfd simulation of the flow over a 2-dimensional pipe and vortex induced vibration of the pipe with 1 degree of freedom. Master thesis, University of Stavanger, Stavanger, Norway.

UN, T., December 2018. Climate actions.
URL `https://www.un.org/sustainabledevelopment/climate-action/`

Velarde, J., 06 2016. Design of monopile foundations to support the dtu 10 mw offshore wind turbine. Master thesis, Norwegian University of Science and Technology, Trondheim.

Versteeg, H. K., Malalasekera, W., 2007. An introduction to computational fluid dynamics: the finite volume method, 2nd Edition. Prentice Hall/ Pearson Education.

Wang, W., Kamath, A., Bihs, H., 2018. Cfd simulations of multi-directional irregular wave interaction with a large cylinder.
URL `http://hdl.handle.net/11250/2568634`

Wienke, J., Oumeraci, H., 2005. Breaking wave impact force on a vertical and inclined slender pile – theoretical and large-scale model investigations. Coast. Eng. 52, 435–462.

Williams, P. S., Moon, M. H., Xu, Y., Giddings, J. C., 1996. Effect of viscosity on retention time and hydrodynamic lift forces in sedimentation/steric field-flow fractionation. Chemical engineering science 51, 4477 – 4488.

Younis, N., 2010. The role of turbulent integral length scale on the drag og a circular cylinder in cross flow. Electronic theses and dissertations 216.

Zang, J., Taylor, P. H., Morgan, G., Stringer, R., Orszagova, J., Grice, J., Tello, M., 2010. Steep wave and breaking wave impact on offshore wind turbine foundations – ringing re-visited. International Workshop on Water Waves and Floating Bodies (IWWWFB25).

Appendix A - OpenFOAM Input Scripts 2D

Job execution script - Wave simulations

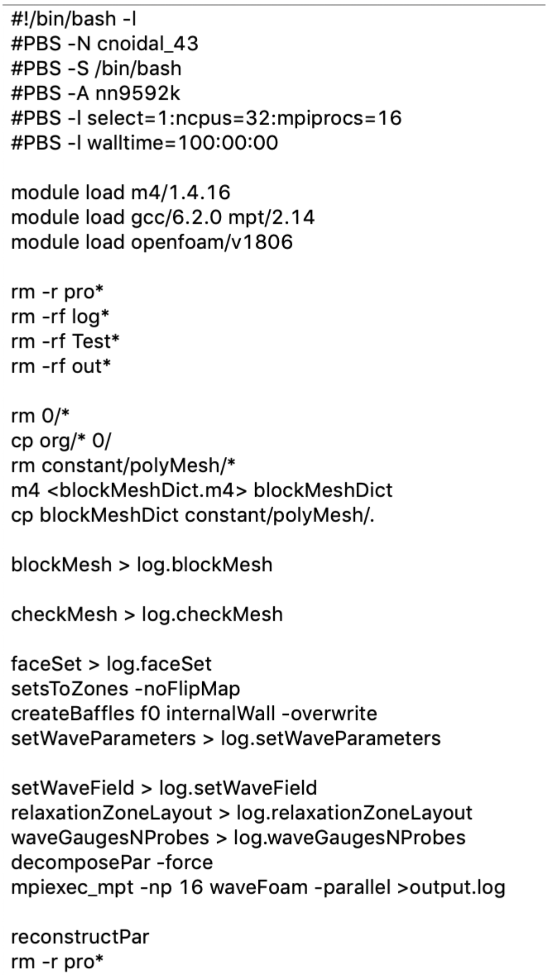

```
#!/bin/bash -l
#PBS -N cnoidal_43
#PBS -S /bin/bash
#PBS -A nn9592k
#PBS -l select=1:ncpus=32:mpiprocs=16
#PBS -l walltime=100:00:00

module load m4/1.4.16
module load gcc/6.2.0 mpt/2.14
module load openfoam/v1806

rm -r pro*
rm -rf log*
rm -rf Test*
rm -rf out*

rm 0/*
cp org/* 0/
rm constant/polyMesh/*
m4 <blockMeshDict.m4> blockMeshDict
cp blockMeshDict constant/polyMesh/.

blockMesh > log.blockMesh

checkMesh > log.checkMesh

faceSet > log.faceSet
setsToZones -noFlipMap
createBaffles f0 internalWall -overwrite
setWaveParameters > log.setWaveParameters

setWaveField > log.setWaveField
relaxationZoneLayout > log.relaxationZoneLayout
waveGaugesNProbes > log.waveGaugesNProbes
decomposePar -force
mpiexec_mpt -np 16 waveFoam -parallel >output.log

reconstructPar
rm -r pro*
```

M4 Mesh File - 2D cylinder

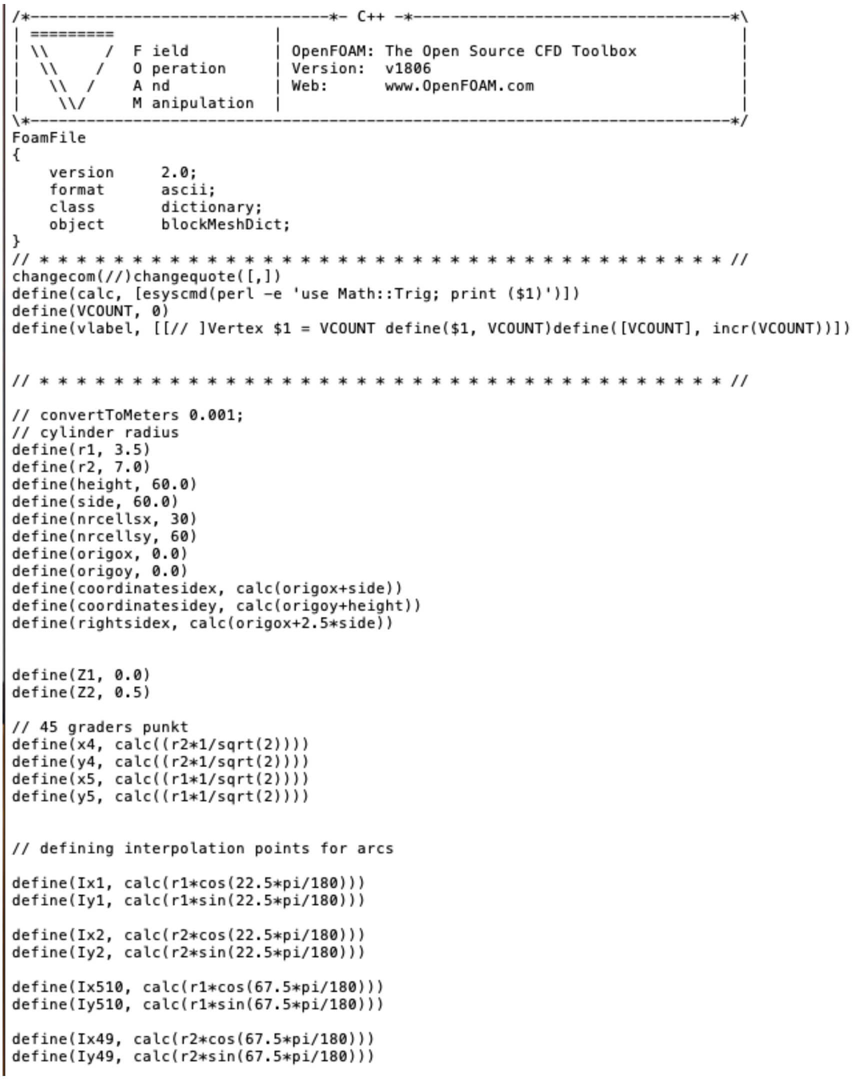

```
/*--------------------------------*- C++ -*----------------------------------*\
| =========                 |                                                 |
| \\      /  F ield         | OpenFOAM: The Open Source CFD Toolbox           |
|  \\    /   O peration     | Version:  v1806                                 |
|   \\  /    A nd           | Web:      www.OpenFOAM.com                      |
|    \\/     M anipulation  |                                                 |
\*---------------------------------------------------------------------------*/
FoamFile
{
    version     2.0;
    format      ascii;
    class       dictionary;
    object      blockMeshDict;
}
// * * * * * * * * * * * * * * * * * * * * * * * * * * * * * * * * * * * * * //
changecom(//)changequote([,])
define(calc, [esyscmd(perl -e 'use Math::Trig; print ($1)')])
define(VCOUNT, 0)
define(vlabel, [[// ]Vertex $1 = VCOUNT define($1, VCOUNT)define([VCOUNT], incr(VCOUNT))])


// * * * * * * * * * * * * * * * * * * * * * * * * * * * * * * * * * * * * * //

// convertToMeters 0.001;
// cylinder radius
define(r1, 3.5)
define(r2, 7.0)
define(height, 60.0)
define(side, 60.0)
define(nrcellsx, 30)
define(nrcellsy, 60)
define(origox, 0.0)
define(origoy, 0.0)
define(coordinatesidex, calc(origox+side))
define(coordinatesidey, calc(origoy+height))
define(rightsidex, calc(origox+2.5*side))


define(Z1, 0.0)
define(Z2, 0.5)

// 45 graders punkt
define(x4, calc((r2*1/sqrt(2))))
define(y4, calc((r2*1/sqrt(2))))
define(x5, calc((r1*1/sqrt(2))))
define(y5, calc((r1*1/sqrt(2))))


// defining interpolation points for arcs

define(Ix1, calc(r1*cos(22.5*pi/180)))
define(Iy1, calc(r1*sin(22.5*pi/180)))

define(Ix2, calc(r2*cos(22.5*pi/180)))
define(Iy2, calc(r2*sin(22.5*pi/180)))

define(Ix510, calc(r1*cos(67.5*pi/180)))
define(Iy510, calc(r1*sin(67.5*pi/180)))

define(Ix49, calc(r2*cos(67.5*pi/180)))
define(Iy49, calc(r2*sin(67.5*pi/180)))
```

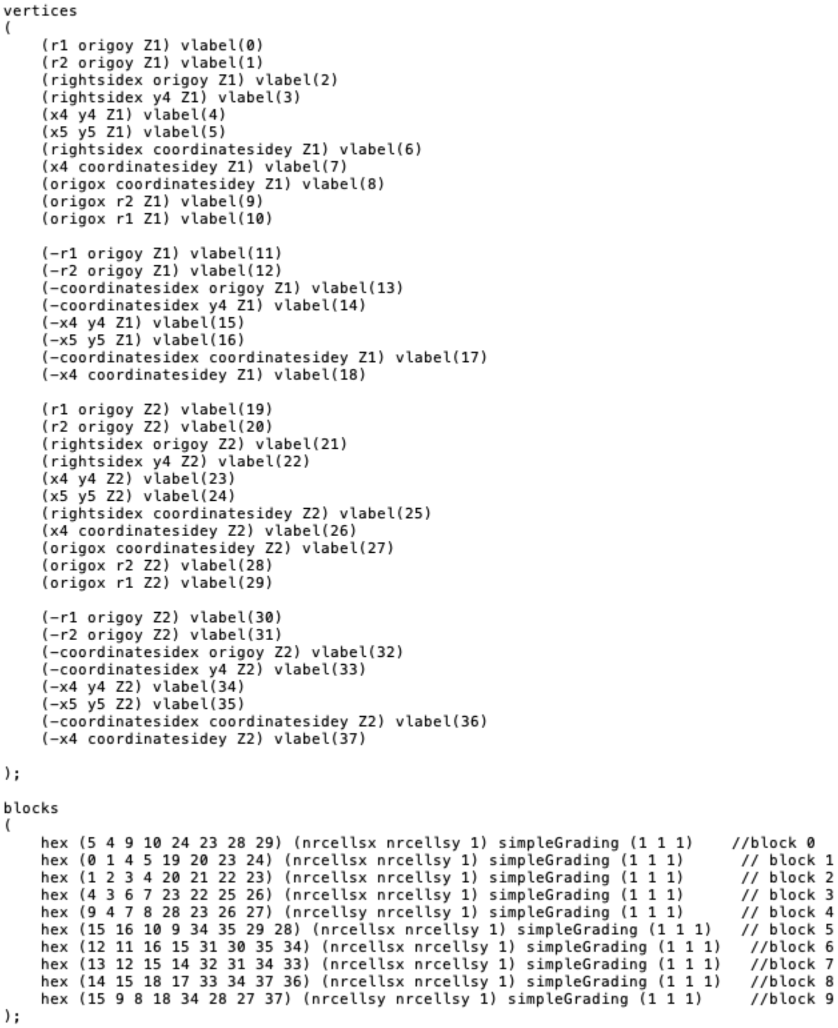

```
vertices
(
    (r1 origoy Z1) vlabel(0)
    (r2 origoy Z1) vlabel(1)
    (rightsidex origoy Z1) vlabel(2)
    (rightsidex y4 Z1) vlabel(3)
    (x4 y4 Z1) vlabel(4)
    (x5 y5 Z1) vlabel(5)
    (rightsidex coordinatesidey Z1) vlabel(6)
    (x4 coordinatesidey Z1) vlabel(7)
    (origox coordinatesidey Z1) vlabel(8)
    (origox r2 Z1) vlabel(9)
    (origox r1 Z1) vlabel(10)

    (-r1 origoy Z1) vlabel(11)
    (-r2 origoy Z1) vlabel(12)
    (-coordinatesidex origoy Z1) vlabel(13)
    (-coordinatesidex y4 Z1) vlabel(14)
    (-x4 y4 Z1) vlabel(15)
    (-x5 y5 Z1) vlabel(16)
    (-coordinatesidex coordinatesidey Z1) vlabel(17)
    (-x4 coordinatesidey Z1) vlabel(18)

    (r1 origoy Z2) vlabel(19)
    (r2 origoy Z2) vlabel(20)
    (rightsidex origoy Z2) vlabel(21)
    (rightsidex y4 Z2) vlabel(22)
    (x4 y4 Z2) vlabel(23)
    (x5 y5 Z2) vlabel(24)
    (rightsidex coordinatesidey Z2) vlabel(25)
    (x4 coordinatesidey Z2) vlabel(26)
    (origox coordinatesidey Z2) vlabel(27)
    (origox r2 Z2) vlabel(28)
    (origox r1 Z2) vlabel(29)

    (-r1 origoy Z2) vlabel(30)
    (-r2 origoy Z2) vlabel(31)
    (-coordinatesidex origoy Z2) vlabel(32)
    (-coordinatesidex y4 Z2) vlabel(33)
    (-x4 y4 Z2) vlabel(34)
    (-x5 y5 Z2) vlabel(35)
    (-coordinatesidex coordinatesidey Z2) vlabel(36)
    (-x4 coordinatesidey Z2) vlabel(37)

);

blocks
(
    hex (5 4 9 10 24 23 28 29) (nrcellsx nrcellsy 1) simpleGrading (1 1 1)    //block 0
    hex (0 1 4 5 19 20 23 24) (nrcellsx nrcellsy 1) simpleGrading (1 1 1)      // block 1
    hex (1 2 3 4 20 21 22 23) (nrcellsx nrcellsy 1) simpleGrading (1 1 1)      // block 2
    hex (4 3 6 7 23 22 25 26) (nrcellsx nrcellsy 1) simpleGrading (1 1 1)      // block 3
    hex (9 4 7 8 28 23 26 27) (nrcellsy nrcellsy 1) simpleGrading (1 1 1)      // block 4
    hex (15 16 10 9 34 35 29 28) (nrcellsx nrcellsy 1) simpleGrading (1 1 1)   // block 5
    hex (12 11 16 15 31 30 35 34) (nrcellsx nrcellsy 1) simpleGrading (1 1 1)   //block 6
    hex (13 12 15 14 32 31 34 33) (nrcellsx nrcellsy 1) simpleGrading (1 1 1)   //block 7
    hex (14 15 18 17 33 34 37 36) (nrcellsx nrcellsy 1) simpleGrading (1 1 1)   //block 8
    hex (15 9 8 18 34 28 27 37) (nrcellsy nrcellsy 1) simpleGrading (1 1 1)     //block 9
);
```

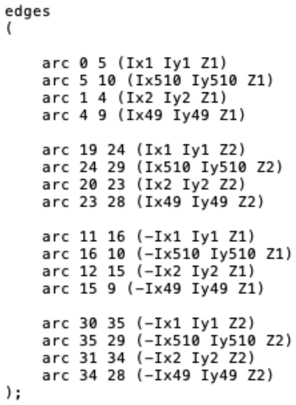

```
edges
(

    arc 0 5 (Ix1 Iy1 Z1)
    arc 5 10 (Ix510 Iy510 Z1)
    arc 1 4 (Ix2 Iy2 Z1)
    arc 4 9 (Ix49 Iy49 Z1)

    arc 19 24 (Ix1 Iy1 Z2)
    arc 24 29 (Ix510 Iy510 Z2)
    arc 20 23 (Ix2 Iy2 Z2)
    arc 23 28 (Ix49 Iy49 Z2)

    arc 11 16 (-Ix1 Iy1 Z1)
    arc 16 10 (-Ix510 Iy510 Z1)
    arc 12 15 (-Ix2 Iy2 Z1)
    arc 15 9 (-Ix49 Iy49 Z1)

    arc 30 35 (-Ix1 Iy1 Z2)
    arc 35 29 (-Ix510 Iy510 Z2)
    arc 31 34 (-Ix2 Iy2 Z2)
    arc 34 28 (-Ix49 Iy49 Z2)
);
```

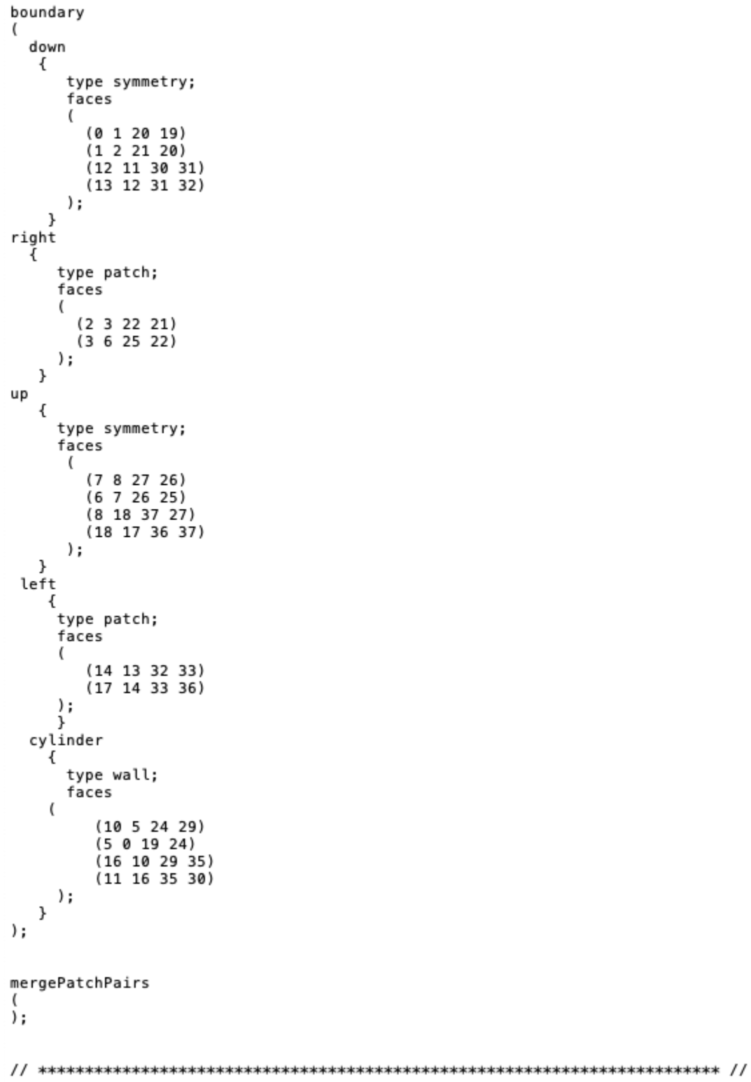

```
boundary
(
  down
   {
      type symmetry;
      faces
      (
        (0 1 20 19)
        (1 2 21 20)
        (12 11 30 31)
        (13 12 31 32)
      );
    }
right
  {
     type patch;
     faces
     (
       (2 3 22 21)
       (3 6 25 22)
     );
   }
up
   {
     type symmetry;
     faces
      (
        (7 8 27 26)
        (6 7 26 25)
        (8 18 37 27)
        (18 17 36 37)
      );
   }
 left
    {
     type patch;
     faces
     (
        (14 13 32 33)
        (17 14 33 36)
     );
     }
  cylinder
    {
      type wall;
      faces
    (
         (10 5 24 29)
         (5 0 19 24)
         (16 10 29 35)
         (11 16 35 30)
     );
   }
);


mergePatchPairs
(
);


// ************************************************************************* //
```

Mirror Mesh File

```
/*--------------------------------*- C++ -*----------------------------------*\
| =========                 |                                                 |
| \\      /  F ield         | OpenFOAM: The Open Source CFD Toolbox           |
|  \\    /   O peration     | Version:  2.1.x                                 |
|   \\  /    A nd           | Web:      www.OpenFOAM.org                      |
|    \\/     M anipulation  |                                                 |
\*---------------------------------------------------------------------------*/
FoamFile
{
    version     2.0;
    format      ascii;
    class       dictionary;
    object      mirrorMeshDict;
}
// * * * * * * * * * * * * * * * * * * * * * * * * * * * * * * * * * * * * * //

planeType           pointAndNormal;

pointAndNormalDict
{
    basePoint       (0 0 0);
    normalVector    (0 1 0);
}

planeTolerance      1e-3;

// ************************************************************************* //
```

Control File - 2D cylinder

```
/*--------------------------------*- C++ -*----------------------------------*\
| =========                 |                                                 |
| \\      /  F ield         | OpenFOAM: The Open Source CFD Toolbox           |
|  \\    /   O peration     | Version:  v1806                                 |
|   \\  /    A nd           | Web:      www.OpenFOAM.com                      |
|    \\/     M anipulation  |                                                 |
\*---------------------------------------------------------------------------*/
FoamFile
{
    version     2.0;
    format      ascii;
    class       dictionary;
    location    "system";
    object      controlDict;
}
// * * * * * * * * * * * * * * * * * * * * * * * * * * * * * * * * * * * * * //

application     pisoFoam;

startFrom        startTime;

startTime       0;

stopAt           endTime;

endTime         500;

deltaT          0.005;

writeControl     timeStep;

writeInterval    100;

purgeWrite      0;

writeFormat     ascii;

writePrecision  6;

writeCompression off;

timeFormat      general;

timePrecision   6;

runTimeModifiable true;
```

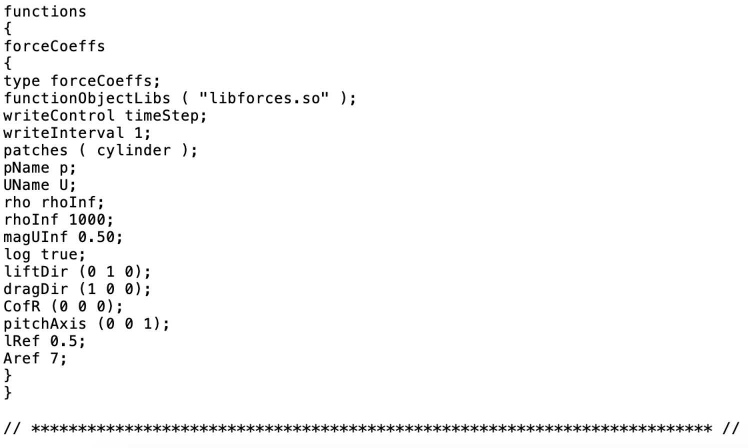

```
functions
{
forceCoeffs
{
type forceCoeffs;
functionObjectLibs ( "libforces.so" );
writeControl timeStep;
writeInterval 1;
patches ( cylinder );
pName p;
UName U;
rho rhoInf;
rhoInf 1000;
magUInf 0.50;
log true;
liftDir (0 1 0);
dragDir (1 0 0);
CofR (0 0 0);
pitchAxis (0 0 1);
lRef 0.5;
Aref 7;
}
}

// ************************************************************************* //
```

Probes Function

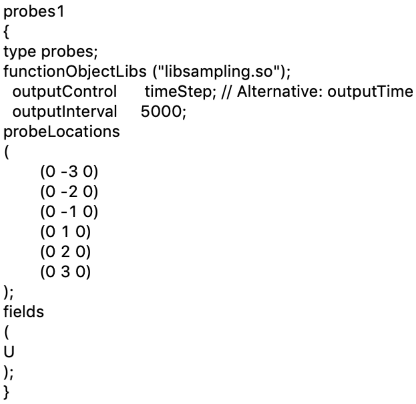

```
probes1
{
type probes;
functionObjectLibs ("libsampling.so");
  outputControl      timeStep; // Alternative: outputTime
  outputInterval     5000;
probeLocations
(
      (0 -3 0)
      (0 -2 0)
      (0 -1 0)
      (0 1 0)
      (0 2 0)
      (0 3 0)
);
fields
(
U
);
}
```

Appendix B - 2D Simulation Results

Drag forces from 2D simulations with unsteady BC at the inlet:

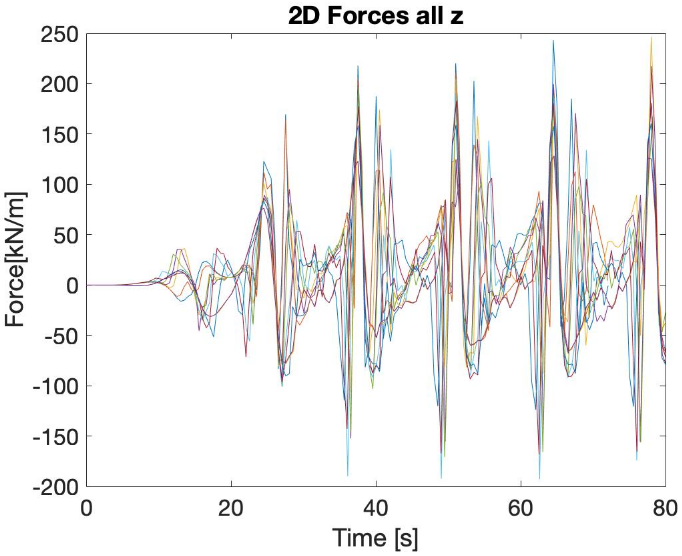

Drag- and lift forces from every simulation with at different z:

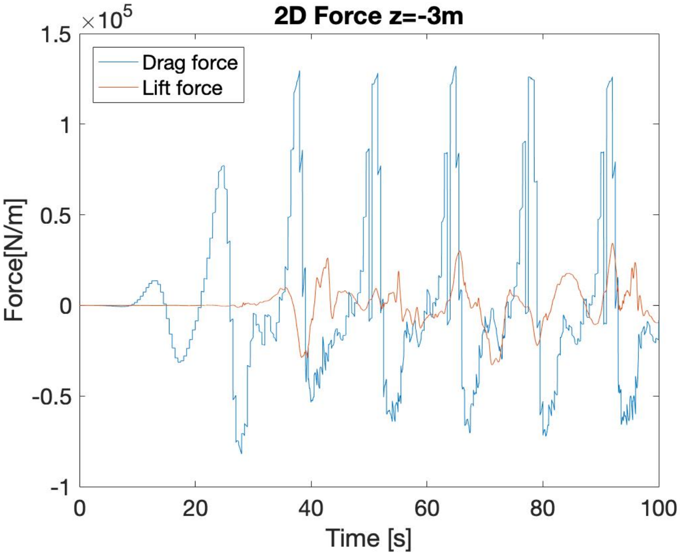

Figure 8.1: 2D forces, z=-3 [m]

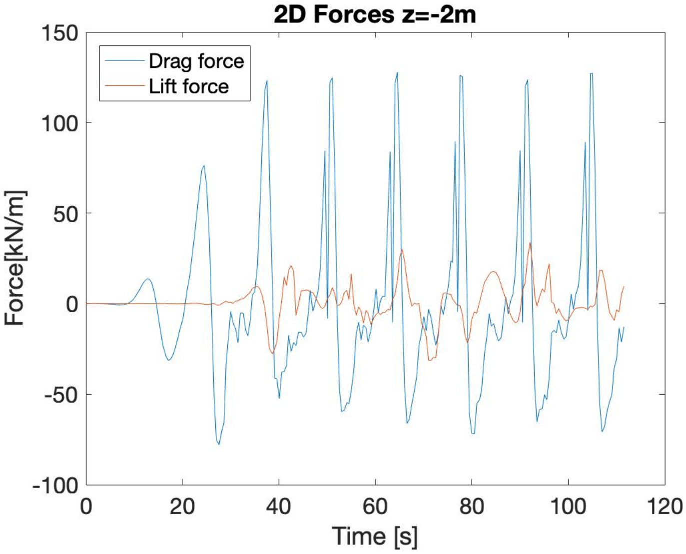

Figure 8.2: 2D forces, z=-2 [m]

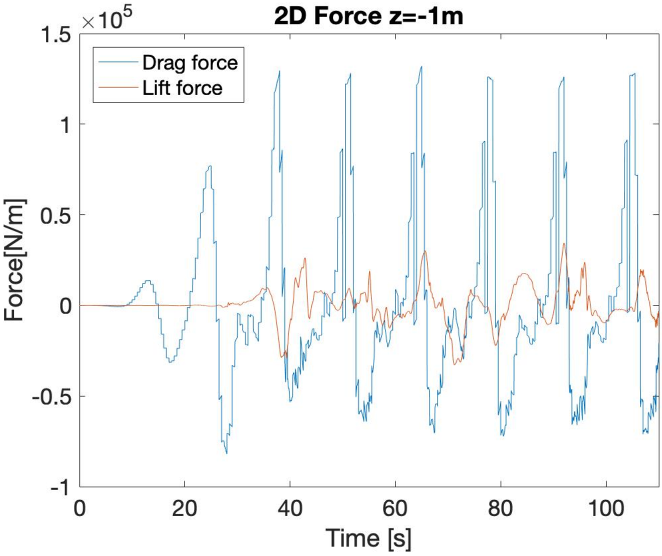

Figure 8.3: 2D forces, z=-1 [m]

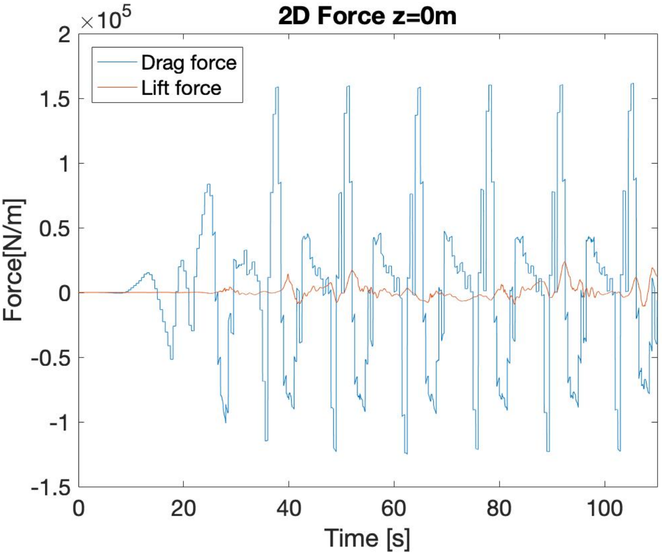

Figure 8.4: 2D forces, z=0 [m]

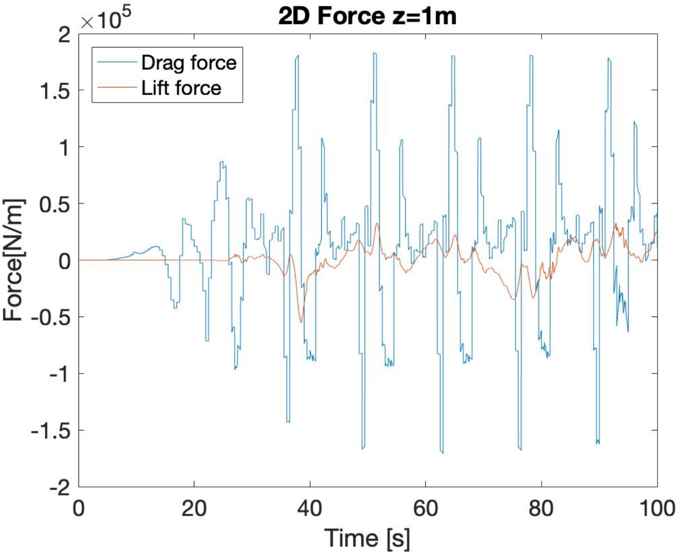

Figure 8.5: 2D forces, z=1 [m]

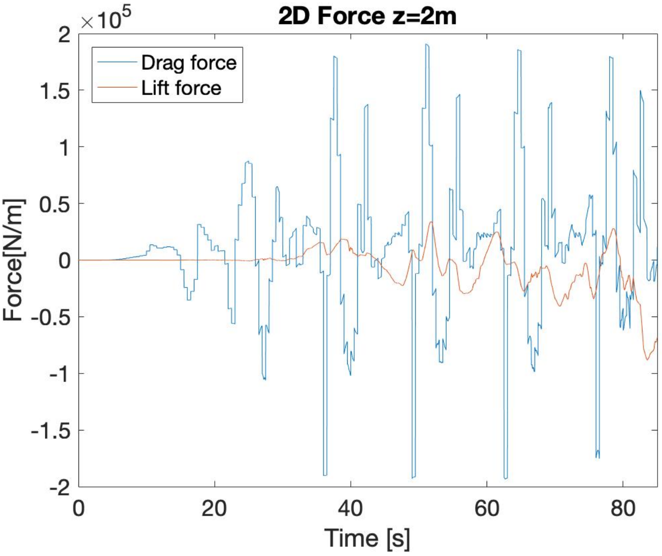

Figure 8.6: 2D forces, z=2 [m]

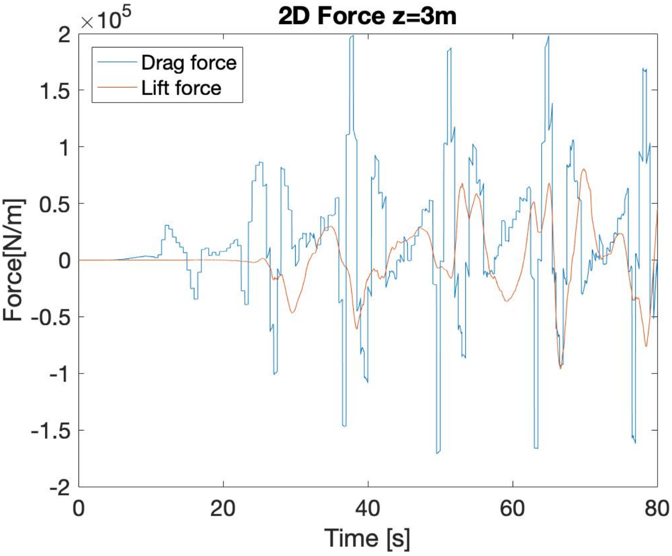

Figure 8.7: 2D forces, z=3 [m]

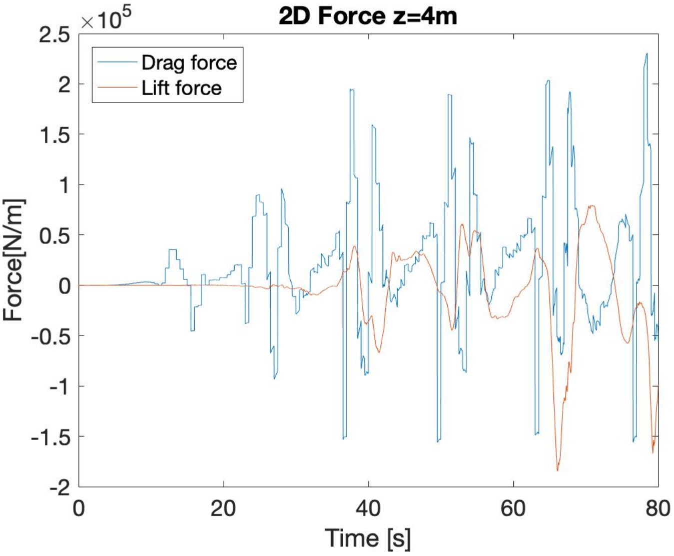

Figure 8.8: 2D forces, z=4 [m]

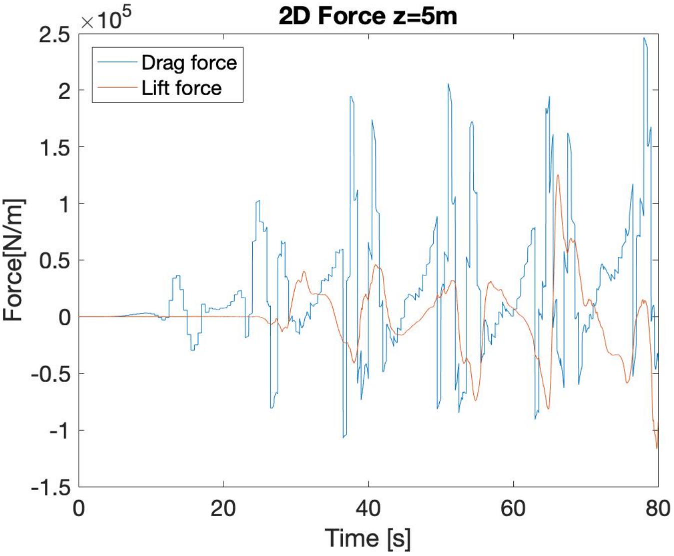

Figure 8.9: 2D forces, z=5 [m]

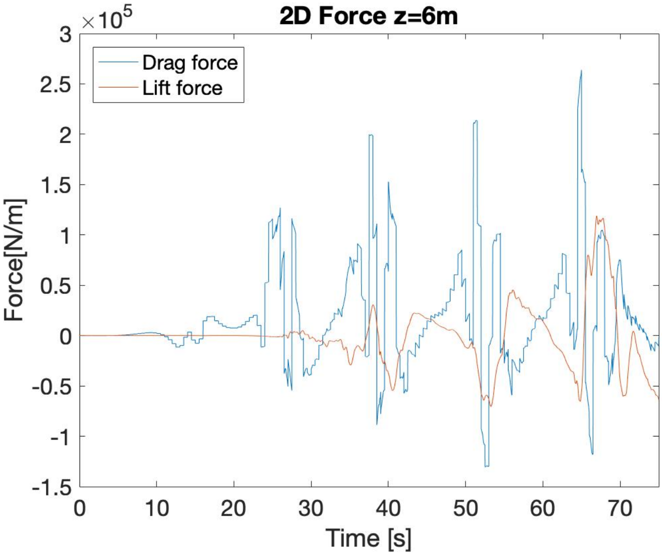

Figure 8.10: 2D forces, z=6 [m]

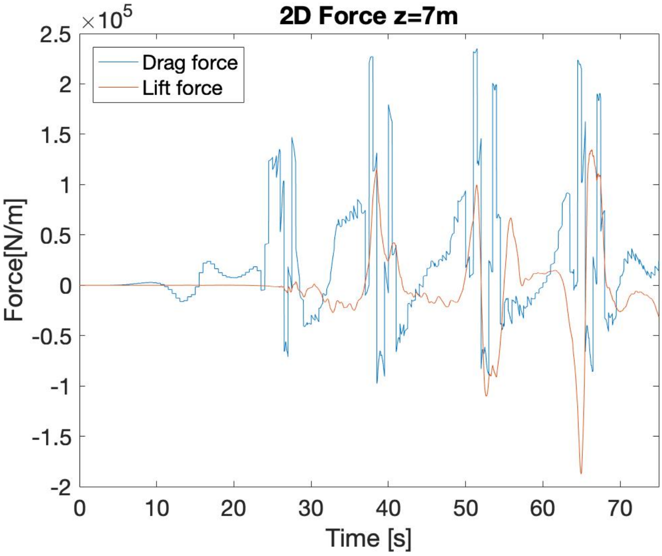

Figure 8.11: 2D forces, z=7 [m]

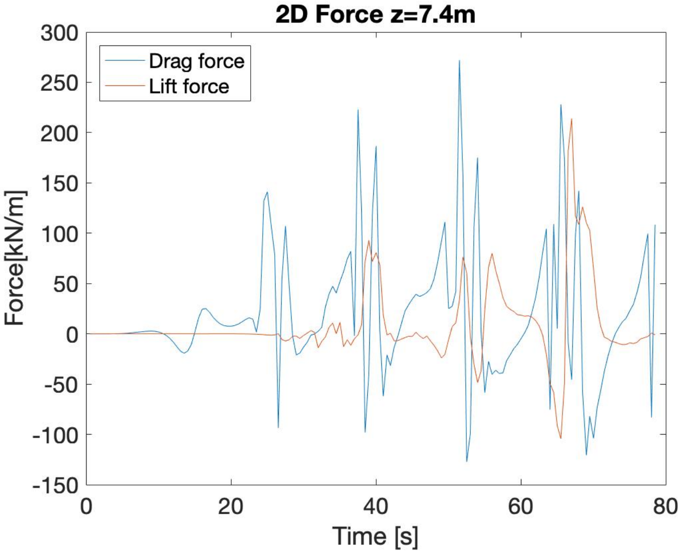

Figure 8.12: 2D forces, z=7.4 [m]

Appendix C - Additional OpenFOAM Input Scripts for 3D

snappyHexMeshDict - 3D cylinder with waves

```
/*--------------------------------*- C++ -*----------------------------------*\
| =========                 |                                                 |
| \\      /  F ield         | OpenFOAM: The Open Source CFD Toolbox           |
|  \\    /   O peration     | Version:  2.4.0                                 |
|   \\  /    A nd           | Web:      www.OpenFOAM.org                      |
|    \\/     M anipulation  |                                                 |
\*---------------------------------------------------------------------------*/
FoamFile
{
    version     2.0;
    format      ascii;
    class       dictionary;
    object      snappyHexMeshDict;
}

// * * * * * * * * * * * * * * * * * * * * * * * * * * * * * * * * * * * * * //

// Which of the steps to run
castellatedMesh true;
snap            true;
addLayers       true;


// Geometry. Definition of all surfaces. All surfaces are of class
geometry
{
    cylinder.stl
    {
        type triSurfaceMesh;
        name cylinder;
    }

    //- Refine a bit extra around the small centre hole
     refinementBox
    {
        type    searchableCylinder;
        point1 (0 0 40);
        point2 (0 0 -20);
        radius 40;
    }





                 refinementBox1//Water area + crest height
                {
                    type searchableBox;
                    min (-245 -20 -20);
                    max (400  20 12);
                }

                refinementBox2//refining by the inlet
               {
                   type searchableBox;
                   min (-250.5 -20 -20);
                   max (-245  20 40);
               }
             };



             // Settings for the castellatedMesh generation.
             castellatedMeshControls
             {

                 // Refinement parameters
                 maxLocalCells 10000000;

                 maxGlobalCells 20000000;

                 minRefinementCells 0;

                 nCellsBetweenLevels 6;

                 // Explicit feature edge refinement

                 features
                 (
                     { file "cylinder.eMesh"; level 1; }
                 );
```

```
        // Surface based refinement

        refinementSurfaces
        {
            cylinder
            {
                // Surface-wise min and max refinement level
                level (2 2);
    patchInfo { type wall; }
            }
        }

        resolveFeatureAngle 30;

        // Region-wise refinement

        refinementRegions
        {
            refinementBox
            {
                mode inside;
                levels ((100 3));
            }
            refinementBox1
            {
                mode inside;
                levels ((10 2));
            }
            refinementBox2
            {
                mode inside;
                levels ((10 2));
            }
        }


        // Mesh selection
        allowFreeStandingZoneFaces true;
    }
```

```
// Settings for the snapping.
snapControls
{
    //- Number of patch smoothing iterations before finding correspondence
    //  to surface
    nSmoothPatch 3;
    //nSmoothPatch 5;

    //- Relative distance for points to be attracted by surface feature point
    //  or edge. True distance is this factor times local
    //  maximum edge length.
    tolerance 1.0;

    //- Number of mesh displacement relaxation iterations.
    nSolveIter 300;

    //- Maximum number of snapping relaxation iterations. Should stop
    //  before upon reaching a correct mesh.
    nRelaxIter 5;
    //nRelaxIter 10;

    // Feature snapping

        //- Number of feature edge snapping iterations.
        //  Leave out altogether to disable.
        nFeatureSnapIter 10;

        //- Detect (geometric) features by sampling the surface
        implicitFeatureSnap false;

        //- Use castellatedMeshControls::features
        explicitFeatureSnap true;

        //- Detect features between multiple surfaces
        //  (only for explicitFeatureSnap, default = false)
        multiRegionFeatureSnap true;
}
```

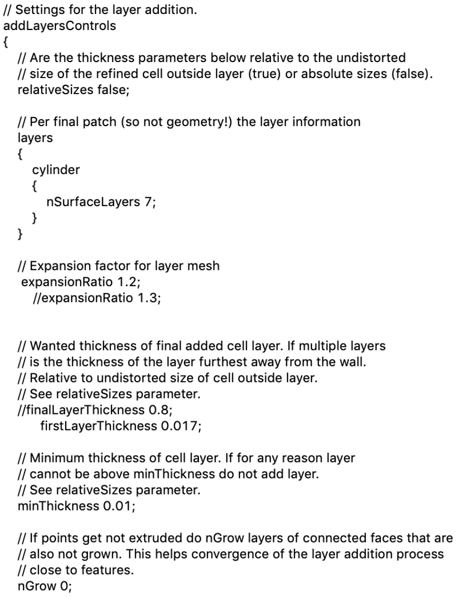

```
// Settings for the layer addition.
addLayersControls
{
    // Are the thickness parameters below relative to the undistorted
    // size of the refined cell outside layer (true) or absolute sizes (false).
    relativeSizes false;

    // Per final patch (so not geometry!) the layer information
    layers
    {
        cylinder
        {
            nSurfaceLayers 7;
        }
    }

    // Expansion factor for layer mesh
     expansionRatio 1.2;
        //expansionRatio 1.3;


    // Wanted thickness of final added cell layer. If multiple layers
    // is the thickness of the layer furthest away from the wall.
    // Relative to undistorted size of cell outside layer.
    // See relativeSizes parameter.
    //finalLayerThickness 0.8;
          firstLayerThickness 0.017;

    // Minimum thickness of cell layer. If for any reason layer
    // cannot be above minThickness do not add layer.
    // See relativeSizes parameter.
    minThickness 0.01;

    // If points get not extruded do nGrow layers of connected faces that are
    // also not grown. This helps convergence of the layer addition process
    // close to features.
    nGrow 0;
```

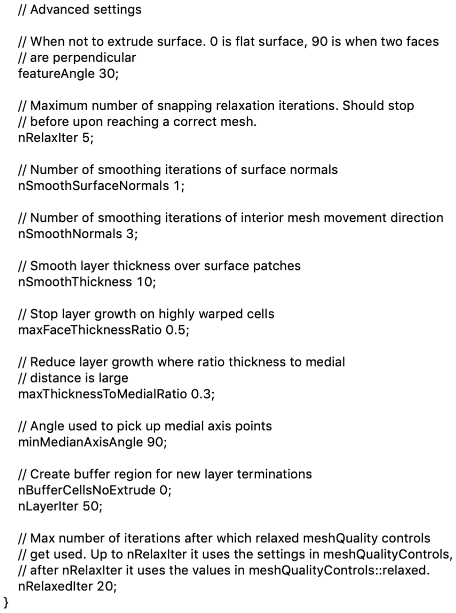

```
        // Advanced settings

        // When not to extrude surface. 0 is flat surface, 90 is when two faces
        // are perpendicular
        featureAngle 30;

        // Maximum number of snapping relaxation iterations. Should stop
        // before upon reaching a correct mesh.
        nRelaxIter 5;

        // Number of smoothing iterations of surface normals
        nSmoothSurfaceNormals 1;

        // Number of smoothing iterations of interior mesh movement direction
        nSmoothNormals 3;

        // Smooth layer thickness over surface patches
        nSmoothThickness 10;

        // Stop layer growth on highly warped cells
        maxFaceThicknessRatio 0.5;

        // Reduce layer growth where ratio thickness to medial
        // distance is large
        maxThicknessToMedialRatio 0.3;

        // Angle used to pick up medial axis points
        minMedianAxisAngle 90;

        // Create buffer region for new layer terminations
        nBufferCellsNoExtrude 0;
        nLayerIter 50;

        // Max number of iterations after which relaxed meshQuality controls
        // get used. Up to nRelaxIter it uses the settings in meshQualityControls,
        // after nRelaxIter it uses the values in meshQualityControls::relaxed.
        nRelaxedIter 20;
   }
```

```
meshQualityControls
{
   #include "meshQualityDict"

   // Optional : some meshing phases allow usage of relaxed rules.
   // See e.g. addLayersControls::nRelaxedIter.
   relaxed
   {
      //- Maximum non-orthogonality allowed. Set to 180 to disable.
      maxNonOrtho 75;
   }

   // Advanced

   //- Number of error distribution iterations
   nSmoothScale 4;
   //- amount to scale back displacement at error points
   errorReduction 0.75;
}

// Advanced

// Write flags
writeFlags
(
   scalarLevels    // write volScalarField with cellLevel for postprocessing
   layerSets       // write cellSets, faceSets of faces in layer
   layerFields     // write volScalarField for layer coverage
);

// Merge tolerance. Is fraction of overall bounding box of initial mesh.
mergeTolerance 1E-5;


// ************************************************************************* //
```

surfaceFeatureExtractDict - 3D cylinder with waves

```
/*--------------------------------*- C++ -*----------------------------------*\
| =========                 |                                                 |
| \\      /  F ield         | OpenFOAM: The Open Source CFD Toolbox           |
|  \\    /   O peration     | Version:  2.4.0                                 |
|   \\  /    A nd           | Web:      www.OpenFOAM.org                      |
|    \\/     M anipulation  |                                                 |
\*---------------------------------------------------------------------------*/
FoamFile
{
   version     2.0;
   format      ascii;
   class       dictionary;
   object      surfaceFeatureExtractDict;
}
// * * * * * * * * * * * * * * * * * * * * * * * * * * * * * * * * * * * * * //

cylinder.stl
{
   // How to obtain raw features (extractFromFile || extractFromSurface)
   extractionMethod    extractFromSurface;

   extractFromSurfaceCoeffs
   {
      // Mark edges whose adjacent surface normals are at an angle less
      // than includedAngle as features
      // - 0  : selects no edges
      // - 180: selects all edges
      includedAngle   150;
   }

   // Write options

      // Write features to obj format for postprocessing
      writeObj                yes;
}

// ************************************************************************* //
```

Karoline Eriksen

Numerical investigation of a bottom-fixed wind turbine

NTNU
Kunnskap for en bedre verden